A Surface Leach Test Facility for SNO

by

John Howard Mark Cowan

Department of Physics and Astronomy

Submitted in partial fulfillment
of the requirements for the degree of
Master of Science in Physics

Faculty of Graduate Studies
Laurentian University
Sudbury, Ontario
August 2000

0-612-61255-4

ACKNOWLEDGEMENTS

I would like to thank my supervisor, Dr. Doug Hallman, and my committee members. Dr. Clarence Virtue and Dr. Rizwan Haq, for their help in completing this thesis.

To all my friends in Sudbury, thanks for your support and comradery over the past few years. Our discussions and good times will always be remembered.

Thanks to my family for their love and support. This would not have been possible without you. A special thanks to Christine who gave me strength when I needed it most.

Finally, many thanks to Dr. Henry Lee and Dr. Jacques Farine for their unending help and support. Your gifts of knowledge and kindness will go much farther with me than this thesis.

ABSTRACT

A leach test facility (LTF) prototype was designed and constructed to assay the surfaces of some high purity materials. The facility was designed to use two established techniques to determine the emanation rate of ^{222}Rn and the leach rates of ^{224}Ra and ^{226}Ra from materials in a high purity acrylic tube filled with ultrapure water. This was done in order to study the potential impact such materials would have on the intrinsic background concentrations of ^{232}Th and ^{238}U in the cavity D_2O in the Sudbury Neutrino Observatory (SNO). In addition, a relationship between the ^{222}Rn emanation rate and the ^{226}Ra leach rate for a material can be measured.

The first technique required nitrogen gas to be bubbled through the water to remove the radon gas emanated from the sample material. The gas was transferred from the leach facility to a gas board with a series of cold traps, where water vapour and volatile gases were removed. The ^{222}Rn was then transferred to a low background, ZnS coated cell and counted on a photomultiplier tube. The ^{222}Rn background activity for the LTF was measured to be 61.63 ± 3.67 dpd. The results for two assays of a viton material gave an average ^{222}Rn emanation rate of 1409 ± 105 Rn/hr$\cdot$m^2.

The second technique utilized a high purity polypropylene column filled with MnO_x coated acrylic beads. When the water from the facility was pumped through the column the leached Ra was absorbed onto the beads. The column was then dried and placed on an electrostatic counter where the charged Po daughters were collected on a silicon photodiode and decay alpha particles were counted. The LTF background concentration levels for ^{232}Th and ^{238}U in ultrapure water (UPW) had upper limits of 9.8×10^{-12} g/g and 3.6×10^{-12} g/g respectively. The lower limits for both were 0.0. The upper limit for the ^{224}Ra background activity was measured to be 45 dpd. The upper limit for the leach rate of ^{224}Ra from a viton sample was measured to be 16 ^{224}Ra/day$\cdot$m^2.

The LTF prototype was shown to be a very useful facility for measuring radon emanation rates for materials immersed in UPW, but it was not sensitive enough to measure their associated radium leach rates. The possibility of a full scale facility for radon monitoring in SNO has been proven. On the basis of this work a larger system with increased sensitivity to radium was proposed, which would have the capability of measuring associated radon emanation and radium leach rates for a material immersed in UPW.

For Christine Ann Wright

TABLE OF CONTENTS

LIST OF FIGURES

LIST OF TABLES

Chapter 1

Introduction

1.1 Solar Neutrinos

For centuries mankind has been in awe of the universe around us. The stars and planets have been studied extensively with many questions remaining unanswered. The discovery of the neutrino in particle physics has led to new questions and theories in astronomy and astrophysics. How, you may ask?

It has been established that the best source of information available, describing the energy-releasing reactions which take place within a star, such as the Sun, are the neutrinos that escape the dense core. Scientists have developed good theoretical models of our Sun which predict, among other things, the flux of these neutrinos from the various reactions that take place at the core. However, solar neutrino experiments have measured counting rates that do not agree with theoretical rates.

This has led to new theories about the production of solar neutrinos, as well as the design of new experiments to better detect them. One such project, the Sudbury Neutrino Observatory (SNO), and its ability to better detect solar neutrinos, is the focus of this thesis.

1.1.1 The Standard Solar Model

The standard solar model (SSM) of Bahcall and Pinsonneault (BP98)[1] is calculated using known parameters of our Sun, known nuclear reaction sequences and parameters, and assumptions of the Sun's state and physics, allowing us to test theories of stellar structure and evolution. Photon luminosity, mass, radius, limiting value for oblateness and age are all measured parameters of our Sun, used in the SSM.

In the model, it is assumed that the Sun is a perfectly spherical, main sequence star with a homogeneous composition, that is in hydrostatic equilibrium. That is, the particle pressures exactly balance gravity, otherwise the Sun would collapse in a free-fall time of less than an hour. Energy transport in the deep interior is primarily by photon diffusion, while the primary source of energy for radiated photons and neutrinos is nuclear fusion.

The SSM[2] predicts that more than 98% of the solar energy in the Sun is generated by a series of nuclear reactions known as the proton-proton (*pp*) chain. It is from these reactions, and the lesser important (for the Sun) carbon-nitrogen-oxygen (CNO) cycle, that the solar neutrinos are born. In Table 1.1[2], the competing branches of the *pp* chain are described with their associated neutrino energies. The neutrino spectrum predicted by the BP98 SSM is shown in Figure 1.1[3], along with the associated solar neutrino experiments.

The ν_e fluxes of the *pp* and *pep* chains, $\Phi(pp)$ and $\Phi(pep)$, depend on the solar luminosity and extensively calculated neutrino cross-sections, and therefore have a lower sensitivity to the fine details of the model. On the other hand, the production rates of ^{7}Be and ^{8}B are critically dependent on core temperature, causing $\Phi(^7\mathrm{Be})$ and $\Phi(^8\mathrm{B})$ to be strongly dependent of the input parameters of the SSM. The production rate for the *hep* reaction is the least temperature dependent[4].

The SNO detector is only sensitive to solar neutrinos produced by the ^{8}B and *hep* reactions[4].

Helioseismology data has provided new tests of solar models mainly for properties of the outer regions of the Sun. However, the data can provide information describing the mean molecular weight of the solar interior[2].

Reaction	ν Energy (MeV)
$p + p \rightarrow {}^2H + e^+ + \nu_e$	≤ 0.424
or	
$p + e^- + p \rightarrow {}^2H + \nu_e$	1.422 (*pep*)
${}^2H + p \rightarrow {}^3He + \gamma$	
${}^3He + {}^3He \rightarrow \alpha + 2p$	
or	
${}^3He + {}^4He \rightarrow {}^7Be + \gamma$	
${}^7Be + e^- \rightarrow {}^7Li + \nu_e$	(90%) 0.861
	(10%) 0.383
${}^7Li + p \rightarrow 2\alpha$	
or	
${}^7Be + p \rightarrow {}^8B + \gamma$	
${}^8B \rightarrow {}^8Be^* + e^+ + \nu_e$	< 15
${}^8Be^* \rightarrow 2\alpha$	
or	
${}^3He + p \rightarrow {}^4He + e^+ + \nu_e$	$\leq$ 18.77 (*hep*)

Table 1.1: Nuclear reactions in the proton-proton (*pp*) chain.

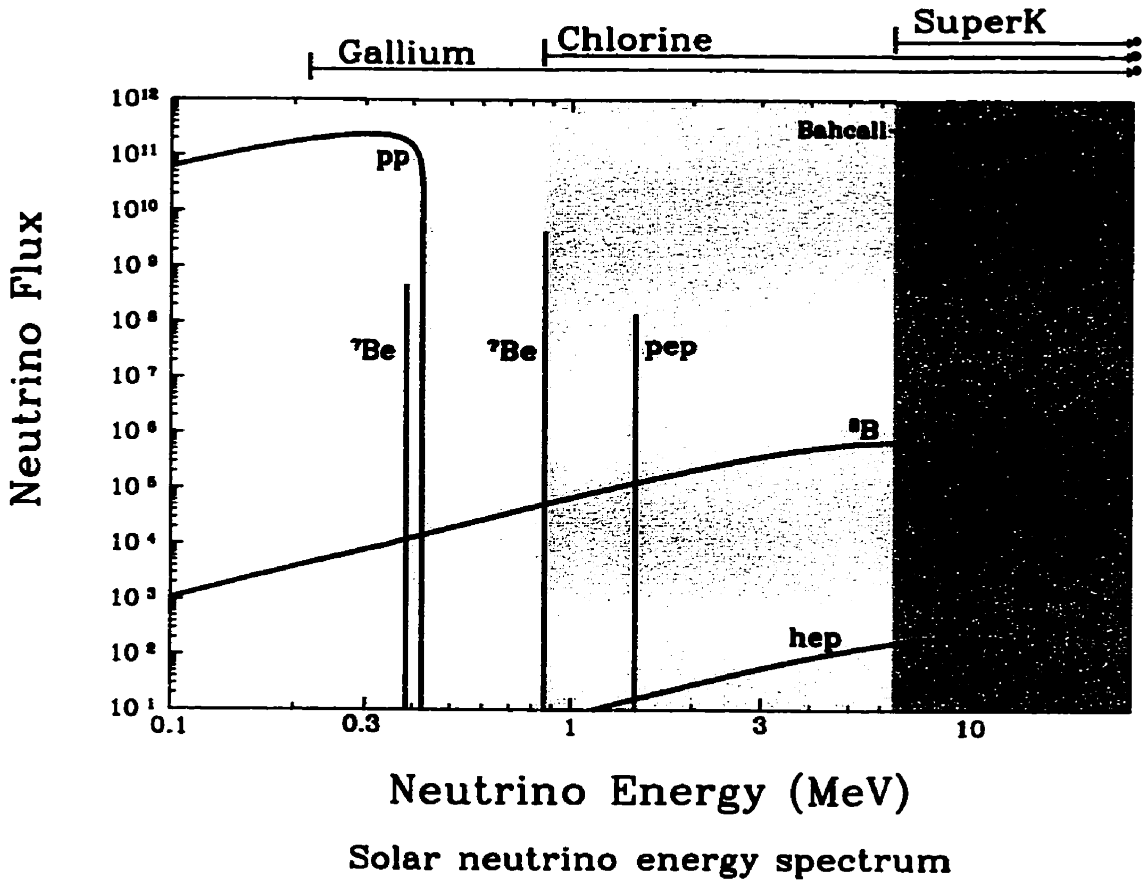

Figure 1.1: An updated plot of the standard solar neutrino energy spectrum from www.sns.ias.edu/ jnb[3]. The units of the neutrino flux are cm^{-2} s^{-1} for the monoenergetic lines and cm^{-2} s^{-1} MeV^{-1} for the continuous spectra.

1.1.2 The Solar Neutrino Problem

The first operating solar neutrino experiment was the ^{37}Cl experiment of Davis et al.[5], in the Homestake mine, in Lead, South Dakota. The reaction it used to detect neutrinos is

$$\nu_e + {}^{37}\mathrm{Cl} \rightarrow e^- + {}^{37}\mathrm{Ar} \tag{1.1}$$

which has a threshold energy of 0.8 MeV[2]. After years of data collection it could be seen that the ^{37}Ar production rate from the ^{8}B neutrinos (75% of total), was much lower than that predicted by the SSM. Tests of the radiochemical extraction efficiency and the neutrino capture cross-section in ^{37}Cl have shown the detector to be well understood[5]. Thus was born the solar neutrino problem (SNP).

If the known background rate (atoms per day) of a detector is subtracted from the production rate (atoms per day), the result is the known capture rate. The unit associated with the capture rate is the solar neutrino unit or SNU, and is defined as 10^{-36} interactions per target atom per second[6].

At present, there are other solar neutrino experiments that have collected sufficient data to reliably show a discrepancy between their capture rates and those predicted by the SSM. Their results are summarized in Figure 1.2[3]. Some new solar neutrino experiments are in the development stage or have just come online. Table 1.2 lists the current experiments, the neutrinos of interest, their techniques and the date they began operation[7].

Modifying the nuclear reaction cross-sections and opacity parameters in the SSM lowers $\Phi(^8\mathrm{B})$, however separate experiments have shown that large errors in these input parameters are unlikely. Some nonstandard models try to solve the SNP by postulating lower core temperatures that do not affect the surface chemical composition or luminosity, but are only plausible on short time scales.

Exotic nuclei, quark catalysis, weakly interacting massive particles and finite neutrino magnetic moments are all being studied as alternative ways to lower the ^{8}B

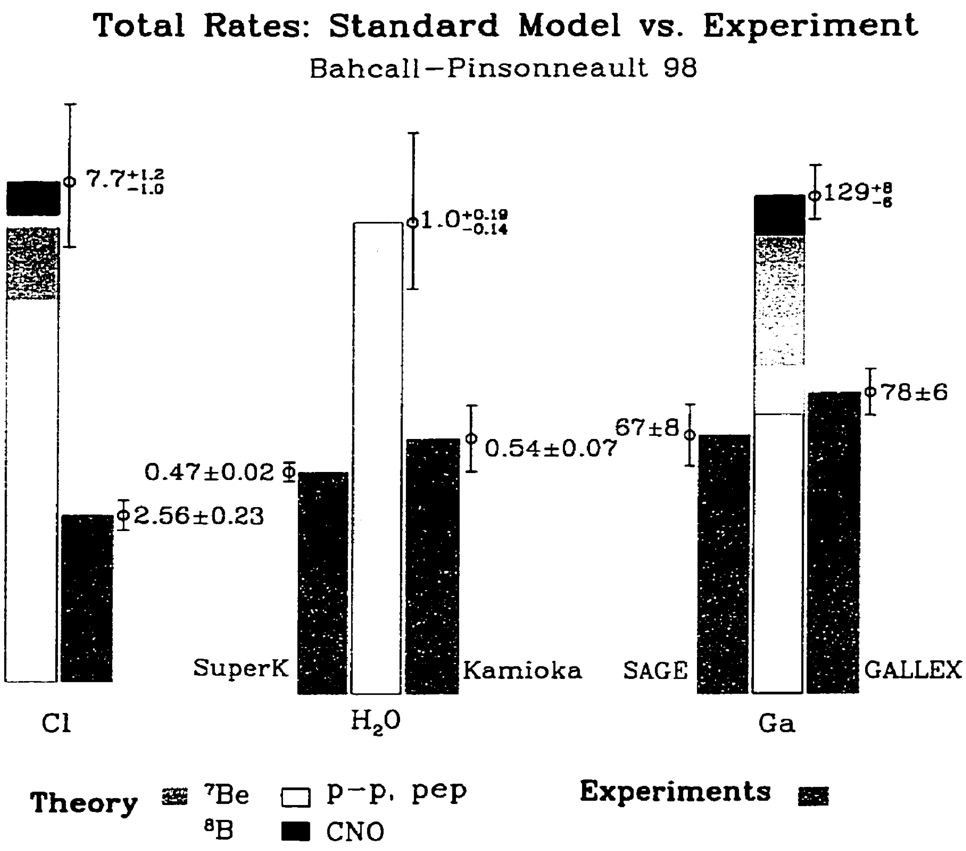

Figure 1.2: The capture rates predicted by the SSM (BP98), for various detector types, compared to actual rates measured by operating detectors. The plot is an updated one found in[3] taken from www.sns.ias.edu/ jnb. The theoretical uncertainties are $\pm 1\sigma$, while the experimental uncertainties are those measured by the respective detector.

Collaboration	$\nu's$	Technique	Date
Super-Kamiokande	^{8}B, *hep*	ν-e scattering	April 1996
SNO	^{8}B, *hep*	ν_e scatt., CC, NC	April 1999
GNO	*pp*, *hep*, ^{7}Be + ...	radiochemical	April 1998
Iodine	^{7}Be, *hep*, ^{8}B + ...	radiochemical	2001
ICARUS	^{8}B, *hep*	ν_e abs., TPC	2001
BOREXINO	^{7}Be, *hep*	ν-e scattering	2001
KamLAND	^{7}Be, *hep*	ν-e scattering	2001
HELLAZ	*pp*, ^{7}Be, *hep*	ν-e scattering	Development (TPC)
HERON	*pp*, ^{7}Be, *hep*	ν-e scattering (superfluid, rotons)	Development (TPC)

Table 1.2: New solar neutrino experiments.

production rate.

Another possible theory, of particular interest to SNO, is that the left-handed ν_e undergoes a conversion to another type of neutrino as it travels from the Sun's core to Earth; one possible "neutrino oscillation" predicted by the theory is outlined below[4].

1.1.3 Neutrino Oscillations

A possible solution to the SNP was proposed twenty years ago by Bruno Pontecorvo[8]. He theorized that if the neutrinos emitted in weak decay were not mass eigenstates, but linear combinations of neutrino mass eigenstates, then neutrino oscillations may be possible and may explain the deficits of the SNP.

More recently, Mikheyev and Smirnov[9], working within the theoretical framework of Wolfenstein[10], have shown that neutrino oscillations may be greatly enhanced within the solar interior; an effect which has come to be known as the MSW effect. The mixing involved is the same as that of the quark sector; for instance s and d quarks are mixed. In addition, the neutrino masses consistent with the SNP explanations arise naturally in some grand unification theories[4].

If we consider the oscillation theory of two neutrino mass eigenstates ν_1 and ν_2, with masses m_1 and m_2, we can write, for example, the electron- and muon-flavour eigenstates as

$$|\nu_e\rangle = |\nu_1\rangle\cos\theta + |\nu_2\rangle\sin\theta \tag{1.2}$$

$$|\nu_\mu\rangle = -|\nu_1\rangle\sin\theta + |\nu_2\rangle\cos\theta \tag{1.3}$$

where θ is the vacuum mixing angle.

When a ν_e is produced, the probability of it being a ν_e after travelling a distance L (meters) is given by

$$P(\nu_e \to \nu_e) = 1 - \sin^2(2\theta)\sin^2\left(\frac{1.27\Delta m^2 L}{E}\right) \tag{1.4}$$

where Δm^2 equals m_2^2 - m_1^2 measured in eV^2 and E is the energy in MeV.

Two types of experiments have been carried out on Earth to try to verify oscillations. The first type measures the flux of antineutrinos ($\bar{\nu}_e$) at various distances from nuclear reactors, in hopes of seeing a reduction of the type in equation (1.4). The results have ruled out values of $\Delta m^2 > 10^{-2}$ eV^2 for large mixing angles. Experiments at particle accelerators are looking for the conversion of high energy ν_μ's and ν_e's but have found no evidence of oscillations[2]. Figure 1.3[11] shows the regions in the MSW plane allowed by current solar neutrino experiments on Earth, using the Bahcall-Pinsonneault (BP) SSM at a C.L. of 95%.

Solar neutrino experiments have the ability to make some of the most sensitive tests for neutrino oscillations. Observations at the distances required cannot be made by terrestrial experiments but the large distance from the Sun to the Earth could yield oscillation evidence for values of Δm^2 as low as 10^{-10} eV^2. In addition, neutrinos passing through matter may have their oscillations greatly enhanced by ν_e's interacting with electrons through the charged-current reaction (CC), while other neutrino types are unaffected. The Sun is a large mass that may have a distinct effect on neutrino oscillations, as is the Earth. A day-night effect due to neutrinos traversing varying thicknesses of the Earth's matter has been looked for but results thus far show only a small (4%) effect.[12].

Most recently, the Super-Kamiokande experiment has shown evidence for a neutrino mass taken from higher energy atmospheric-neutrino data[13]. This result gives new support for the theory of neutrino oscillations, but more detailed exploration of oscillation parameters is required.

SNO is unique in that it can detect all flavours of solar neutrinos. This not only allows for a unique study of neutrino oscillations, but also the further determination of neutrino mass parameters.

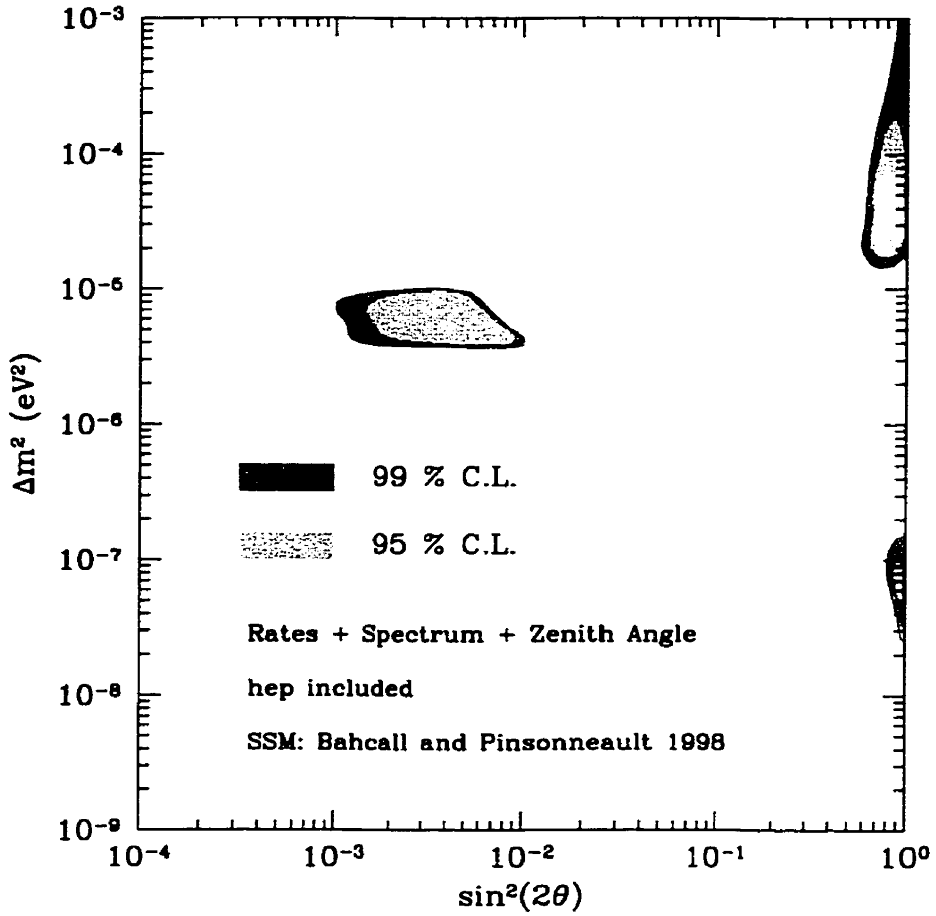

Figure 1.3: Regions in the MSW plane that are consistent with the total rates observed in four solar neutrino experiments (chlorine, SuperKamiokande, GALLEX and SAGE) and with the electron recoil energy spectrum and zenith angle distribution measured by SuperKamiokande.[11].

1.2 The Sudbury Neutrino Observatory

At the 6800 foot level of INCO's Creighton Mine near Sudbury, a second generation water Cerenkov detector known as the Sudbury Neutrino Observatory is now in operation. SNO's 1000 tonne heavy water core is a detection medium, unique to solar neutrino detectors, which allows for the observation of all three flavours of neutrinos. This ability will allow SNO to make stringent tests of the MSW effect for low energy electron neutrinos from the Sun, and hence shed new light on the SNP. Table 1.3 lists some of the characteristics of the detector.

Location	INCO's Creighton Mine, Sudbury, Ontario
Depth	6800 ft. (2070 m)
Containment	Spherical acrylic vessel
Detecting Medium	D_2O
Total Mass of Medium	1 kiloton
Threshold	$\sim$ 5 MeV
D atoms	6.02×10^{31}
Solar Neutrino sensitivity	^{8}B, *hep*

Table 1.3: Characteristics of the SNO detector

1.2.1 Solar Neutrino Detection

The first objective of SNO is to accurately measure the flux and energy spectrum ^{8}B neutrinos produced by the Sun[4]. The mechanism by which the energy spectrum of these neutrinos are measured is the charged-current (CC) reaction.

$$\nu_e + d \rightarrow p + p + e^- \tag{1.5}$$

In reaction (1.5), monoenergetic ν_e produce almost monoenergetic electrons given by $E_{e^-} = E_{\nu_e} - 1.44$ MeV. The large cross-section of the CC reaction and high sensitivity of the detector will allow SNO to determine a ^{8}B energy spectrum to high statistical accuracy.

The second reaction of interest to SNO is the electron scattering (ES) reaction.

$$\nu_x + e^- \rightarrow \nu_x + e^- \tag{1.6}$$

where ν_x is a neutrino of any flavour. As mentioned before, electron-type neutrinos react in a unique way with electrons, causing their scattering cross-section to be much larger than that for ν_μ or ν_τ. Thus, reaction (1.6) is mainly sensitive to the ν_e flux, however, with a separate measurement of the ν_e flux from reaction (1.5), the total neutrino flux can be determined. The ES reaction also gives valuable directional information that has been used to establish the Sun as the source of detected neutrinos[14].

The total neutrino flux, independent of neutrino flavour, can be measured using the neutral current (NC) reaction.

$$\nu_x + d \rightarrow \nu_x + p + n \tag{1.7}$$

A measurement of the NC reaction holds particular importance to solving the SNP, as it is a direct determination of the solar ^{8}B spectrum, independent of oscillations[15]. The reaction is identified by the γ-rays produced subsequent to neutron capture a short time after the NC reaction. In order to obtain the best γ-ray signal with high capture efficiency, SNO will utilize a salt additive to the D_2O in which a chlorine neutron capture reaction will be detected.

Minimizing radioactivity which can affect the measurement of γ-rays produced by reaction (1.7), or which can produce a neutron background, is the motivation for the development of a leach test facility (LTF) for SNO materials.

SNO is unique in its materials purity and cleanliness levels, allowing for a very low energy threshold and background rate. This, in turn, allows for a high statistical accuracy in the measurement of the neutrino spectrum from ^{8}B decay. The shape of a neutrino energy spectrum, from any individual neutrino source, is determined by nuclear physics alone, independent of any solar influence, to an accuracy of 1 part in 10^5[16]. This allows for an excellent comparison between an experimental spectrum and that predicted by theory. Figure 1.4 shows the best estimated (standard) ^{8}B spectrum λ, with the limit spectra $\lambda^{\pm}$ allowed by the maximum ($\pm\ 3\sigma$) theoretical and experimental uncertainties[17].

1.2.2 Construction and Design

The center of SNO's acrylic detector vessel is 1730 m below mean sea level in a cavity 25 m in diameter[18]. The surface is 309 m above sea level; the 2039 m of granite rock overburden corresponds to approximately 6000 m water equivalent. At this depth, the rate of muons passing through the detector is < 100 per day.

SNO's 1000 tonnes of heavy water (D_2O) are contained in a high purity acrylic sphere, 12 m in diameter and 5.5 cm thick (nominal), suspended by ten sets of vectran ropes. The D_2O, on loan from AECL and produced at the Ontario Hydro Bruce heavy water plant, has an isotopic purity of 99.997%.

Surrounding the acrylic vessel (AV) is a region with 1700 tonnes of ultrapure light water (UPW), then a giant, stainless steel geodesic sphere (the photomultiplier tube support structure (PSUP)), which includes panels housing 9546 photomultiplier tubes (PMTs), their light concentrators and associated hardware. Of the 9546 tubes, 94 are outward looking (OWL) tubes to view the volume between the PSUP and cavity.

The PMTs, (Hamamatsu Model R1408, 8 inch diameter), were designed not only to be waterproof and pressure resistant, but to be of high material purity as well so as not to compromise the required low radioactivity levels. In addition, the PMTs and associated electronics must have a low threshold down to one quarter photon-electron sensitivity. The effective photocathode coverage of the PMT sphere with the light

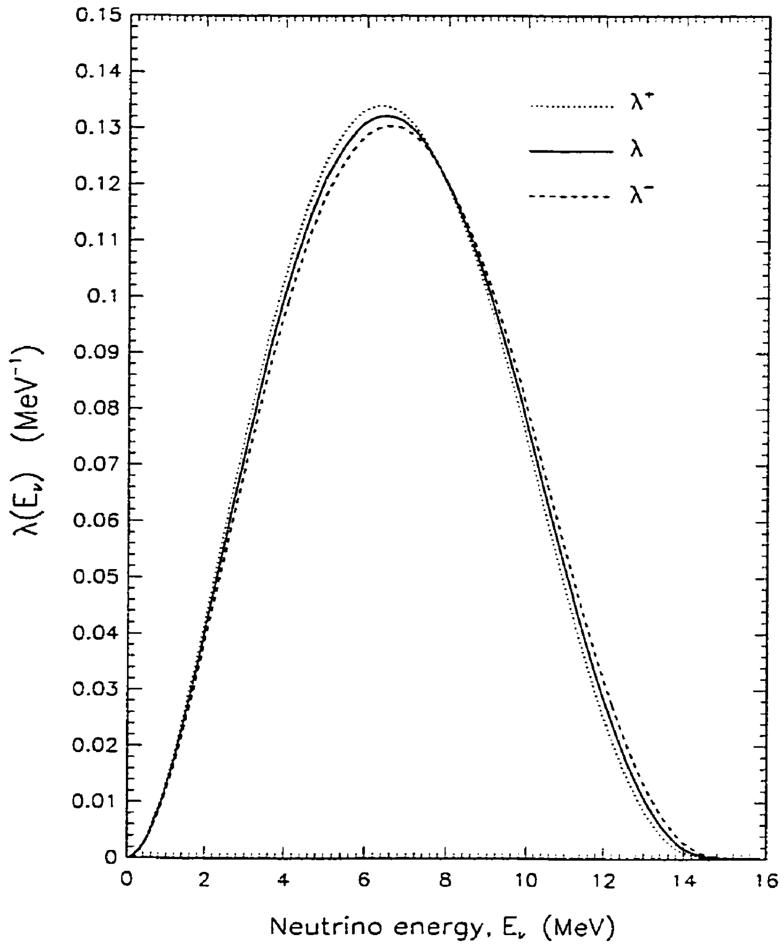

Figure 1.4: Standard neutrino spectrum from ^{8}B decay with the limit spectra allowed by theoretical and experimental uncertainties.

concentrators is 64%.

The region between the PSUP and the cavity walls contains an additional 5300 tonnes of UPW. All UPW entering the detector does so between the AV and the PSUP, causing this region to have higher water purity than the outer region which contains the PSUP cables, connectors, PMT bases, supports and the cavity liner. A 99.99% leak-tight plastic barrier seals this inner region from the dirtier outer region.

The cavity walls are coated with a 1 cm thick layer of polyurethane (Urylon) to prevent radon gas from the rock from entering into the cavity water and to water-proof the cavity. Figure 1.5 shows a cross-section of the detector.

All materials going into the detector construction had to be of the utmost cleanliness in order to achieve a low enough radioactivity level to reach the uniquely low energy threshold available for the detector.

1.2.3 Radioactive Background

The radioactive background level of the SNO detector must be extremely low, to interfere as little as possible with an expected solar neutrino signal rate of approximately twenty events per day. Two contributing factors to the background level are cosmic rays and radiation produced by naturally occurring radionuclides[4].

As mentioned before, the only surviving cosmic ray components are muons and neutrinos, due to the depth of the observatory. Only 1.5 muons per day are expected to produce detectable spallation events above the detector energy threshold[4]. These events can be identified by their time signature of a high-energy muon signal followed by decay electrons, gammas and neutrons.

The more pervasive of the two background sources is the radiation component. Naturally occurring radionuclides such as ^{40}K, ^{232}Th, ^{235}U and ^{238}U not only directly contribute radiation but can indirectly contribute added nuclides produced by α-particles and neutrons.

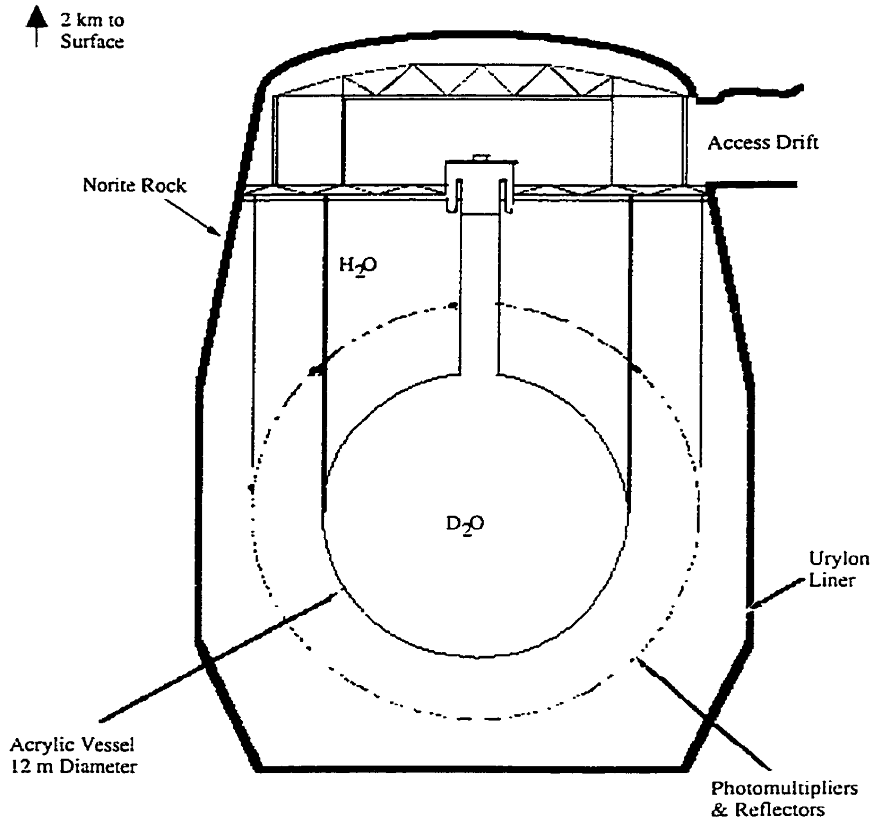

Figure 1.5: A cross-section of the SNO detector.

The D_2O volume can contain materials that may increase the radioactivity levels. Some of this radioactivity can produce free neutrons which are a background source to the neutrons produced in the NC reaction (1.7). The most important source of these free neutrons is the photodisintegration of the deuteron by γ-rays with an energy level above 2.223 MeV. The main source of these γ-rays are two products in the decay chains of ^{232}Th and ^{238}U.

In the ^{232}Th decay chain, Figure 1.6[19], ^{208}Tl decays to ^{208}Pb with the release of a 2.615 MeV γ-ray in 36% of the ^{232}Th disintegrations, assuming secular equilibrium. The 2.615 MeV γ-ray has a cross-section for photodisintegration of the deuteron of

1.2 mb and a cross-section for collision with an electron of 125 mb. Considering that every D_2O molecule has two deuterons and ten electrons, and that approximately 11.5% of the Compton-scattered photons have enough residual energy to cause photodisintegration, one neutron is produced per 470 2.615 MeV γ-rays.

In secular equilibrium, ^{232}Th gives 126 γ-rays $\mu g^{-1} d^{-1}$ of energy 2.615 MeV, which means 3.7μg of ^{232}Th would produce one neutron per day in the D_2O, compared to 18 neutrons per day estimated by the SSM. In 1000 tonnes of D_2O this amounts to a ^{232}Th concentration of 3.7×10^{-15} $g^{232}Th/gD_2O$.

Similarly, in the ^{238}U decay chain, Figure 1.7[19], ^{214}Bi decays to ^{214}Po with the release of a 2.445 MeV γ-ray at a rate of 16.8 γ-rays $\mu g^{-1} d^{-1}$ of ^{238}U, in secular equilibrium. The γ-ray has a cross-section for photodisintegration of 0.8 mb and a Compton cross-section of 130 mb, of which 7.2% have enough residual energy to cause photodisintegration.

This leads to 750 2.445 MeV γ-rays producing one neutron in the D_2O and corresponds to 45 μg of ^{238}U. Again, in 1000 tonnes of D_2O a rate of one background neutron per day is produced by a concentration of 4.5×10^{-14} $g^{238}U/gD_2O$.

The total radiation background level in the D_2O is comprised of radioactivity in the D_2O itself and from all materials placed in it. A facility designed to leach test these materials for radioisotope release must have an extremely low background and good sensitivity.

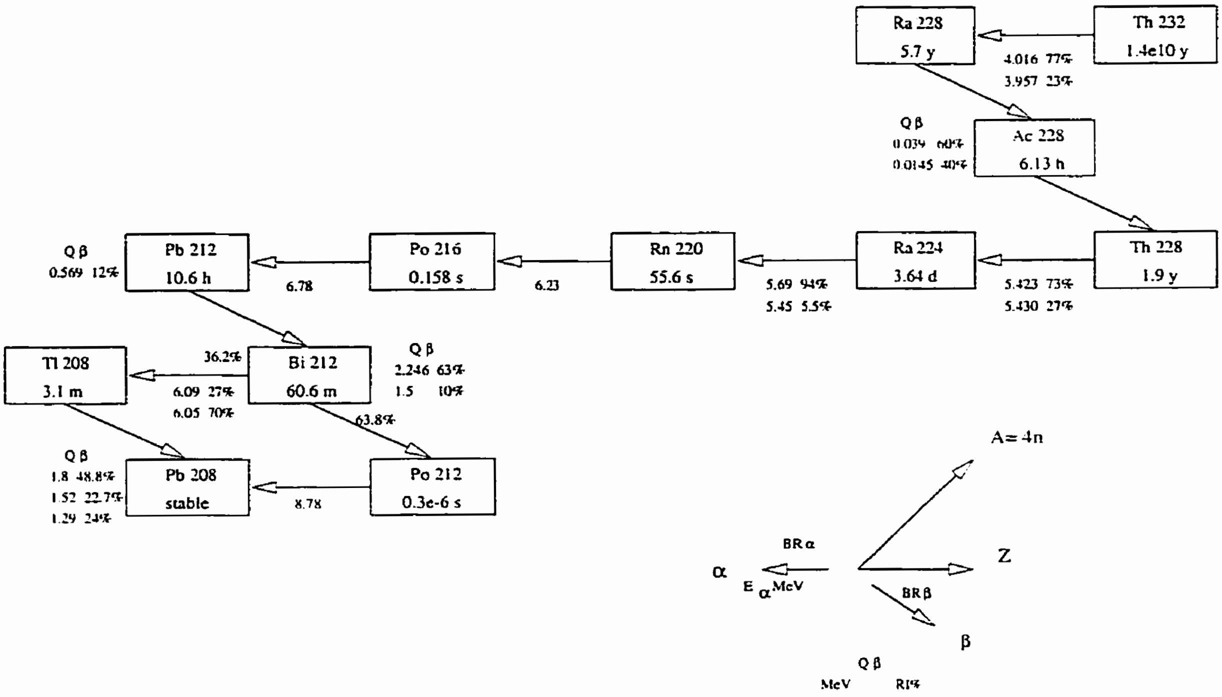

Figure 1.6: The ^{232}Th decay chain[19].

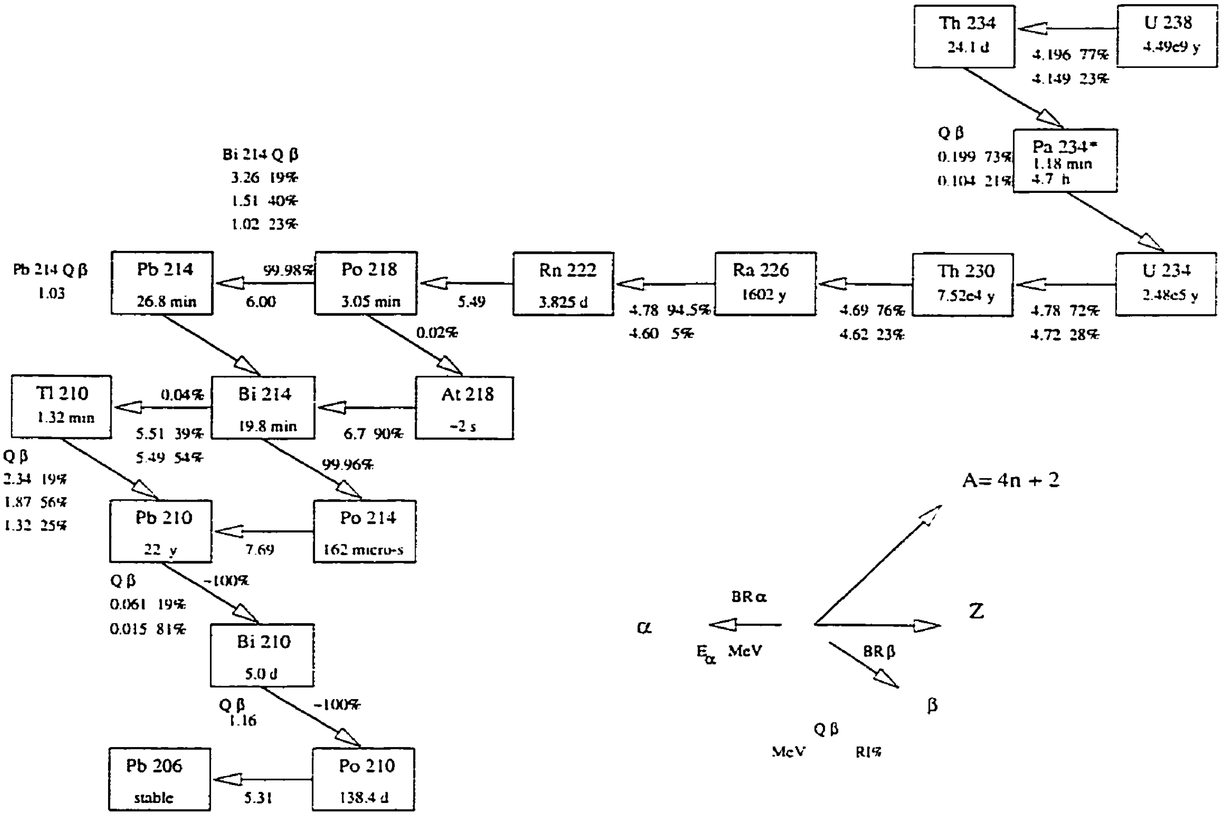

Figure 1.7: The ^{238}U decay chain[19].

Chapter 2

The Leach Test Facility

2.1 Introduction

All substances entering the AV or involved in its construction, must have extremely low intrinsic radionuclide levels in order to be able to lower and sustain SNO's D_2O internal radiation levels to 3.7×10^{-15} $g^{232}Th/gD_2O$ and 4.5×10^{-14} $g^{238}U/gD_2O$. Various methods of radiation detection and control have been specially designed and used to measure the radioactivity levels within SNO to make the detector as clean as possible in all respects.

Contributions to the internal D_2O radiation level may arise from radon (Rn) and radium (Ra) which make their way into the detector by diffusion and leaching out of materials that are submerged. Although strict measures are taken to use pure materials and assure cleanliness in manufacturing, assembling and transporting, a facility to measure Rn and Ra levels leached from a material immediately prior to its addition to the cavity would be beneficial. If this measurement is done with the object submerged in a typical ultrapure sample of cavity water, a true estimate of its contribution to the detectors background can be made.

One large potential contributor to the internal background is the neutral current detector (NCD) assembly that will be used to detect the free neutrons from the NC reaction (1.7). The NCDs are ^{3}He-filled proportional counters that use the reaction

$$^3\text{He} + n \rightarrow p +^3 \text{H} + 764\, keV \tag{2.1}$$

to detect these neutrons, taking advantage of a huge neutron cross-section, 5330 b for ^{3}He , through a well developed technique[18]. Although the counters are made of ultrapure nickel, the large surface area of the array to be placed in the D_2O volume require testing for the emanation of Rn and leaching of Ra.

A proposal was made in July 1998, by Cowan, Hallman, Lee and Seifert, to design, construct and fabricate a system to leach test a number of NCDs, using the well developed Ra assay techniques SNO uses in the testing of its water systems.

A total of 96 strings of NCDs are to be placed in the AV, having a total length of 770 m and a total surface area of 125 m^2[18]. The radioactivity specifications for the NCDs is not to exceed 10% of the total allowable inner radioactivity in both ^{238}U and ^{232}Th.

The proposed system was to measure single, 3 m long detectors. If the maximum allowable level of ^{232}Th is taken to be 3.7×10^{-15} g^{232}Th/gD$_2$O, and secular equilibrium in the decay chain is assumed, this corresponds to a ^{224}Ra activity of 1302 decays per day (dpd) for 1000 tonnes of D_2O. Similarly, a ^{226}Ra activity of 4.82×10^4 dpd results from a maximum level of 4.5×10^{-14} g^{238}U/gD$_2$O. Considering that leaching from the NCDs is to be restricted to 10% of the total radiation level and it was proposed to test 9.74% of the total counters (25 units), this gives maximum acceptable activity levels of 12.7 dpd and 470 dpd in the water of the LTF for ^{224}Ra and ^{226}Ra respectively.

The extraction, emanation, transport and detection efficiencies of the system will reduce these activity levels even further, requiring the allowable intrinsic background levels of the system to be extremely low in order to have a discernable leaching signal with good statistics.

Although it was believed that the system could measure the Ra leaching levels of the NCDs with sufficient sensitivity, there were a number of other factors that had to be considered. To achieve these low background levels, it was proposed to use a large, acrylic chamber for holding the counters. This would significantly raise the cost of the system. In addition, it was not feasible to submerge the counters in D_2O, so UPW would have to be used. This could raise the background level of the system and would require the plumbing of a dedicated UPW line. Lastly, an alternative system was proposed at Los Alamos National Laboratories (LANL) which used an analytical radiochemistry approach to measure the Ra levels[20]. Preliminary results for this system were promising and it has now been put into operation.

In September 1998 a new proposal was made to design, construct and fabricate a prototype leaching facility. The motivation behind the second proposal was the belief that such a system could be used to leach test other materials while providing useful design information for the performance of a larger, more sensitive system. The prototype system could be constructed using available materials and equipment, resulting in a low total cost.

The design of the leach test facility (LTF) began in October, 1998. This system would not only have the ability to measure Ra leached from materials, as in the first proposal, but a separate system to measure emanated ^{222}Rn was added to the design. This would allow for a comparison of the ^{222}Rn emanation rate and ^{226}Ra leach rate for a given material.

2.2 LTF Design and Fabrication

A 70.5" long section of a 3.0" I.D.ultrapure acrylic pipe was available and was chosen as a suitable chamber for the prototype system. With the detection methods being established on site, the system could be designed and fabricated quickly.

2.2.1 The LTF Chamber

In order for the LTF to be effective, the chamber had to be designed to have an excellent seal against lab air Rn.

Two top flanges and a bottom flange were designed and machined to complete the chamber. These flanges were made of acrylic, of a sufficient thickness to not allow the ingress of Rn from lab air, and to keep the chamber material as free of intrinsic background radioactivity as possible.

The specific criteria for the design of the bottom flange were to have a good sealing surface with the acrylic tube (using a PS-30 acrylic cement bond), and to provide a large enough support for the pipe when standing vertical. The choice of a vertical chamber over a horizontal one was dictated by available space underground and the requirement for bubbles of nitrogen gas to flow throughout the entire chamber, during the Rn collection process.

A narrow groove was machined in the bottom flange for the pipe to fit in for bonding while not allowing any PS-30 to enter the inside of the chamber, as it would be impossible to sand away. The flange was designed to be 4.75" O.D. to allow for stability, although a stand was also fabricated to secure the chamber.

The fabrication of the two top flanges involved more crucial design criteria. The first of the flanges neede to be bonded onto the pipe, leaving the 3.0" I.D. of the chamber open, while having six 1/4" bolt holes, 60^o apart from one another, to secure the second flange to it. In addition, a groove for an 1/8" thick o-ring needed to be machined to seal the two flanges together. Figure 2.1 shows how the dimensions of the groove were calculated. This configuration allowed for the flanges to be separated to open the system to add water (since there was no dedicated line from the SNO UPW water systems), and to add samples of materials. The o-ring groove was machined in the bottom of the two flanges so that the o-ring would remain in place when the cover was removed or set in place.

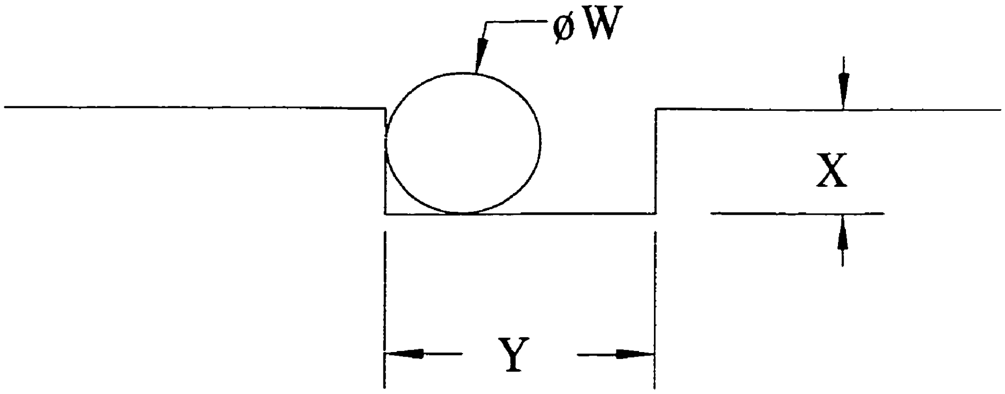

W = 0.125"

X = 0.7W = 0.0875"

Y = 1.28W = 0.160"

Figure 2.1: The design criteria for the o-ring groove.

The second of the top flanges, or the cover flange, needed to be the same O.D. as the first, with matching holes for 1/4" bolts. These holes would allow for four stainless steel (SS) Swagelok™ fittings[1], with o-rings, that were machined through to allow for SS tubing to enter the system. The holes were designed such that any tubing inside the chamber would run tight along the side to avoid any material. These feedthroughs would be used for various components of the Rn and Ra extraction systems. The flanges were machined on site to the above specifications. They were then placed in an oven to be annealed before bonding[21]. Figure 2.2 shows a plot of

---

[1] All fittings and valves used in the construction of the LTF were Swagelok™ to ensure the entire system had a good seal to lab air.

the annealing process temperature profile.

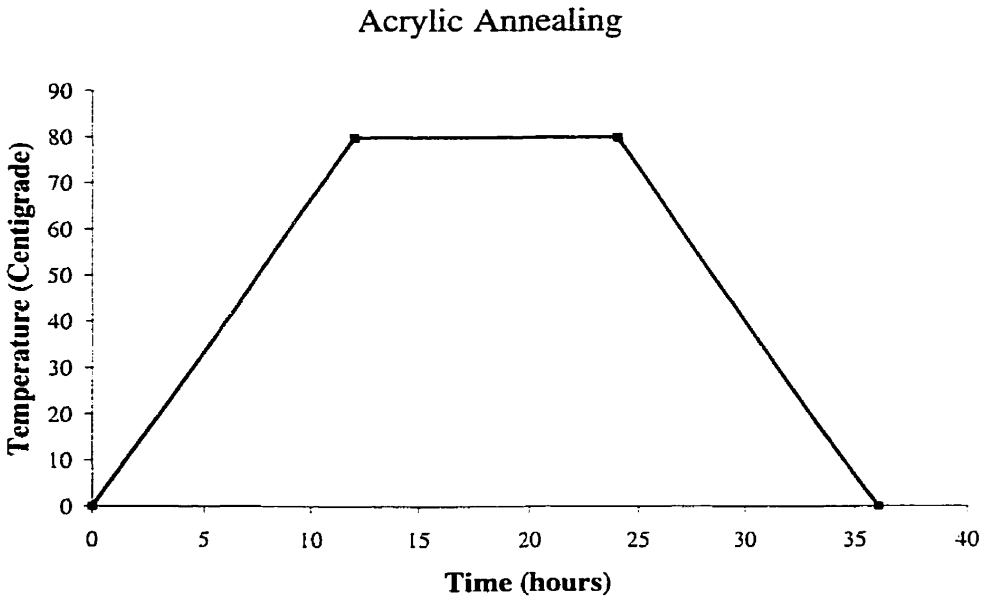

Figure 2.2: A plot of temperature vs. time for the acrylic flange annealing process.

After the annealing of the flanges was completed, all the acrylic parts were cleaned with UPW and Alcanox detergent and sanded on surface under a high efficiency particulate (HEPA) filter to reduce particles in the air. All the acrylic was bagged, sealed and shipped underground where it was cleaned again. On January 25, 1999, the bottom flange and first top flange were bonded to the pipe, using PS-30.

A stand for the system was then designed and constructed. The stand's main purpose was to secure the chamber without damaging the acrylic. A sturdy platform to stand on was also needed in order to remove the LTF cover to add water or samples. A moveable stand was also designed for the MnO_x column used for Ra extractions and to mount any flowmeters and lines.

The second action at this time was to place the SS fittings in the cover flange to test their seal. It was found that the holes had been tapped slightly off the vertical and the fittings would not compress their o-rings properly. Two more cover flanges had to be machined and annealed before the difficult seals were made.

All the fittings and tubing required in sealing the system were then installed. This included SS tubing and SS valves for all three lines entering the system and the line leaving the system. This fourth line included an assembly of a pressure gauge, to measure the pressure in the chamber, and a pressure relief valve, to ensure the chamber pressure did not rise above 15 psi, otherwise the chamber would have to be certified as a pressure vessel[22].

The cover flange was then bolted to the top flange and it could be seen that the 0.125" diameter o-ring compressed nicely. All four valves were closed to seal the partially complete system as it is shown in Figure 2.3. Since all tubing and valves are included in the chamber volume of 8.5 l, the lengths of tubing leading back to the valves were kept as short as possible to minimize the background Rn load.

In this state it was possible to leak test the system, as no additional components would be added to the sealing volume of the chamber. The system was pumped down through the outlet line using a Balzers HLT 150 Helium Leak Detector. An initial leak rate was obtained, of 5.2×10^{-8} cc/s [or (mbar$\cdot$ l/s)], noting that a level of 10^{-6} indicates there are no gross leaks. The tracer ^{4}He gas was sprayed around the surface of the chamber, paying special attention to bonding and sealing areas. In twenty minutes no leaks were found and a level of 2.7×10^{-8} cc/s was reached. The valve to the LTF was then closed and the detector was vented. The next step was to construct the LTF sections required for the Rn and Ra extraction systems.

2.2.2 The LTF Radon Extraction System

In the Rn extraction system, nitrogen (N_2) gas is bubbled through the chamber to strip Rn from the water and any air volumes sealed there. The gas mixture then

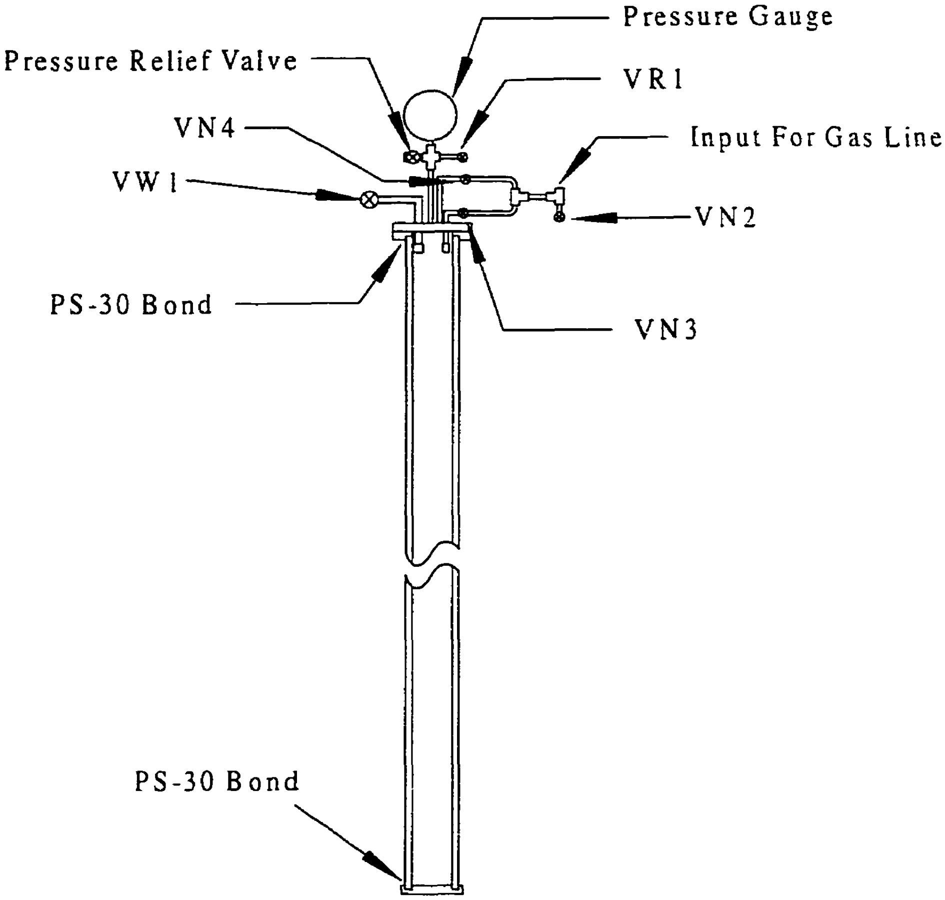

Figure 2.3: A schematic of the LTF chamber assembly.

flows from the LTF chamber to a gas board where it passes a cold trap, that extracts water vapour, and then to a preliminary Rn cold trap. Other volatile gases are then boiled away while the Rn stays trapped. Then the Rn is transferred to a smaller Rn cold trap. Finally, this trap is then gradually warmed and the Rn is transferred to a high purity acrylic, ZnS-lined Lucas cell[23]. This cell is brought to surface, then placed in a PMT detector to count the scintillations from Rn decays.

The LTF portion of the Rn extraction system was designed to keep the chamber volume sealed from outside air and it had to be constructed from pure materials under clean conditions[2]. In addition, the volume of tubing up to the valves that sealed the system had to be kept to a minimum, since this volume would be included in the extraction. The N_2 gas used must have a very low intrinsic Rn content and the bubbles must cover the entire volume of the UPW in the LTF chamber.

Keeping these requirements in mind, the LTF Rn system starts with a liquid nitrogen (LN_2) dewar, using the 22 psi boil-off gas outlet. This gas is known to have a lower Rn content than compressed N_2 gas. A 0.2 micron filter was plumbed into the LTF gas line as a further precaution. A SS line runs from the LN_2 Dewar to a brass plug valve (VN1), as shown in Figure 2.3 preceding a variable flowmeter. From the flowmeter outlet a coil of 1/4" O.D. copper (Cu) tubing runs through a filter, up to a SS tee-fitting. Here the line splits to a SS valve (VN2) and a section of 1/4" SS tubing leading to the chamber. A QuickConnect (QC) fitting is attached to the outlet of VN2 to connect the gas board.

Before gas flow to the chamber is started, the lines can be vented through the QC at VN2[3], even though the lines are filled with clean N_2 gas at all times. This removes any Rn that has diffused into the lines or has emanated out of the tubing. For this reason a coil of Cu tubing is used in this section, giving flexibility when removing the cover flange as well as reducing cost. All other tubing and fittings included in the chamber volume are SS or Teflon as they have lower intrinsic levels of Rn.

The section of SS tubing runs to another SS tee-fitting which separates into two SS lines. These lines run through SS valves (VN3 and VN4) then through the cover

---

[2] All materials, except acrylic, are wiped with methanol then ultrasonically cleaned prior to being used in the construction of the LTF. Cleaned pieces are bagged in clear plastic and latex gloves are worn during assembly.

[3] A QC feedthrough fitting had to be connected to allow gas to flow out

flange fittings, into the chamber. The sections of tubing from the first t-fitting to the two valves is kept short as it is a deadleg in the system. A line can be connected to the QC fitting at the outlet of VN2, to use the gas board pump to pump out this deadleg prior to a Rn extraction. This eliminates any Rn that has built up in the lines, leading to the chamber, from increasing the system background or skewing the extraction results.

The first of the lines entering the chamber is used in the Ra system and will be discussed in the next section. The second of these lines passes through the cover fitting and extends a small distance into the chamber. Here a SS 1/4" union is used to switch from SS to high purity Teflon tubing. This minimizes any Ra from leaching out of, or plating onto, any submerged SS tubing in the chamber. In addition, the chamber is never filled to a level where the SS fittings or tubing are submerged. The Teflon line extends to the bottom of the chamber where it is plugged with a Teflon fitting. Holes of diameter 1/32" were drilled in the tubing in a uniform pattern to create a wide dispersion for the N_2 gas flow throughout the chamber.

A short piece of SS tubing runs from the third fitting in the cover flange, and is connected to a SS union cross. The cross connects to a pressure relief valve, to ensure the chamber pressure does not exceed 15 psi, a pressure gauge and a SS line with another 1/4" valve (VR1). This line is the outlet line to the gas board and is fitted with a QC fitting. Since the tubing and fittings atop the chamber are included in its volume, all are SS and all tubing lengths are kept short. The tubing on the outlet side of the valve, leading to the QC fitting, is a deadleg and is pumped out prior to any Rn extraction in the same manner as the other system deadleg.

The mixture of N_2, Rn, water vapour and other volatile gases is transfered from the LTF to the gas board through the gas board extraction line, connected at the QC fitting on the outlet of VR1.

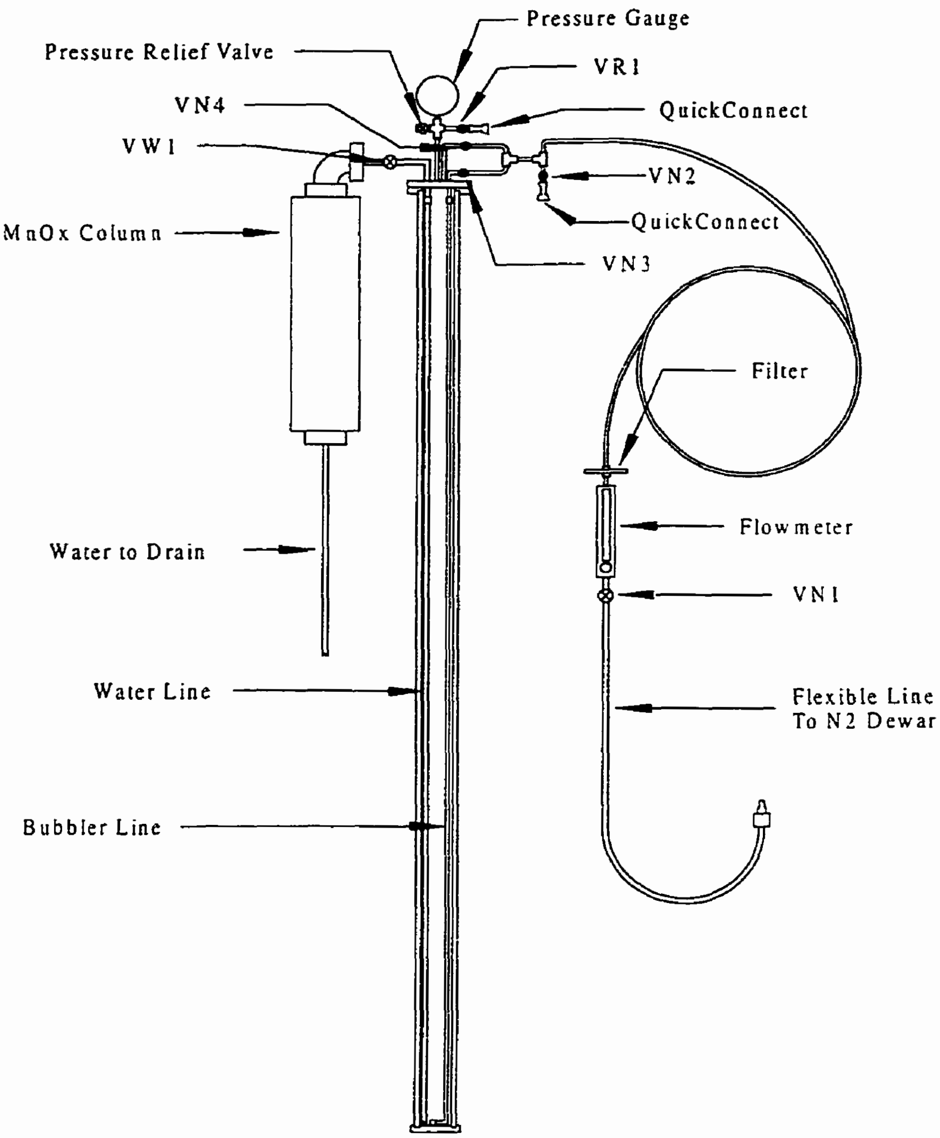

Figure 2.4: The full LTF system diagram.

2.2.3 The Radium Extraction System

SNO uses a polypropylene (PP) column filled with acrylic beads, uniformly coated with MnO_x, to extract Ra from both the UPW and D_2O systems. This column is then placed on a specially designed electrostatic counter (ESC) to count the Po daughters of both ^{226}Ra and ^{224}Ra[24]. This extraction method is also used by the LTF, however, the LTF method differs in that it does not recirculate the UPW and the MnO_x column is not flushed with UPW prior to a Ra extraction. Recirculating the UPW in the system would require a highly expensive diaphragm pump, while flushing a column requires a specific procedure to be run within the full SNO UPW system.

In designing the Ra extraction system all the aforementioned criteria apply to sealing the lines and the chamber, and to cleanliness and purity of the materials.

The LTF Ra extraction system makes use of the N_2 gas line, previously described as part of the Rn extraction system. The gas is used to pressurize the chamber, so as to force the UPW out. The flowmeter in the gas line is used to control the flow of water by adjusting the pressure in the chamnber.

Knowing that at a gauge pressure of 15 psi, water will rise to a maximum height of 10 m through a small diameter tube[25], we can calculate that a pressure of 3 psi is needed to raise water to a height of 2 m. This is well below the 15 psi pressure limit the chamber is restricted to.

The N_2 flows through the flowmeter, past VN2 to the SS tee-fitting, then to VN4, as shown in Figure 2.4. When VN4 is opened, the gas then flows through a piece of SS tubing runs from VN4, through a fitting in the cover flange and into the chamber.

The UPW flows through a 3/8" Teflon tube, which is connected, through a union fitting, to a 3/8" SS tube on the top of the chamber as shown in Figure 2.4. This SS tube runs out of the chamber through a fitting in the cover flange to a SS valve (VW1). A short piece of SS tubing then joins to a 1.0" PP elbow via a special SS fitting welded to the tubing.

At the bottom of the elbow there is a special PP nut that connects to the MnO_x column, when it is in place. The column is supported by an adjustable SS plate, that can be raised so that the column rests tightly against the tubing when connected.

The UPW slowly runs through the beads in the column where the Ra is extracted. Another SS fitting is connected by a PP nut at the bottom of the column, where a flexible PVC line is connected to carry the water to drain. The column is then disconnected and taken to the surface chemistry and physics laboratory for counting.

2.2.4 Obtaining UPW

A high purity container was needed in order to fill the LTF chamber with UPW. A length of 2.0" I.D. PP pipe (made from SV258 resin) with a 1/2" valve on one end was found and cleaned with radiac wash. This special, high purity resin is used in all PP components of the SNO water systems. The container was then rinsed thoroughly with UPW and sealed on both ends.

The PP container has an approximate volume of 2.0 l, requiring it to be filled four times to fill the LTF chamber. The volume of UPW in the LTF is calculated by measuring the height of the water and using the inside to diameter, measured to be 3.0" on average. Again, the UPW should not cover the SS union fittings inside the chamber to avoid leaching of the SS.

All UPW going into the LTF is taken from a sample line at valve V-566, just after the 254 nm light source (UVO2) and prior to the chiller loop. Figure 2.5[18] shows the various elements that comprise SNO's UPW system. The first fill of the LTF occured during the SNO cavity fill, while water system procedure WAT-PR-127 was being followed. This water came from the INCO feed and did not pass through the process degasser (PDG). All other water for the LTF was obtained while procedure WAT-PR-163 was being used, where cavity water is recirculated through a loop to purify it. This procedure does include the PDG, although it is not essential to LTF performance that the UPW be degassed.

Table 2.1 lists the estimated background Rn activity levels for the chamber volume. The ^{222}Rn rates are from [26][27] and the N_2 gas ^{222}Rn content from[28]. The level of

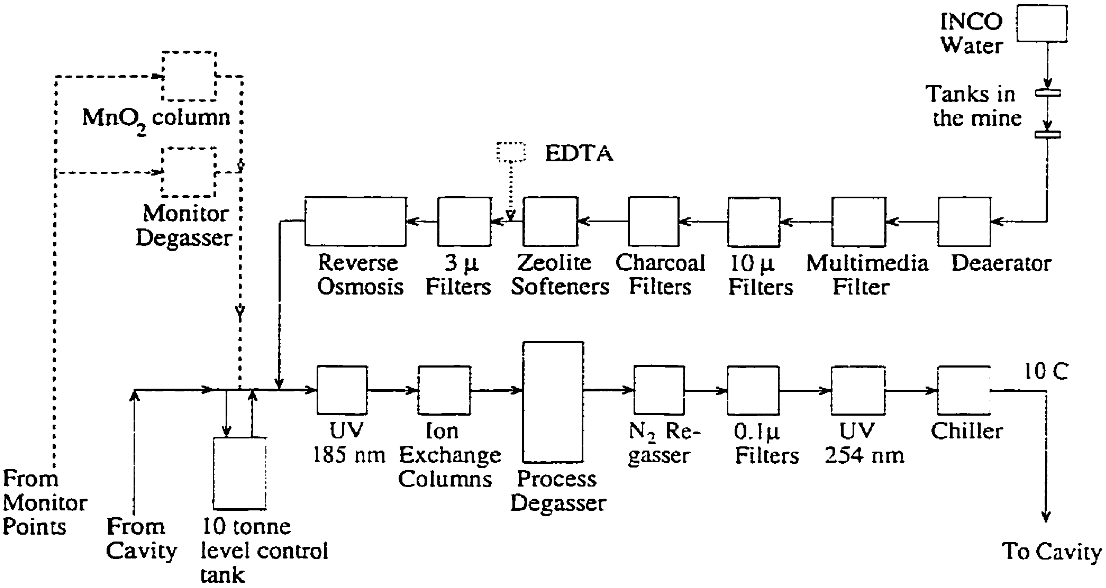

Figure 2.5: A schematic of the SNO H_2O water purification and re-circulation system[18].

^{238}U content in the UPW is the average of the last three 'cavity to cavity' Ra results listed in Table 2.2[29]. All the numbers were taken from the 'A' results of the 'A to B' series experiments. These numbers can then be compared to the extracted Rn background levels to examine and understand the LTF systematics.

Material	Area (m^2)	^{222}Rn Emanation Rate $Rn/hr \cdot m^2$	Activity (dpd)
Acrylic	0.43	0.1	1.03
Stainless Steel	0.29	0.3	2.09
Teflon	0.089	4.4	9.4
Butyl Rubber	8.9×10^{-04}	0.1	2.1×10^{-03}
Total			12.5
Substance	Quantity	Content	Activity (dpd)
UPW	7.5×10^{03} (g)	1.2×10^{-14} $g^{238}U/gH_2O$	0.096
N_2 Gas	75 (l)	0.05 $^{222}Rn/l$	0.68
Total			0.77
Material	Area (m^2)	^{222}Rn Diffusion Rate $Rn/hr \cdot m^2$	Activity (dpd)
Butyl O-ring	2.7×10^{-04}	6480	42.0
Acrylic	0.54	8.3×10^{-21}	N/A
Total			42.0
Total Rn Activity	(chamber and contents)		55.3

Table 2.1: Estimated background Rn activity levels for the chamber volume.

Extraction Date	Type	Water Volume (kl)	ESC	g Th/cm^3 H$_2$O	g U/cm^3 H$_2$O	Goodness of Fit Prob. (%)
99/02/11	Cavity to cavity A	17.9	5	$2.1 \times 10^{-14}(1^{+0.35}_{-0.31})$	$0.0\ (0.0\text{-}2.1 \times 10^{-15})$	5.
99/02/11	Cavity to cavity B	17.9	3	$2.0 \times 10^{-13}(1^{+0.11}_{-0.10})$	$0.0\ (0.0\text{-}2.5 \times 10^{-15})$	22.
99/05/10	Cavity to cavity A	55.5	4	$1.7 \times 10^{-13}(1^{+0.10}_{-0.09})$	$1.5 \times 10^{-14}(1^{+0.06}_{-0.06})$	37.
99/05/10	Cavity to cavity B	55.5	4	0.0 (0.0-0.0 0))	$4.4 \times 10^{-15}(1^{+0.65}_{-0.66})$	68.
99/06/07	Cavity to cavity A	56.5	4	$2.1 \times 10^{-13}(1^{+0.07}_{-0.08})$	$2.0 \times 10^{-14}(1^{+0.07}_{-0.08})$	23.
99/06/07	Cavity to cavity B	56.5	5	$8.6 \times 10^{-14}(1^{+0.15}_{-0.14})$	$7.0 \times 10^{-15}(1^{+0.20}_{-0.19})$	73.

Extraction Date	ESC	Type	Counting Time (d)	Overlap (%)	Decays ^{224}Ra/day	Decays ^{228}Th/day	Decays ^{226}Ra/day	Decays ^{222}Rn/day	Fit Prob. (%)
99/02/11	5	Blank	8.88	1.5	69(57-83)	69(57-83)	545(520-571)	172(151-193)	26.
	5	Sample	8.39	1.5	156(130-185)	0(0-14)	518(492-545)	119(99-139)	5.
99/02/11	3	Blank	7.13	1.9	100(83-119)	100(83-119)	578(543-614)	225(201-250)	24.
	3	Sample	8.51	1.9	1007(914-1105)	208(129-290)	448(423-472)	52(34-71)	22.
99/05/10	5	Blank	12.77	1.5	74(63-85)	74(63-85)	466(448-484)	338(315-363)	3.
	5	Sample	2.38	1.5	1625(1513-1742)	0(0-253)	1407(1264-1546)	39(18-65)	71.
99/05/10	4	Blank	8.01	1.1	29(21-39)	29(21-39)	373(351-395)	53(38-68)	75.
	4	Sample	2.51	1.1	13(0-50)	78(0-205)	605(454-754)	270(232-309)	68.
99/06/07	4	Blank	10.51	1.1	60(50-71)	60(50-71)	255(241-270)	73(59-87)	61.
	4	Sample	5.38	1.1	1692(1556-1799)	35(0-226)	1029(973-1084)	71(48-96)	23.
99/06/07	5	Blank	10.63	1.5	57(46-68)	57(46-68)	441(421-461)	171(151-192)	6.
	5	Sample	5.63	1.5	752(655-854)	329(191-473)	706(659-754)	143(119-168)	73.

Table 2.2: Results of analysis of MnO$_x$ extraction experiments of cavity H$_2$O.

Chapter 3

Radon Detection

This chapter describes in detail the radon assay methods and capabilities of the LTF. It includes the intrinsic background levels of the system and the radon emanation rate for a viton material.

3.1 Radon Extraction

The purpose of extracting ^{222}Rn from the LTF is to make inferences about the levels of its parent nucleus, ^{226}Ra, for comparison with Ra extraction results from the LTF for the same sample. This type of comparison is made in view of the fact that the ^{226}Ra leach rates for the sample is unknown and will allow us to examine the accuracy of Ra extraction methods and mechanisms. Precautions must be taken in the extraction process to eliminate other sources of ^{222}Rn aside from that supported by ^{226}Ra in the sample material.

In addition, the measured ^{222}Rn emanation rates from samples in the LTF can be compared to previously measured rates for the same sample in order to examine the radon extraction methods and establish the systematic uncertainties involved.

In the future, a refined radon emanation assay of this type could be utilized to test the potential radon load to the cavity water from various components intended to be added for long periods of time.

3.1.1 Extraction from the LTF

Once a sample has been added to the LTF and the chamber has been sealed, nitrogen gas is used to sweep away all the ambient radon in the chamber, as well as any radon that immediately outgases from the sample. This sweep is done by bubbling nitrogen into the system (in the same manner used for the extraction) and venting it to the lab air through a feedthrough fitting connected at VR1, as shown in Figure 2.4.

The exposure time begins at the end of the sweep used to 'zero' the Rn levels and lasts until the beginning of the extraction sweep. During the exposure time, Rn that is supported by Ra trapped in the material will emanate from the material into the water. At the same time, Rn that has been trapped in the interstitial spaces of the material will diffuse into the water. It is therefore necessary to define the two sources of Rn and to take measures to distinguish between them when extracting.

Radon Emanation Supported by Radium Decay

Materials with intrinsic uranium and thorium levels are sources of emanated radon. The most important radon isotope for emanation studies is ^{222}Rn because it has the longest half-life and is an inert gas, allowing it to emanate easily from materials, once in the pore space[30]. ^{222}Rn that is supported by ^{226}Ra trapped in the grains or crystals of a material may emanate in two ways. The Rn[1] atoms can recoil directly from Ra decay near the materials surface or can diffuse from decaying Ra located deeper in the material. For both these cases we can assume a steady emanation rate that is independent of time[31]. The number of atoms emanated is given by the radioactivity growth curve

$$N = P_0(1 - e^{-\lambda t})/\lambda \tag{3.1}$$

where P_0 is the emanation rate of Rn, λ is the decay constant for Rn (ln2/3.82 d) and N is the number of Rn atoms at a time (t).

---

[1] For the remainder of this chapter Rn will refer to the ^{222}Rn isotope.

Radon Emanation by Radon Outgassing

Radon emanation may take place if Rn is trapped in the pores of a material[32]. Assuming this Rn diffuses, or outgases, from the material with a probability proportional to the number of Rn atoms trapped, we can write

$$dN_1/dt = -(\lambda' + \lambda)N_1 \tag{3.2}$$

$$dN_2/dt = \lambda' N_1 - \lambda N_2 \tag{3.3}$$

where λ is the decay constant of Rn, λ' is the probability of outgassing the trapped Rn (or the diffusion rate of Rn), N_1 is the number of Rn atoms trapped inside the pores of the material and N_2 is the number of Rn atoms outside the pores (or in the chamber).

These two differential equations can be solved to give

$$N_1 = N_0 e^{-(\lambda'+\lambda)t} \tag{3.4}$$

$$N_1 + N_2 = N_0 e^{-\lambda t} \tag{3.5}$$

$$N_2 = N_0 e^{\lambda t}(1 - e^{-\lambda' t}) \tag{3.6}$$

where N_0 is the total Rn trapped inside the pores at a time (t=0).

If λ' greater than λ (most materials), then after 3.8 days the emanated Rn atoms into the chamber follows the typical decay curve

$$N_2 = N_0 e^{-\lambda t} \tag{3.7}$$

with a 3.82 day half-life.

If λ' is less than λ, then the diffusion rate is quite slow, with a decrease of emanated Rn over several half-lives.

By bubbling N_2 gas through the LTF chamber to 'zero' the Rn levels we eliminate some of the outgassed Rn. An exposure time of two weeks will allow for virtually all of the remaining outgassed Rn to decay away. When the extraction is done, the remaining Rn is assumed to be supported Rn that has emanated from the sample. If this is not the case a plot of $N/(1-e^{-\lambda t})$ will show the excess counts from outgassing, but the need to distinguish between the two Rn sources is unlikely.

At the end of the exposure time, N_2 gas is once again bubbled through the LTF. By flowing a volume of gas ten times larger than the chamber volume (85 *l*), we can expect an extraction efficiency, for Rn from the chamber, of greater than 95%[33]. This efficiency is limited by the finite contact time of the bubbles with the water, where a typical bubble has a 1 cm diameter and the nitrogen flow rate is 1 liter/minute (*lpm*). It is also dependent on the intrinsic purity of the N_2 gas, another reason why boil-off N_2 is used. Although a source was not available to calibrate the LTF extraction efficiency, similar systems have shown high Rn extraction efficiencies using even lower N_2 to water ratios[34]. If data is collected for a sample of known emanation, it is possible to compare the LTF results, to the accepted results to evaluate the extraction efficiency.

The flow of combined gases is then carried to the cover gas Rn board where water vapour and volatile gases are separated from the extracted Rn.

3.1.2 Gas Board

When the SNO cover gas Rn board (CGRB) is used for an LTF extraction, gas flow through the traps is produced by the pressure of N_2 gas, instead of using a vacuum pump. This keeps the gas flow pure and prevents any water from the chamber from being drawn into the extraction line. Figure 3.1 shows the relevant sections of the CGRB used in an LTF Rn extraction.

Once a steady flow of approximately 1 *lpm* has been established and the pressure in the CGRB is sufficiently high, the gas extracted from the LTF is flowed through a water vapour trap (WT) and a large Rn trap (trap A). The water trap is cooled with a methanol (CH_3OH) slush bath to a temperature of approximately -50 °C. This

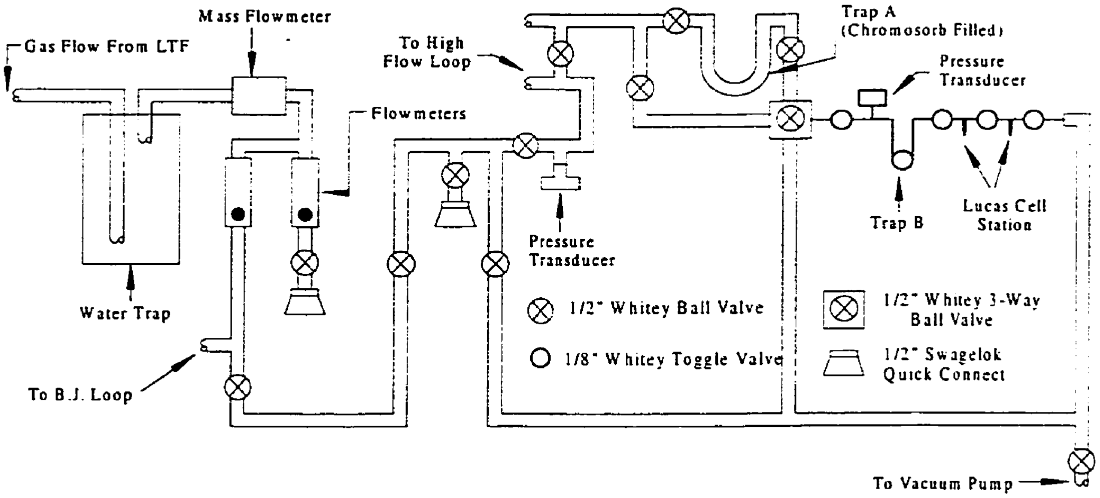

Figure 3.1: A schematic of the cover gas Rn board. The Bonderenko Jar (B.J.) loop (big jar connected to this loop) and High Flow loops are not used in these assays.

is achieved by adding liquid nitrogen (LN_2) to methanol until methanol ice starts to form, then breaking the ice into slush. When the flow of gases from the LTF passes the water trap, the water vapour is frozen, while the other gases continue flowing toward trap A. Table 3.1 shows the boiling points (at 1 atmosphere) of gases of interest in a Rn extraction[35].

Trap A is cooled to -195.8 °C by a liquid nitrogen bath and is filled with Chromosorb. Chromosorb is a large organic molecule that presents a large, cold surface for gas to be trapped on[28]. Most of the remaining gas, except for He, will become trapped in trap A during the flow. The trapping efficiency for Rn on trap A is 100%.

Once a sufficient volume of N_2 has been bubbled through the LTF chamber and

Gas	Boiling Point (°C)
H_2O	0
Rn	-61.8
CO_2	-78.5
Xe	-108.1
Kr	-153.4
O_2	-183.0
Ar	-186.0
N_2	-195.8
He	-268.6

Table 3.1: Boiling points of various gases[35].

passed through the CGRB, the flow is stopped, trap A is isolated and the vacuum pump for the gas board is turned on. Trap A is gradually opened to the vacuum pump to remove any residual gases, then isolated again. At this point the LN_2 bath on trap A is switched with a methanol slush bath. All the remaining volatile gases will boil from the trap, as their boiling points are lower than that of the bath, while Rn remains trapped. Trap A is gradually opened to the vacuum pump again to remove these gases. By monitoring the pressure in trap A it is possible to deduce when all the unwanted gases have been removed. Trap A is then isolated once again.

Only Rn gas should remain in the system now. By gradually heating trap A with heat tape we can release the Rn in the Chromosorb and transfer it to a smaller Rn trap (trap B), that has been cooled by a LN_2 bath. Trap B is filled with brass wool and has a trapping efficiency, for Rn, of 100%. This transfer requires one hour to ensure a transfer efficiency of 100%. Once completed, trap B is isolated.

The Rn gas is freed by heating trap B with a heat gun, in order to transfer it to a Lucas cell. There is a slight possibility that small amounts of CO_2 still remain trapped at this point. The volume of trap B is only 2 cc so the pressure in the trap must be monitored carefully for a large rise. In the event of a large rise the gas volume must be shared immediately with the larger Lucas cell. Otherwise, the trap can be heated gradually before transferring to the cell. This transfer has a duration of ten minutes and an efficiency of 69 ± 1.7%. The total transfer efficiency for the gas board is 69 ± 1.7%[28].

The Lucas cell is taken to surface and placed on a photomultiplier tube (PMT) to count the decays of Rn and its daughters.

3.1.3 SNO Lucas Cell

The Lucas cell is one of the most widely used devices in Rn detection. The scintillation mechanism for inorganic scintillators, such as ZnS, depends on the crystal lattice of the material[36].

As shown in Figure 3.2, the valence band represents electrons that are essentially bound at the lattice states. The conduction band represents electrons that are free to migrate through the crystal. The band gap represents an intermediate band of energies in which electrons can never be found in the pure crystal.

Given the absorption of sufficient energy, electrons can be elevated from the valence band, to the conduction band, leaving a hole. In a pure crystal, the return of electrons to the valence band, accompanied by visible photon emission, is an inefficient process. The addition of an activator, such as Ag, creates special sites in the lattice at which the normal energy band structure is modified from the pure crystal. Energy sites are created within the band gap through which an electron can deexcite back to the valence band. Selection of the appropriate activator is required in order for the scintillation photon to be in the visible range.

The SNO Lucas cell was designed to have an ultralow background. This was

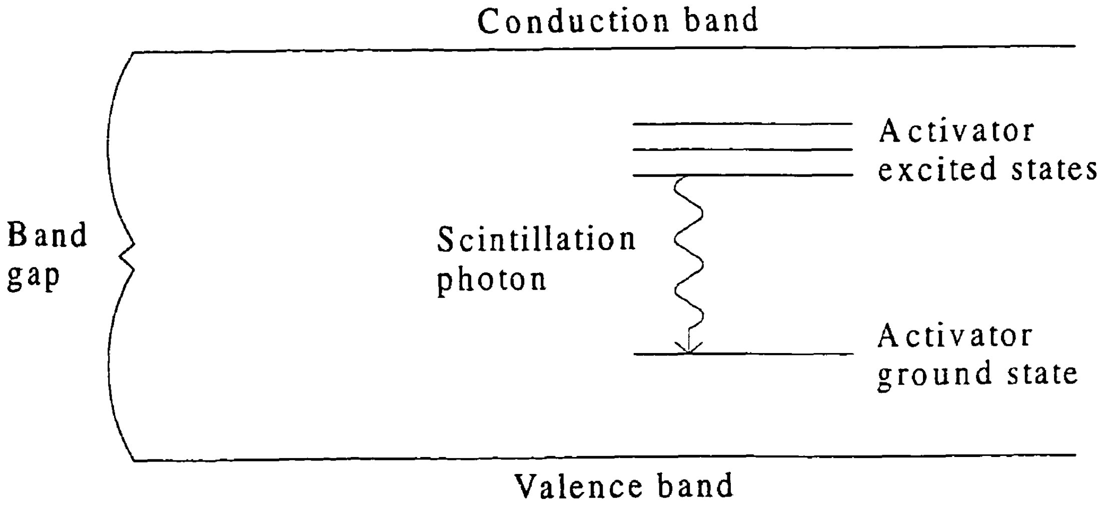

Figure 3.2: Energy band structures of an activated crystalline scintillator[36].

achieved by using acrylic for the hemispherical cell and the window as shown in Figure 3.3[32].

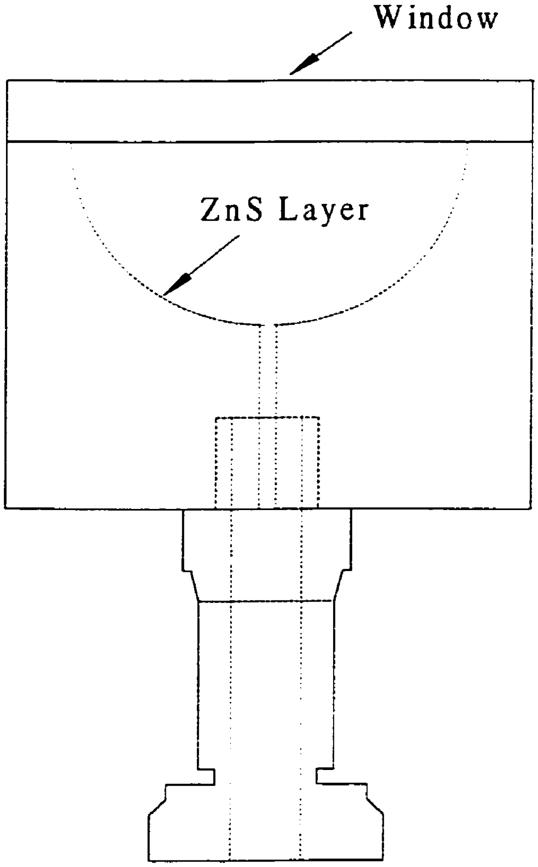

Figure 3.3: Diagram of the SNO Lucas cell[32].

Pure zinc sulfide is mixed with approximately 2% sodium chloride and 0.005% silver and fired in a nonoxidizing atmosphere to produce a coating.

The 2" diameter of the cell best matches the Phillips XP2262B photomultiplier tube (PMT)[33]. The ZnS (silver-activated) layer has a thickness of 10 mg/cm^2 corresponding to the approximate range of a 6 MeV alpha in ZnS. This gives the best ratio between ZnS background and scintillation pulse height, which should be well separated from the PMT noise[23].

The cell has a 15.5 cm^3 volume and a 20 cm^2 active area. The internal pressure is < 1 atm. A 5 MeV alpha has a range of 3.8 cm at 1 atm, therefore the detection efficiency and pulse amplitude are not significantly affected by pressure effects.

The detection efficiency of the cell was measured to be 63±2% at the Canadian Center for Mining Technology (CANMET), with a Rn source. The cell background, although very low, needs to be measured regularly due to the possibility of contamination.

3.2 Data Acquisition

As previously mentioned, the PMT used to detect the scintillation photons is a Phillips XP2262B with a 2" window and a HV setting of 1000V. An EG&G ORTEC 113 scintillation preamp is used in line with an EG&G ORTEC 855 dual amp. The shape time is set to 3 μs with a gain of approximately 10.

The amplifier input is fed into a sixteen input ORTEC 920-16 Spectrum Master multi-channel buffer (MCB)[33]. The MCB is read by Maestro II (ver. 1.30) DOS program to display one of sixteen 1024 channel spectra, to set regions of interest and to find peak areas. The DOS Multi-Tasker (A19-BI, ver. 2.2) program saves each spectrum and writes the counts in the region of interest into a log file every few hours (as specified by the user)[25].

3.3 Data Analysis

^{222}Rn is a daughter of ^{238}U, as shown in Figure1.7. When Rn decays to ^{218}Po, through alpha decay, the alpha energy is absorbed by the ZnS (silver-activated) scintillator which produces a photon. These scintillation photons are detected by the PMT and recorded by the DAQ as a count, with a 63% efficiency, as mentioned previously. In addition to ^{222}Rn both ^{218}Po and ^{214}Po produce alphas which result in counts before the chain reaches the long-lived ^{210}Pb daughter.

It takes approximately three hours after filling the Lucas cell before the decay chain reaches equilibrium. After this time we may assume that each ^{222}Rn decay results in three alphas or three counts at 63% efficiency. After determining the total number of counts in a counting interval, this number is divided by three to give the number of counts resulting from the decay of Rn alone.

To determine the number of Rn atoms in the LTF at the time of extraction, we use the expression,

$$N = \left(\frac{C_{fit}}{3}\right) \times \left(\frac{1}{\varepsilon_{det} \times \varepsilon_{trans} \times \varepsilon_{LTF}}\right) \times \left(\frac{1}{1 - e^{-\lambda_{Rn} t_{bin}}}\right) \tag{3.8}$$

where C_{fit} is the number of counts in a three hour bin, from all three alphas, derived from a fit to the differential plot of the counting data, ε_{det} is the 63% Lucas cell detection efficiency, ε_{trans} is the 70% transfer efficiency of the CGRB, ε_{LTF} is the 95% extraction efficiency associated with the LTF and t_{bin} is the time for one counting bin (set to three hours)[33]. Again, the decay constant λ_{Rn} is given by ln2/3.82 d which is derived from the 3.82 day half-life of ^{222}Rn.

For each run of the LTF a log file is produced by the DAQ PC. This file contains information about the start and stop times of the runs, the counting intervals (or bins) and the number of counts in each bin. For most counting intervals the bin time is set to three hours. This means that each three hour time interval has an associated number of counts during this time.

The log files are read into Physics Analysis Workstation (PAW), an analysis software package produced by the Computing and Networks division of CERN in Geneva, Switzerland. First, a cumulative and differential plot of the Lucas cell background data is produced, as shown in Figure 3.4 and Figure 3.5. The cumulative curve is given by

$$C_{LC} = P_1 t \tag{3.9}$$

while the differential is given by

$$dC_{LC} = P_1 \tag{3.10}$$

where P_1 is the number of counts (from the three alphas) per three hour bin[25]. The fit value for P_1 is stored in a file to be used in fitting the data from the experiment.

In all the Rn assays performed using the LTF Lucas cell #10 was used and counted on segment (PMT) #16. This cell was used for its low intrinsic background and was counted on the same segment to reduce the number of parameters affecting the data.

The experiment data is read and a cumulative and differential plot are generated. Using the data from the Lucas cell, a least squares fit is done on the differential plot to give the fit number of counts in a bin. The cumulative plot of the experimental data is given by

$$C_{exp} = P_1 t + P_2(1 - e^{-\lambda_{Rn} t}) \tag{3.11}$$

while the differential is given by

$$dC_{exp} = P_1 + P_2 e^{-\lambda_{Rn} t} \tag{3.12}$$

where C_{exp} is the total number of counts from the Lucas cell and the experiment and P_2 is the total number of counts per bin. The fit number of counts, C_{fit}, is given by dC_{exp} - dC_{LC}. This value of C_{fit} is then used in equation (3.8) to determine the number of atoms in the LTF chamber when the extraction was performed[25]. The cumulated plot and differential plot with the data fit, for an LTF Rn assay are shown in Figure 3.6 and Figure 3.7.

The rate of decay can be determined by the expression

$$R = \left(\frac{N \lambda_{Rn}}{1 - e^{-\lambda_{Rn} t_{exposure}}} \right) \tag{3.13}$$

where N is the number atoms in the system and $t_{exposure}$ is the exposure time of the system. The expression $1 - e^{-\lambda_{Rn} t_{exposure}}$ is known as the saturation factor.

Similarly, cumulative (Figure 3.8) and differential (Figure 3.9) plots of experimental data can be made using PAW. The fit number of counts can then be converted

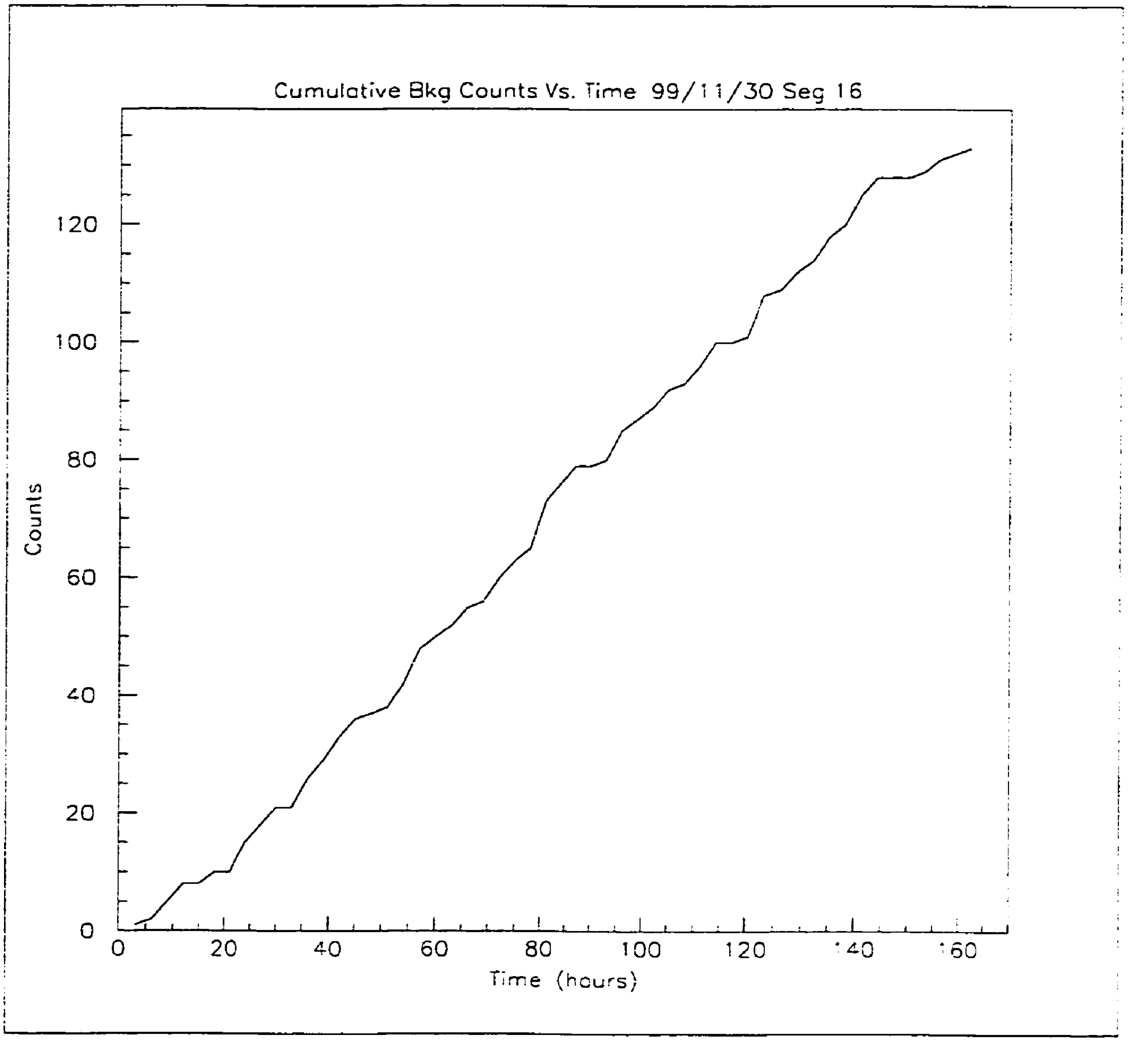

Figure 3.4: Cumulative plot of Lucas cell background data.

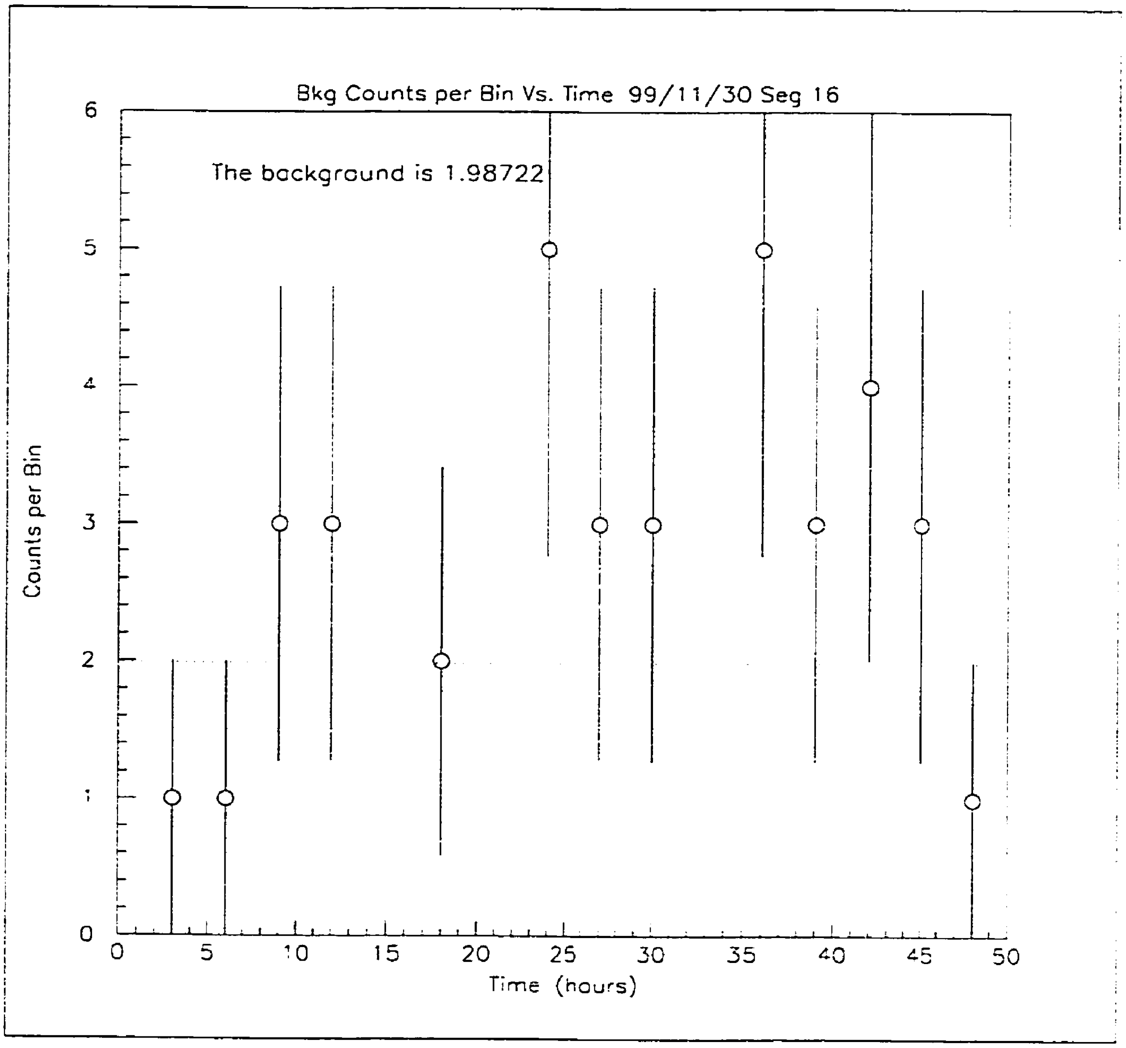

Figure 3.5: Differential plot and fit of Lucas cell background data. The dotted line is the PAW fit of equation 3.9 to the data.

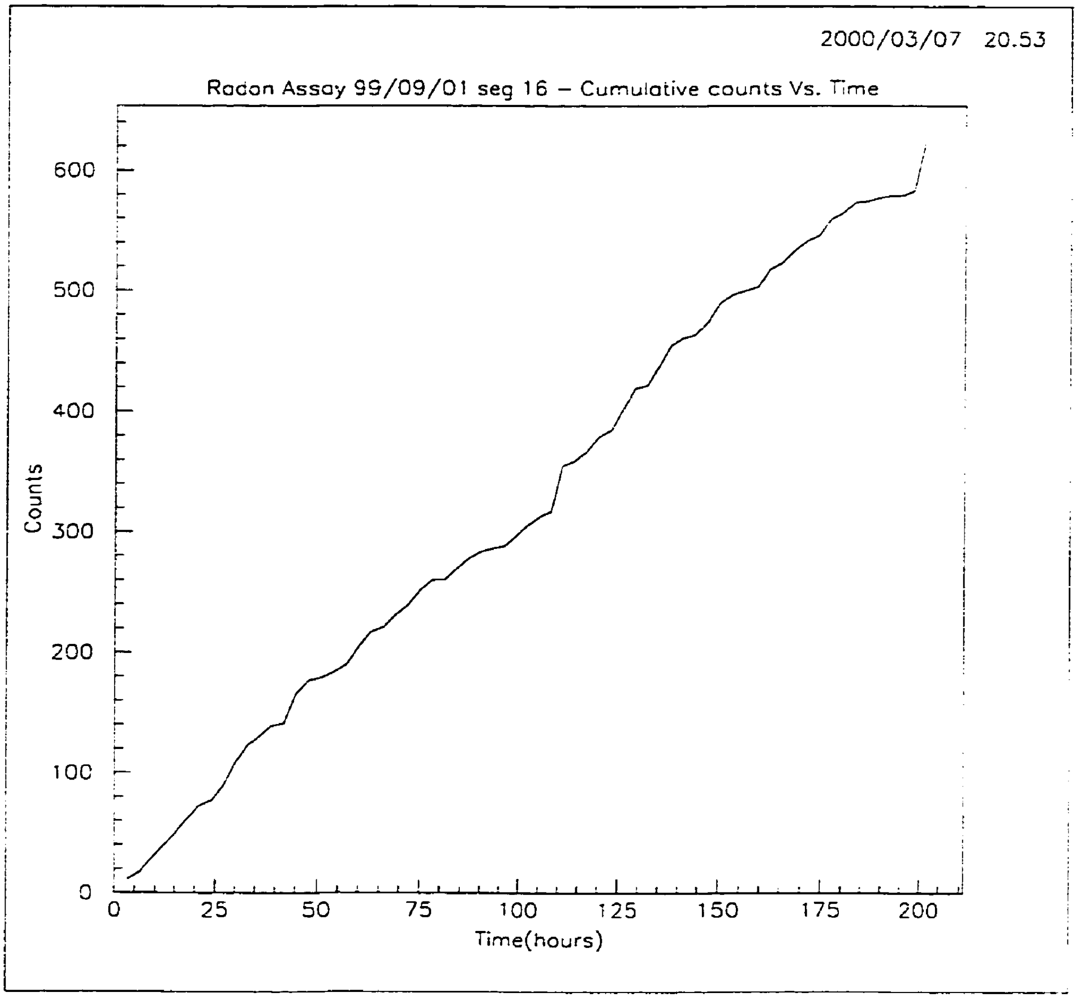

Figure 3.6: Cumulative plot of an LTF Rn background experiment.

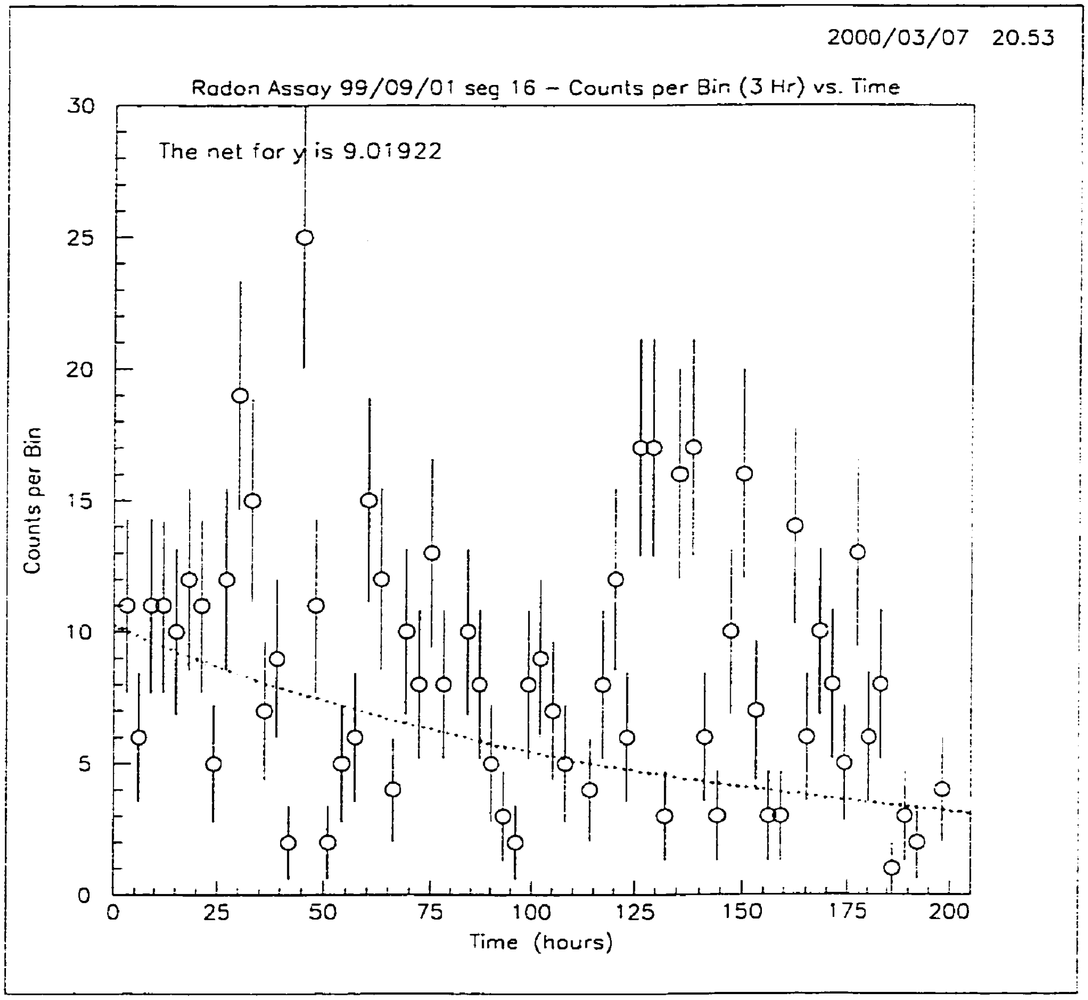

Figure 3.7: Differential plot and fit of an LTF Rn background experiment. The dotted line shows the PAW fit of equation 3.10 to the data (y-intercept at approximately 10.1). The net count intercept is given as 9.02.

to an equivalent number Rn atoms at the time of extraction. The value of the LTF background, as determined from fits similar to Figure 3.8, is subtracted, leaving us with the true number of Rn atoms emanated from the material under test.

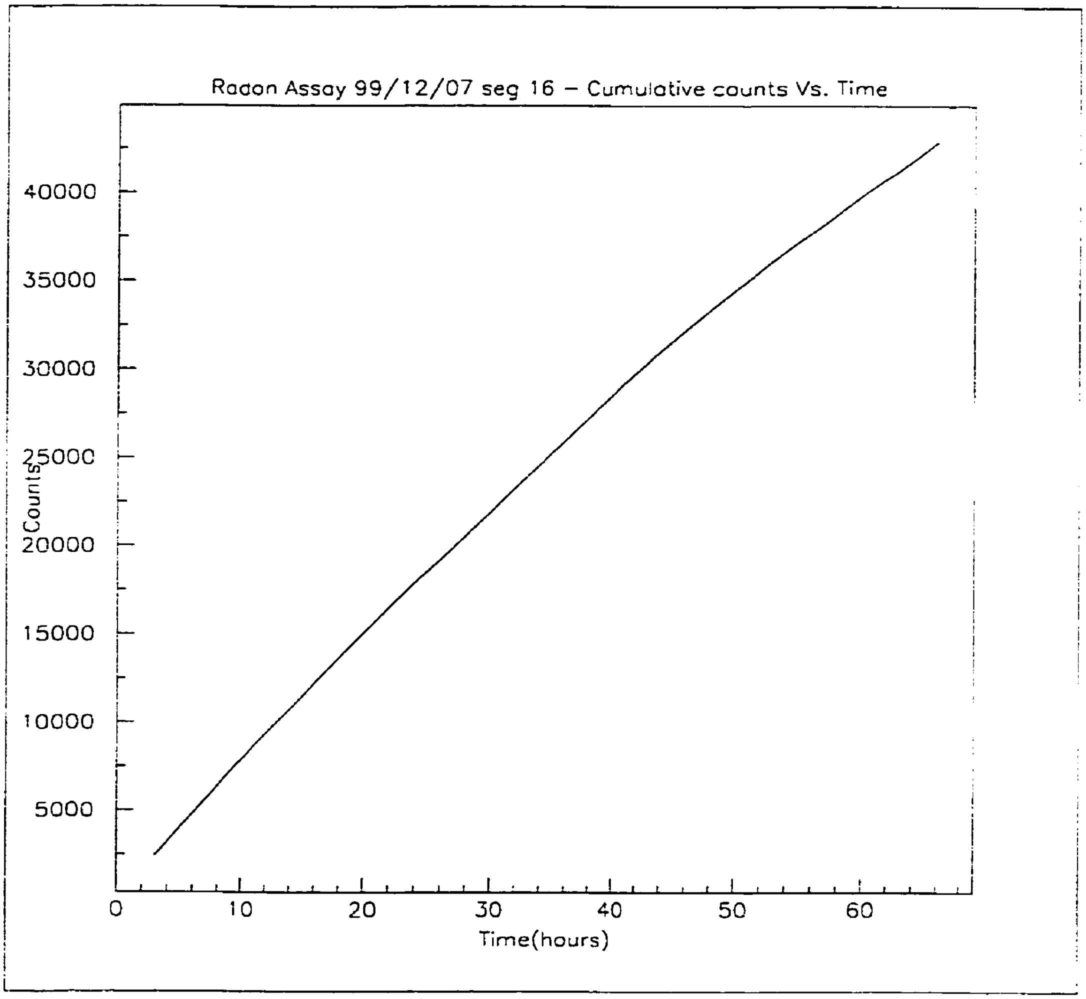

Figure 3.8: Cumulative plot of an LTF Rn experiment.

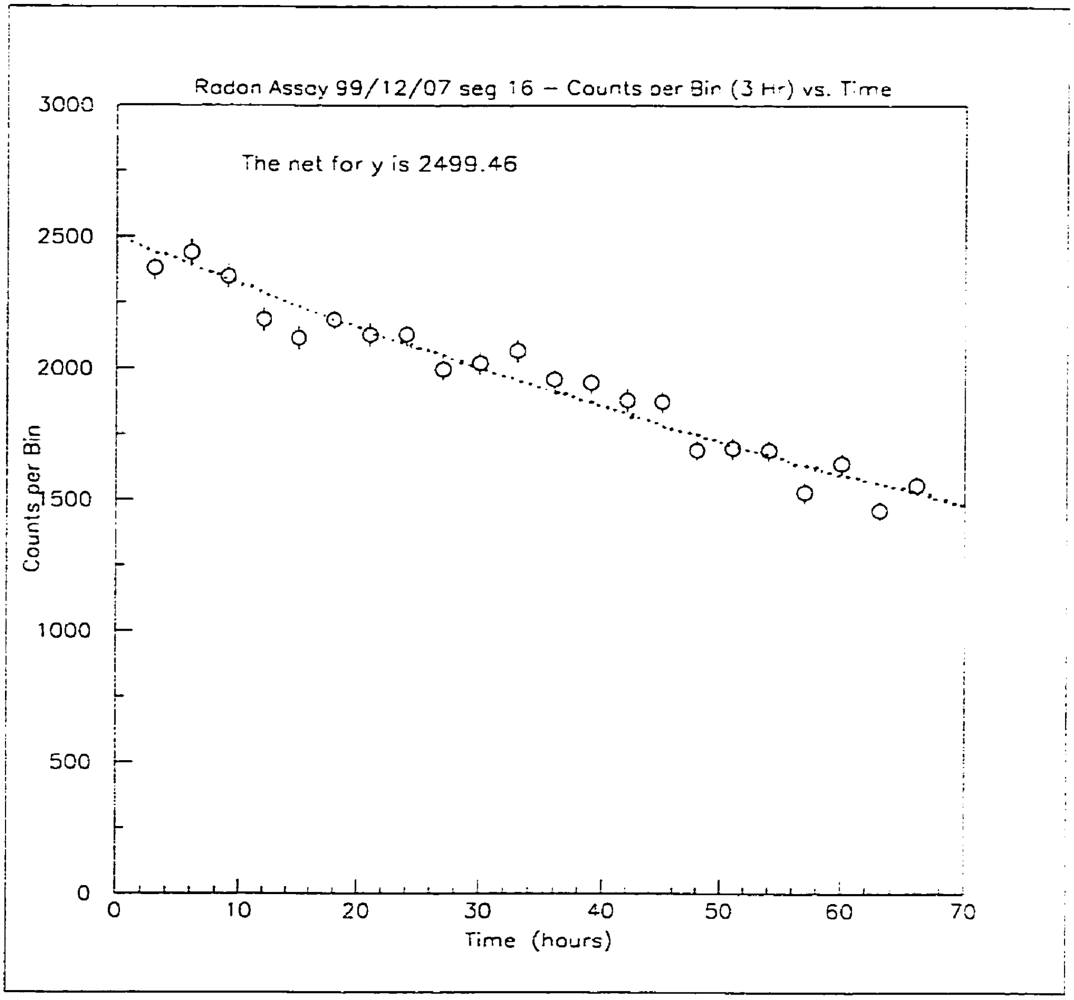

Figure 3.9: Differential plot and fit of an LTF Rn experiment. The dotted line shows the PAW fit of equation 3.10 to the data. One can now use equation 3.8 to convert the number of counts (net y-intercept) to Rn atoms at the time of extraction, then subtract the value of the LTF Rn background to give the true value.

Method of Least Squares Fitting

If an assumption is made that the data follows a statistical distribution, different values of C_{fit} can be used to try to maximize the probability

$$\max(P) \rightarrow \max(\sum P_i) \rightarrow \min(-\ln(\prod P_i)) \tag{3.14}$$

where P is the normal (parent) distribution and P_i are the individual probability functions from the data set[37] of the form

$$P_i = \frac{1}{\sqrt{2\pi}\sigma_i} e^{-\frac{1}{2}\sum\left(\frac{x_i-\mu_i}{\sigma_i}\right)} \tag{3.15}$$

where σ_i and μ_i are the standard deviation and mean of the individual functions. As shown above, maximizing P is the equivalent to minimizing the argument of the exponential from P_i[38] which gives:

$$\min(-\ln(\prod P_i)) = \min\left(\sum_{i=1}^{n} \frac{(x_i - \mu_i^2)}{\sigma_i^2}\right) \tag{3.16}$$

By using PAW to maximize the fit, a reliable value for C_{fit} is obtained quickly. PAW also provides the χ^2 value per degree of freedom, or the reduced χ^2 (χ^2_ν). The expectation value of this quantity is equal to one for a perfect fit. Values of the reduced χ^2 much larger than one indicate large deviations from the assumed distribution, poor measurements, incorrect uncertainties or an incorrect probability function. Values much less than 1 indicate over-estimated uncertainties or a serious flaw in the experiment[38].

Three experiments were performed to determine the Rn background of the LTF system. Once the background was established, two experiments were performed using viton cord as a sample.

3.4 The LTF Radon Background

The first Rn assay of the LTF background was performed using the Monitor Degasser (MDG) Rn board. This board was used in the absence of the CGRB to establish initial levels for the LTF system.

This particular Rn assay only involved the empty LTF chamber. The chamber was sealed for an exposure time of approximately twenty days. After this time it was connected to the MDG Rn board vacuum pump. The pump was used in place of the N_2 sweep gas to remove all gases from the LTF chamber. The remainder of the assay is very similar to those using the CGRB, except that the pump was used at all times during this assay.

Since this was the first assay of the system, our goal was to try to determine whether there were any large oversights in construction, whether the system functioned as we hoped and estimate whether we could achieve low enough background levels to be able to assay materials.

The following two assays were LTF Rn backgrounds that included a water filled chamber. An N_2 gas flow and the CGRB were used for these and all other Rn assays. The results of the assays are listed in Table 3.2.

Extraction Date	Type	Water Volume (l)	Exposure Time (d)	Activity (dpd)	χ^2_ν
99/05/25	Empty chamber (MDG Rn Board)	N/A	19.93	22.26 ± 2.60	1.5
99/09/01	First Rn background (CGRB)	7.5	15.15	61.72 ± 3.97	3.8
99/10/08	Second Rn background (CGRB)	7.9	21.92	61.55 ± 3.36	2.0

Table 3.2: Results of analysis of Rn extraction backgrounds on the LTF.

We found very good agreement between the two LTF background assays where the system was run as designed. The errors associated with the activities are purely statistical, however, the results lie within this uncertainty limit of one another.

The average of the results gives an activity for LTF background Rn of 61.63 ± 3.67 decays per day (dpd). If we compare this result to the estimated activity level for the system in Table 2.1, we see an 11.4% relative uncertainty between the 55.3 dpd estimated level and the 61.63 ± 3.67 dpd experimental result. Although the experimental value does not appear to be within experimental uncertainties of the estimated value, no uncertainty was associated with the estimate. Furthermore, the uncertainty of the experimental value is statistical, requiring a systematic uncertainty to be determined for the system in the future.

An activity of 61.63 ± 3.67 dpd will be used when determining the emanation rate of the viton sample.

3.5 Radon Emanation from Viton

A variety of o-rings were required in the construction of the Sudbury Neutrino Observatory. As an example, each pipe connector and valve for the SNO water systems requires an o-ring. If the ^{222}Rn permeation through the o-ring is high, these particular o-rings alone can account for a significant percentage of the intrinsic background in the water of the SNO detector. Radon emanation from these o-rings was also a potential background source.

Many types of o-rings were measured for their Rn permeation and emanation rates. The emanation studies in particular led to much of the refinement of the assaying techniques used in the LTF. The results are very useful for making comparisons and inferences to Rn emanation rates exhibited by other materials.

The two emanation experiments performed using the LTF were done using a sample of carbon black viton cord with a surface area of 0.437 ± 0.051 m^2. This particular viton cord has been previously measured to have a significant rate.

The difficulty in comparing samples lies in the makeup of each. One batch of viton can be slightly different than another. This will cause the Rn emanation rate to change, making comparisons difficult.

The sample used in the LTF was comprised of three pieces of the same viton cord. Both experiments were performed on the same sample, so that the Rn emanation rate is identical. The motivation for using the same sample is associated with the Ra experiments to be described later. The results of the two experimental assays are listed in Table 3.3.

The average Rn activity is 14777 ± 472 dpd. Calculations, using this result, give a Rn emanation rate, for 0.437 ± 0.051 m^2 of viton, of 1408.9 ± 105.0 Rn m^{-2} h^{-1}. This result is compared to those of other similar materials in Table 3.4[39].

The results of the LTF assays of viton are consistent with the measured emanation rates of other similar materials. It would be advantageous to perform this experiment a number of times to gain better statistics and be more certain of the actual rate.

A calibration of the LTF system with a Rn standard should be done but is beyond the scope of this thesis. A suitable source, acceptable for use in the SNO lab, requires considerable development work.

The LTF was sited in the SNO laboratory, largely because of the availability of a known source of UPW. However, underground air has a significant Rn content and diffusion of Rn into the assembly could occur. Although we had estimates for this result, it was uncertain as to what these background levels would be. Air with a known Rn content can be a possible calibration source for the LTF.

The UPW volume for these experiments is lower than those of the background runs. Consequently, the background level will be reduced slightly. If an average difference of 3.7 *l* is used, the estimated difference in activity is 0.03 dpd which is well within the uncertainty of the background.

The ^{222}Rn assays of the LTF were successful. The Rn background level has been established within statistical uncertainty and initial results for the emanation rate of viton compare well with similar material types.

Extraction Date	Type	Water Volume (l)	Viton Sample (m^2)	Exposure Time (d)	Activity (dpd)	Adjusted Activity (dpd)	χ^2_ν
99/11/16	First Experiment (Viton)	4.3	0.437 ± 0.051	20.04	13290 ± 51.8	13229 ± 419	2.7
99/09/01	Second Experiment (Viton)	4.2	0.437 ± 0.051	20.78	16386 ± 80.3	16324 ± 526	2.4

Table 3.3: Results of analysis of Rn assays of viton in the LTF.

Material	Emanation Rate (Rn m^{-2} h^{-1})
Chemraz O-ring 784	1879 ± 39
EDPM O-ring	1514 ± 20
Viton (LTF)	1409 ± 105
Viton	1089 ± 26
Red Silicon O-ring	635 ± 10
Silicon Bathtub Sealant	26 ± 1.3
Blown Teflon Gasket	<9
Butyl Rubber	0.1

Table 3.4: Comparison of the LTF viton Rn emanation results with those of similar materials[39].

Chapter 4

Radium Detection

In this chapter the method by which radium is assayed using the LTF will be discussed. The data acquisition and analysis systems will be detailed and the intrinsic background levels for the LTF will be established. Finally, experimental assays of a viton material will be outlined and the radium leach rate for the material presented.

4.1 Radium Extraction

The method for extracting ^{224}Ra and ^{226}Ra using MnO_x coated, Diakon acrylic beads has been well established within SNO[24]. Specific analysis software has been developed to fit the data produced by the electrostatic counters (ESCs) used to count the Po daughters from their respective Ra parent nuclei. This software also calculates the respective mass of ^{232}Th and ^{238}U per mass of ultrapure water (UPW) which flowed through the PP column that houses the MnO_x beads.

The LTF ultilizes this Ra extraction system to measure the ^{232}Th and ^{238}U contents of samples of materials in order to calculate the impact of these materials on SNO's intrinsic background. The systematics and methodology of the radium extractions follow, with descriptions of the MnO_x beads and the extraction parameters.

4.1.1 Extraction from the LTF

Prior to being used for an LTF Ra assay, an MnO_x column is assembled and dried with 60°C compressed air. The air is filtered through a 1 μm filter. The column is then placed on an ESC to count the combined intrinsic background signals of the column and detector. This is referred to as a 'blank' run and it has a duration of approximately seven days. When the counting of the column is finished, the column is sealed with threaded PP caps and taken underground for Ra collection[1]. This activity runs in parallel with the sealing and exposure time of the LTF chamber.

The exposure time required for an LTF radium assay is governed by the half-life of ^{224}Ra. For a background run of the LTF system, ^{224}Ra atoms are already in equilibrium with the water since it is taken from the SNO UPW water systems. However, small contributions from ^{224}Ra leaching from the chamber or tubing in the system will require time to reach equilibrium. The leach rate is unknown so an exposure time of a week, twice the half-life of ^{224}Ra, was established. In addition, some radium assays were coupled with radon assays, so the exposure time accounted for ^{222}Rn to reach equilibrium. Due to the long 1602 year half-life of ^{226}Ra, only ^{224}Ra was considered when establishing exposure times.

Once the exposure time for ^{224}Ra to reach equilibrium in solution is reached, the PP column containing the MnO_x coated beads is attached to the output of the LTF at VW1 (see Figure 2.4). Clean N_2 boil-off gas from a LN_2 Dewar is used to pressurize the LTF chamber, forcing the UPW sample through the Teflon line running to the bottom of the chamber. This water is flushed through the PP column where the Ra is extracted onto the MnO_x beads, then flowed to drain. Time is measured during the flush to calculate the flow rate of the UPW, which should not exceed 20 *lpm*.

---

[1] If a column has been stored before the blank is counted or before being used in an assay, it is flushed with compressed N_2 and capped. This procedure was implemented to eliminate any radon gas that may have absorbed on the beads. Should this occur, the ^{238}U activity curves will show a rise followed by a decrease faster than that of ^{222}Rn[40]

The PP column is then transported to the surface lab to be dried and then counted on an electrostatic counter (ESC).

Radium Leached Into Water

The amount of Ra that leached from a material into solution with the UPW in the LTF chamber is difficult to calculate. It is very dependent on the micro-structure of the material and the intrinsic concentrations of ^{224}Ra and ^{226}Ra. Not all the radium will leave the material, otherwise we could calculate the ^{226}Ra levels for a material by measuring its ^{222}Rn emanation rate. Radium can be distributed throughout the material and can be trapped in the grains or crystal. Some of this Ra will be seen as ^{222}Rn that has emanated from the trapped Ra directly into the UPW or diffused from deeper within the material[31].

When a material is submerged in UPW the radium in the material will leach into the water at a certain rate until equilibrium is reached. The factors which govern the dynamics of the radium leach rate are the concentration difference between radium in the material and radium in the UPW[2], the ability for radium to leave the substrate and the solubility of radium in water. By measuring the number of Ra atoms leached from a material per day per square meter the leach rate for ^{226}Ra and ^{224}Ra can be calculated, just as the emanation rate for Rn was calculated in the previous chapter. This thesis concentrates on experimentally determining the systematics and sensitivity levels of a prototype leach test system in order to be able to measure a given material's radium leach rate. Once the systematics of the LTF are established, further studies may be done using the LTF to determine the relationship

---

[2] The reduction of ^{232}Th and ^{238}U content of the cavity water in the SNO detector results in the lowering of the intrinsic background level of the NC signal but also in an increase in the concentration difference between the water and the cavity materials, thus increasing the potential for leaching. This increases the importance of knowing the intrinsic radium levels of materials before they are submerged in the cavity for long periods of time.

between a selected material's radon emanation rate and its radium leach rate.

Due to the small volume of the LTF chamber, only small volume samples of UPW are flushed through the MnO_x columns. The sensitivity of the system is therefore lower than that of a large volume system, however, useful knowledge of the sensitivity levels of a system of this type can be gained using a smaller volume prototype. Once these levels are established, inferences can be made on the sensitivity levels of a larger system, while the smaller prototype may be utilized to measure higher activity materials.

In order to fully characterize the sensitivity of the LTF, the parameters of the extraction must be known. The following subsection describes the methods by which radium ions are extracted from the sample water.

4.1.2 MnO_x Columns

In order to remove the Ra^{++} aqueous ions, the UPW from the LTF chamber is pumped through a 1 l PP column containing Diakon acrylic beads coated with MnO_x. Once the entire volume of UPW from the LTF has passed through the column it is taken to the surface chemistry and physics laboratory where it is dried and connected to an electrostatic counter (ESC).

Two types of coated beads have been developed by the SNO collaboration at the Centre for Research in Particle Physics (CRPP). The first is an MnO_2 coating produced by prolonged oxidation of an organic matrix with permanganate, at high temperature and in the presence of sulfuric acid, to form a black coating on acrylic beads. The second and more recent coating, MnO_x, is a dark brown intermediate product formed in a controlled and partial oxidation of the beads with the same permanganate reagent. The growth of the coating is controlled to reach a dark brown appearance. The beads are dried, then passed through a series of sieves to retain beads with diameters in the range of 400 to 600 μm[24].

The column itself has a volume of 1 l and contains honeycomb shaped inserts at both ends, which themselves contain 0.1 mm square grid screens that act as holders. These holders are designed to prevent any of the beads from escaping the column, potentially damaging the pump, and entering the SNO water system. If this was to take place, the Ra activity seen for the experiment would be lowered and, more importantly, the stray beads could trap Ra activity and hide it from future assays. The packing fraction and mass of beads placed in the column are controlled as these factors will slightly affect the removal of radium and the transport of radon during counting[42]. Being assured of the uniformity of the beads allows for control of the packing fraction by controlling the mass of beads in a column to be 700.0 ± 0.2 g[41].

Two parameters of the MnO_x assay technique were studied extensively in order to increase the amount of radium extracted during an assay. The product of the radium extraction rate and the radon emanation rate for the beads was established and optimized, as was the retention of extracted radium of the beads.

The distribution coefficient (K_d) of the MnO_x beads gives a quantitative measure of the affinity of the beads to absorb and retain Ra^{++} aqueous ions. Experiments to determine the apparent distribution coefficient were performed using various sized columns filled with MnO_x beads spiked with 30-50 ng ^{226}Ra[24]. These experiments were conducted on two scales; 1.5 cc polycarbonate columns with an aspect ratio (L:D) of 1.5:1 and 30 cc polycarbonate columns with an aspect ratio of 6:2.5. The columns were then leached at 20 BVM (bed volumes per minute) with UPW. The distribution coefficient was determined by

$$K_d = \frac{V_w}{V_r} \times \frac{A_r}{A_w} \tag{4.1}$$

where V_w is the volume of water, V_r is the volume of resin, A_r is the activity of the resin and A_w (A_o - A_r) is the activity of the water[24][42]. The value of the K_d constant of MnO_x was determined to be approximately 1×10^{-6} in 1996[24]. This value is dependent upon equilibrium conditions like the flow of water, the beads used and the aspect ratio of the column. These parameters were kept constant in all subsequent radium assays in the LTF; the same, 1 l volume, columns were used, the beads were selected from batches that had undergone QC in CRPP and the flow was monitored and kept well below the 20 BVM (or liter per minute (*lpm*) for a 1 l column) limit.

The extraction efficiency of MnO_x was measured in CRPP in 1995, by performing runs on an extraction rig using a ^{228}Th spike[43]. The experiment involved flowing 500 l of UPW through two PP columns (A & B) joined in series. The activities of the two columns were measured with the extraction efficiency being determined by the ratio of the activities found on the respective columns as $\varepsilon - \frac{B}{A}$. Seven runs were performed at flow rates from 5 to 20 *lpm* with the average extraction efficiency measured at

86 ± 1%. The 5 *lpm* flow rate resulted in a ^{224}Ra extraction efficiency of 90 ± 1%. This flow rate is the most similar to that used in the LTF Ra assays, therefore a 90 ± 1% extraction efficiency is used in the data analysis of the LTF runs.

The radium extraction efficiencies for the SNO D_2O and UPW systems are measured frequently during assays of the cavity waters and have been consistently high. The average UPW extraction efficiencies have been measured to be 97.4 ± 2.1% for ^{224}Ra and 93.5 ± 22.4% for ^{226}Ra from May 10, 1999 to May 24, 2000[29]. It was noticed that a cooler ambient temperature of the cavity water coincided with reduced radium extraction efficiencies of as low as 63% for cavity assays in May and June of 1999. These trends have not persisted as the extraction efficiencies since have been measured to be consistently high with the same cooler temperature. All the LTF Ra assays were performed with lab temperature UPW, and are not subject to any studies of the effect of lower temperature on the radium extraction efficiencies, if any are deemed as necessary.

At the same time as experiments were conducted to determine the radium extraction efficiency for MnO_x, initial studies were done to determine the effect of fines[43]. Fines are defined as small amounts of the MnO_x coating (needles) that are removed when UPW is flowed through the PP column during an extraction. Just as stray beads can carry away Ra activity from an assay, preliminary results showed that fines >0.1 μm can account for as much as 10% of the total activity extracted in the tests considered. Consequently, measures were taken to ensure that these fines do not enter the cavity of the SNO detector or remain in the light and heavy water systems where fines could hide radium activity levels from further radium assays and reduce the light attenuation length in the detector. Fines $\leq$0.1 μm entering the test system have not been seen to carry away any activity[44].

In order to lower the amount of fines entering the system in a SNO radium assay, MnO_x column are rinsed before being used in extractions. The rinsing is done using the same UPW as that sampled in an assay, so as to not skew the results. The objectives are to lower the amount of fines at the >0.1 μm, thus minimizing the load on all the 0.1μ filters following the MnO_x columns in the SNO water system[44]. It was found that the volume of water needed to remove a high percentage of fines at the >0.1 μm level was two to three 50 l rinse volumes, or 100 to 150 l. However, additional rinsing showed evidence of further generation of >0.1 μm fines, increasing the importance of coarse filters between MnO_x columns and fine filters following them, in the SNO water systems. The procedure in place for the SNO water systems uses 100 - 300 l of water to rinse.

The Ra assays of the LTF were performed with non-rinsed columns, as the rinsing rig available underground is dedicated to Ra assays of the SNO cavity UPW. Consequently, results from radium assays of the LTF can have activity lost in fines. The exact amount of activity lost cannot be known at this time but could be included in extraction efficiency studies specific to the LTF and its systematics.

After a column has been flushed in an extraction it is brought to the surface lab, dried for four hours, then placed on the same counter it was counted on for the blank run so as not to skew the background levels of the assay. This run is referred to as the 'sample'. The activity from the blank run will be subtracted from the sample to give the activity from the assay.

4.2 Data Acquisition

The data acquisition for a radium assay involves measuring the activity of ^{224}Ra and ^{226}Ra through their respective daughter ions. This is done by using an electrostatic counter (ESC) to detect alpha particles. The following subsection outlines the operating principles of the circulation loop and the electrostatic chamber for a SNO ESC and the associated efficiencies.

4.2.1 Electrostatic Counter

The SNO electrostatic counters (ESCs) were designed specifically for the counting of ^{220}Rn, as previous counters did not provide the sensitivity required to analyze the levels targeted for the UPW and D_2O in SNO. These counters were designed and manufactured by the SNO group at the University of Guelph. In the context of a radium assay, the detector's function is to measure the activity of the associated radon daughters that escape from the radium decaying within the MnO_x column. The column is connected to the chamber using mainly clean Tygon and SS tubing in series with a diaphragm pump to force circulation exchange (Figure 4.1). The diaphragm is made from a high purity Teflon to lower the intrinsic background levels of the system. The counter and its circulation loop are filled with a nitrogen carrier gas, which transports the Rn atoms from the column to the chamber[37].

In the ^{232}Th chain, the supporting source of ^{220}Rn is both ^{228}Th and ^{224}Ra as ^{224}Ra is short lived (half-life of 3.64 days). ^{220}Rn decays to ^{216}Po, which has a very

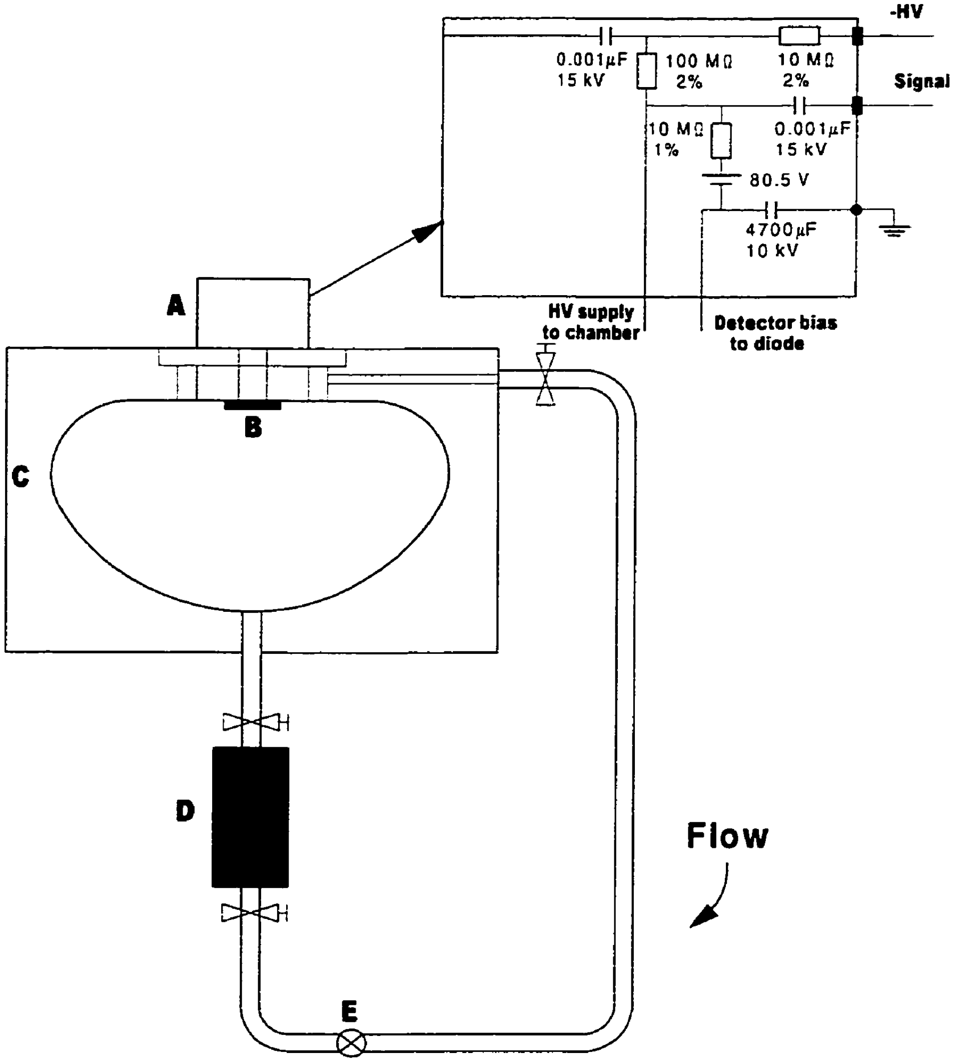

Figure 4.1: A schematic of an electrostatic chamber with its recirculation loop and associated electronics. Section A shows the battery and preamp circuit, B shows the silicon photodiode, C the detector chamber, D the MnO_x column and E represents the diaphragm pump.

short half-life of 0.158 seconds. ^{216}Po then decays to ^{212}Po through ^{212}Pb and ^{212}Bi (see Figure 1.6). The 6288 keV alpha released in the decay of ^{220}Rn is not detected by the ESC, however, the subsequent 6779 keV and 8785 keV alphas from ^{216}Po and ^{212}Po respectively can be identified. In the ^{238}U chain, ^{226}Ra decays to ^{222}Rn with the release of a 4784 keV alpha. ^{226}Ra is the supporting source of ^{222}Rn with a half-life of 1600 years. ^{222}Rn has a half-life of 3.823 days and decays to ^{218}Po with the release of a 5490 keV alpha and ^{218}Po subsequently decays to ^{214}Po through ^{214}Pb and ^{214}Bi (see Figure 1.7). Again, only the subsequent 6002 keV and 7687 keV alphas from the Po daughters are identified.

The parameters to consider in the ESC detection process are the ability of ^{222}Rn and ^{220}Rn to emanate from the MnO_x beads and the efficiency with which the radon gas is carried to the active volume of the chamber. The emanation of radon from the beads was maximized in conjunction with the extraction efficiency and distribution coefficient of the beads. The transport efficiency has been maximized by keeping the volume of the circulation loop small, compared to the chamber volume, and by using an appropriate transport gas (N_2) to carry the radon atoms to the active volume.

Two efficiencies have been characterized for the ESC loop; the emanation efficiency (ε_{eman}) and the transport efficiency (ε_{trsp}). The efficiency of the active volume is embedded in the transport efficiency as it takes into account the amount of time spent in the active volume. The product of ε_{eman} and ε_{trsp} for ^{232}Th and ^{238}U have been measured to be 30 ± 7 % and 75 ± 10 % respectively[41].

The electrostatic radon detector primarily consists of an aluminum chamber and an alpha particle detector. The principle of detection relies on the fact that a significant fraction of the Po daughters for Rn decay are positively charged. The Po ions drift towards the photodiode along the electric field in the chamber. Most are deposited on the alpha-particle detector surface but some ^{216}Po ions will decay in flight. Figure 4.2 shows a spectrum from an ESC using both a ^{226}Ra (^{222}Rn) source and a ^{220}Rn source. The 6070 keV ^{212}Bi peak (36% alpha decay at 6051 and 6090 keV) can be distinguished from the 6002 keV ^{218}Po peak. The high-energy side tail of the ^{212}Po peak is caused by the simultaneous detection of the beta particle from the decay of ^{212}Bi[37]. For the LTF radium assays, ^{212}Po is not used in the fit.

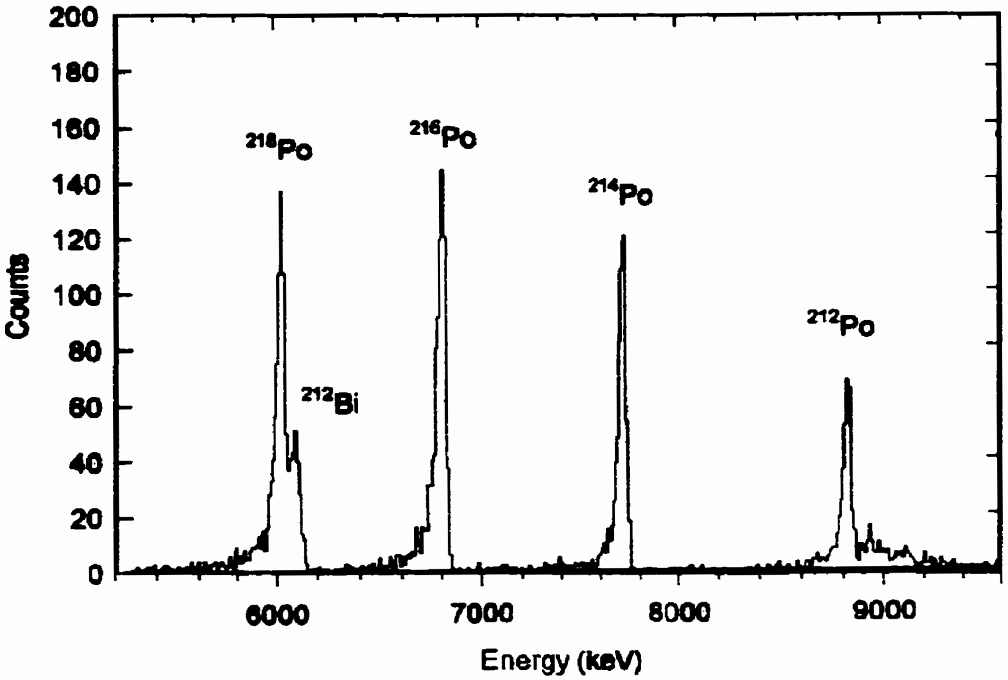

Figure 4.2: Typical spectrum of Po daughter peaks from a ^{220}Rn and ^{222}Rn source[37].

For typical radon detectors the detection efficiency for ^{222}Rn was measured to be about 10%, while that for ^{220}Rn was $< 1\%$. The efficiency of the SNO ESC chamber as a radon detector is given as $\varepsilon = \varepsilon_{geom} \times \varepsilon_D \times \varepsilon_{coll} \times \varepsilon_Q$, where ε_{geom} is the solid angle factor of the alpha detector or the diode geometry, ε_D is the fractional effective area of the alpha-particle detector, ε_{coll} is the collection factor for positively charged ions to be precipitated onto the detector and ε_Q is the fraction of positively charged ions following radon decay. The solid angle efficiency, ε_{geom}, of 50 ± 0% cannot be improved. Similarly, the fraction of positively charged ions from radon decay of 70 ± 3% cannot be improved[41]. The efficiencies that have been improved upon in the SNO ESC are the fractional effective area of the alpha-particle detector and the collection factor for positively charged ions[37].

In order to improve upon ε_{coll}, the shape of the chamber was designed to minimize the dead area where the electric field is very small as much as possible. In addition, the volume was made much larger than that of the MnO_x column so that most of the radon would decay in the chamber. Figure 4.3 shows a two-dimensional model calculation of the electric field in the chamber with 1000 V between the detector and the decay chamber wall[37]. The high voltage (HV), for the electric field between the alpha particle detector and the chamber wall, was provided by an Ortec 566 high voltage supply.

The collection efficiency of ^{216}Po is dependent on the shape of the chamber. the chamber pressure and the high voltage as it has a half-life of 0.158 s. Maximizing ε_{coll} for ^{216}Po will ensure a high collection efficiency for the longer lived ^{218}Po, with a half-life of 3.05 m. The recoil of ^{216}Po is in a random direction and is assumed to take place in one step. Afterwards, the Po ion is considered thermalized, and it follows the chamber electric field. The electric field competes with the random walk of the ion in the carrier gas, and thus requires a lower chamber pressure than other ^{220}Rn detectors. If the Po ion becomes trapped on the chamber wall it is considered lost.

The drift velocity of the Po ion is given as the product of the ion mobility K and the electric field E. A value for K of 2 cm^2 V^{-1} s^{-1} in 1 atm nitrogen gas was used in the Monte Carlo modeling of Tom Andersen[45]. Nitrogen gas was chosen for the transport gas for its availability and safety, although other gases such as helium and argon produced no significant difference on the ^{216}Po transport times. The results of the Monte Carlo studies showed the Po ions to have a flight time of less than 0.158 s

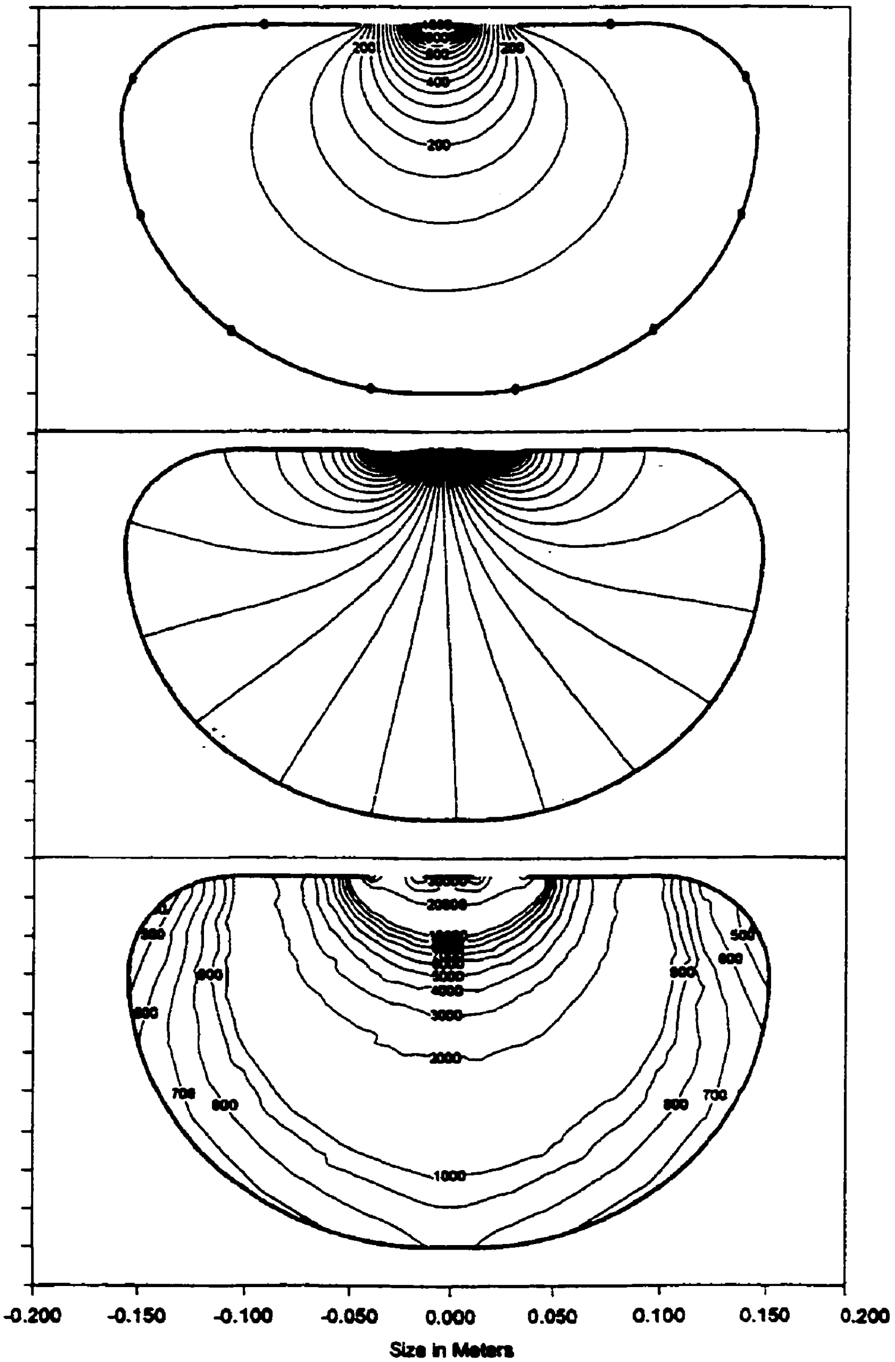

Figure 4.3: Two-dimensional model calculation of the electric field in the ESC chamber with 1000 V between the diode and the chamber wall. Top: electric potential contour lines; Middle: electric field lines; Bottom: field strength contour lines[37].

and consequently only about 20% of the ions are lost to decay during collection. The overall collection efficiency for ^{216}Po is 65 ± 7% while that for ^{218}Po is 100 ± 0%.

It is important to ensure the leak rate for the chamber is kept to below 1 mbar/day, corresponding to a pressure range of 30 to 40 mbar and a counting period of 10 days. Also, the high voltage should not drift as the efficiencies are affected by both parameters, as shown in Figure 4.4.

The use of a silicon photodiode decreases the frontal dead area of the detector, effectively increasing ε_D. The diode used in the SNO ESC is a Hamamatsu with a diode area of 18 × 18 mm^2 on a ceramic base of area 25 × 25 mm^2. A ceramic insulator is used in the base, therefore the fractional effective area of the detector is 100%. The detector is mounted on a Teflon flange with a bias feedthrough, with its surface flush to the top of the chamber, reducing the dead volume not reached by the electric field lines. The intrinsic capacitance of the PIN diode is 400 pF when depleted to more than 90%, which occurs at approximately 70 V provided by the bias battery. A diagram of the operation of a photodiode is shown in Figure 4.5.

The efficiencies for the loop and chamber of ESC7 are summarized in Table 4.1. Including the extraction efficiency, the total efficiency for ^{232}Th is 6.1 ± 1.7% and for ^{238}U is 23.6 ± 3.0%.

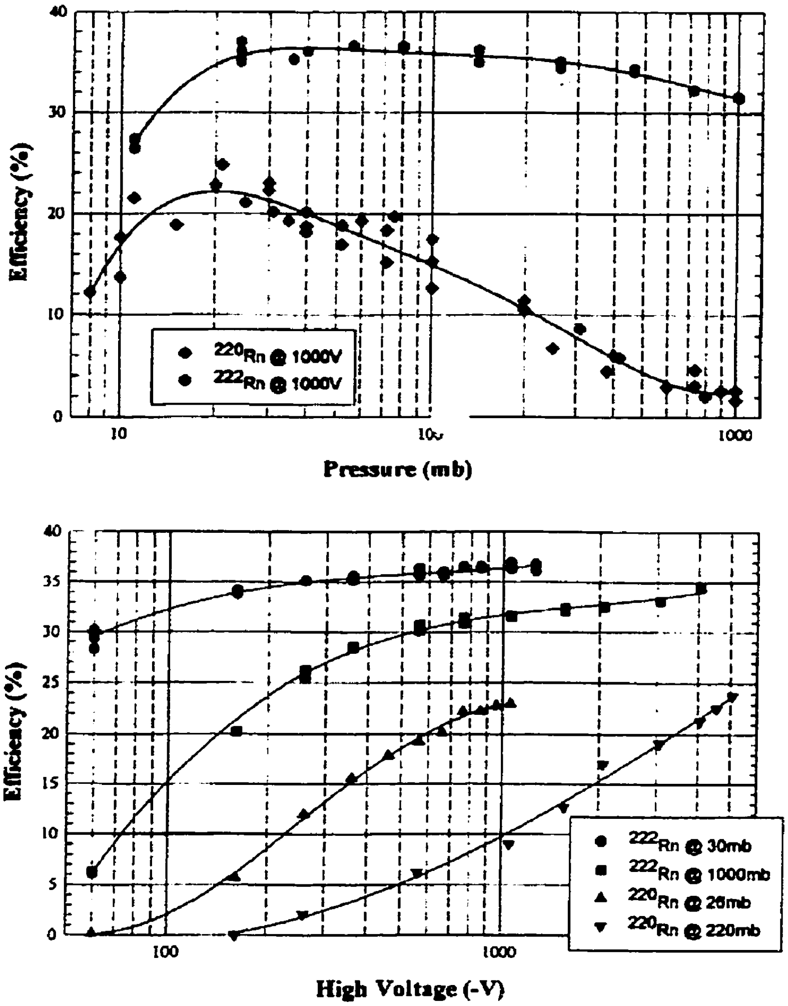

Figure 4.4: ^{220}Rn and ^{222}Rn detection efficiency as a function of pressure and electric field (HV)[37].

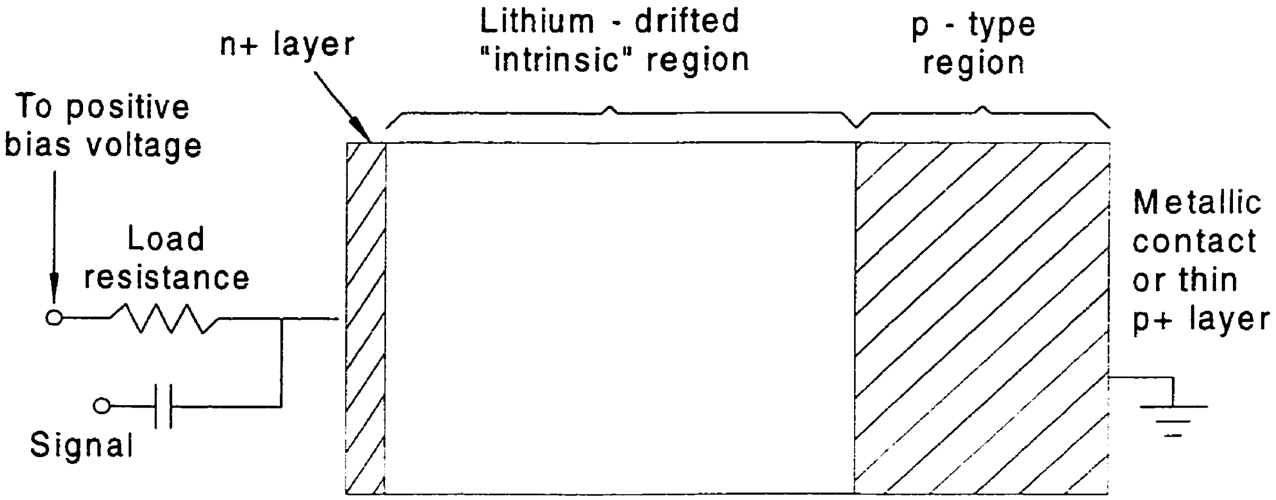

Figure 4.5: A diagram of a PIN silicon photodiode showing the bias and depletion layer[36].

Operation	Efficiency (%)	
	^{232}Th	^{238}U
Emanation + Transport	30 ± 7	75 ± 10
Charge Fraction	70 ± 3	70 ± 3
Collection	65 ± 7	100 ± 0
Geometry	50 ± 0	50 ± 0
Fractional Effective Area	100 ± 0	100 ± 0
Detection (chamber only)	22.8 ± 2.6	35.0 ± 1.5
Detection (for column)	6.8 ± 1.8	26.2 ± 3.0

Table 4.1: The efficiencies and respective uncertainties for ESC7[37][41].

4.2.2 ESC Installation

The ESC used for the LTF assays was originally built for the Neutral Current Detector group at Los Alamos National Laboratories. It was shipped to Sudbury in its original crate, having not been assembled in Los Alamos. The detector chamber, the fittings the o-rings and tubing were all cleaned with methanol at Laurentian University prior to transporting the detector to the clean environment of the surface lab at the SNO site. The chamber was then filled with approximately 12 *l* of UPW in solution with 300 *ml* of radiac wash to remove any ions from the chamber wall. After an exposure period of 3 days the chamber was flushed with 48 *l* of UPW to remove the radiac wash solution. Cables were made for the HV and signal and a Pirani gauge was mounted for monitoring the pressure.

The battery voltage was measured to be 80.5 V (see Figure 4.1), well above the 70 V specification for 90% depletion of the photodiode. In addition, the diode itself was seen to be damaged and was replaced and tested to ensure proper working order. A stand was procured and modified for the ESC. The recirculation pump was a new UN035 TTP KNF with a Teflon diaphragm that was cleaned and greased. Some of the fittings for the vacuum line, the nitrogen gas feedthrough and column top and bottom were specially machined as no spares were available.

Once all the fittings were secured and sealed for the ESC chamber, the chamber was pumped down using a large Alcatel vacuum roughing pump (used for the array of six existing ESCs). Leak checks were done to ensure pressure levels lower than 1 mbar could be reached. Once the fitting seals were established the chamber was pumped down to 4.6×10^{-2} mbar and the pressure rise was recorded overnight by a chart recorder. By morning the pressure had reached a level of 0.28 mbar so the fittings were inspected again and the process was repeated over several days until a low pressure leak rate of 0.29 mbar/day was established.

It is important to ensure the leak rate at low pressure is small, as ^{222}Rn ingress from the lab air can contaminate an ESC run. The ^{222}Rn content in the surface lab air was measured to be 0.33 ± 0.02 pCi/l on September 28, 1999 by flushing 58 mbar of lab air through a cold trap and into ESC7. This level corresponds to 64.2 ± 3.2 atoms/mbar. Given an average leak rate of 0.5 mbar/day, ^{222}Rn ingress would be interpreted as an increase of 32 ± 2 dpd in the activity levels of ^{226}Ra. This level is approximately 10% of the typical signal seen for a column blank. Fluctuations in the lab air radon levels can lead to large systematic errors in the activity levels of an ESC run[41].

A plot of the ESC pressure rise was made in order to extrapolate the time for the chamber pressure to rise from 30 mbar to 40 mbar, as this affects the collection efficiency (ε_{coll}) for ^{216}Po as previously mentioned. The pressure rise was measured by pumping down the chamber below 1 mbar using the large Alcatel vacuum roughing pump, then flushing the chamber with clean nitrogen gas and leaving it at approximately 450 mbar for approximately three minutes. Caution has to be taken not to exceed a pressure of 450 mbar when the recirculation loop is open as this will damage the KNF pump. After three flushes of the chamber a pressure of 30 mbar of nitrogen was established[3]. Data were collected for the pressure rise and the leak rate was shown to be 0.31 mbar per day as extrapolated from the plot of ln(P_{atm} - P_{ESC})[4].

The preamp, signal, and HV electronics were all connected to allow the electric field to be established in the sealed chamber. Before applying high voltage to the new ESC, the line and white noise for the existing ESC3 were measured to be 30 mV and 150 mV respectively, using an oscilloscope. The HV was slowly raised to -1000 V with some arcing being observed that quickly settled. No changes were seen in

---

[3] This is the standard procedure for starting any ESC run.

[4] It was noticed, after the data for the LTF runs were collected, that the Pirani gauge was not calibrated properly. The actual starting pressure for the runs was 18 - 20 mbar instead of 27 - 30 mbar. Recent studies (July, 2000) with a high activity column have shown that the difference in the detection efficiency is only 0.8 ± 1.3%[46]. Data results have been adjusted accordingly

the noise levels of ESC3 when the new ESC (ESC7) had HV applied, indicating no significant ground loops.

Just as for the radon DAQ system, the amplifier input is fed into a sixteen input ORTEC 920-16 Spectrum Master multi-channel buffer (MCB). The MCB is read by Maestro II (ver. 1.30) DOS program to display one of sixteen 1024 channel spectra, to set regions of interest and to find peak areas. The DOS Multi-Tasker (A19-BI, ver. 2.2) program saves each spectrum and writes the counts in the region of interest into a log file every three hours[25].

The chamber was injected with lab air containing ^{222}Rn to calibrate the Po peaks using Maestro II. The overlap percentage of ^{214}Po into ^{216}Po was measured to be 1.60%, which is taken into account in the data analysis. In addition, the counting efficiency of ^{218}Po relative to ^{214}Po was determined to be in the region of 0.9392 ± 0.0052 which is used when the energy windows are set in the analysis in the standard manner (see Section 4.3)[41]. The relative counting efficiencies for ^{216}Po and ^{212}Po are not considered in this thesis as ^{212}Po is not used in the analysis.

4.3 Data Analysis

For the data analysis of radium assays in general, it is assumed that only the isotopes ^{228}Th, ^{224}Ra, ^{226}Ra and ^{222}Rn are present at the start of counting. In the ^{232}Th chain both ^{228}Th and ^{224}Ra are extracted from the water, with extraction efficiencies of about 10% and 90% respectively. In the ^{238}U chain, ^{226}Ra is extracted from the water with an efficiency of 90%, while ^{222}Rn absorbed into the MnO_x may be present at the start of counting and must be accounted for in the fit. All the activities measured, whether for a sample or blank run, are referred to the time of the start of counting. It is also assumed that the activities measured for blank runs are from unsupported ^{228}Th and ^{226}Ra[29].

Two programs are used to analyze the data in an ESC run, and therefore a radium assay. The first, READESC, reads data from an ESC run and produces the time spectra, and calculates the energy efficiency and overlaps. The second, FITESC, calculates the concentration of radium in the water, based on the flow input for the assay[47]. Both programs were written for the purpose of analyzing data specific to SNO ESC runs.

READESC first reads the last binary energy spectrum from an ESC run (or spectrum selected by the user) as written by the acquisition program 'MT'. The energy spectrum is then written as an ascii file with the times of acquisition, then the spectrum is plotted. READESC then evaluates all the previous spectra to determine the number of counts as a function of time. The spectrum is fit to refine the energy window limits and to determine the energy window efficiency, the overlap of one line with another and the peak widths. Dead time corrections are then applied on the times of acquisition[47].

The fit of the spectrum is done in three passes. The first pass starts with the initial coordinates for the energy windows and fits windows 1 (^{218}Po) and 3 (^{214}Po) for a uranium spectrum and 2 (^{216}Po) and 4 (^{212}Po) for a thorium spectrum and then sets the windows to the new values. The second pass then refits the new windows to give improved width and peak positions. The third pass further improves the width and peak positions, then sets the energy scale and calculates the errors on the parameters, the overlap and the energy efficiency[47].

The likelihood function (LF) for an energy bin with l counts is the Poisson probability

$$(l \mid m) = e^{-m} \, \frac{m^l}{l!} \tag{4.2}$$

where m is the predicted number of counts in the energy bin. The number of counts m is dependent on the number of atoms giving observed decay, the counting efficiency, the peak shape parameters and the energy limits of the bin. The LF for each energy window is the product of the Poisson probabilities for each energy bin in that window

$$LF = \prod_i e^{-m(i)} \frac{m(i)^{l(i)}}{l(i)!} \tag{4.3}$$

where $m(i)$ is the mean number of counts in energy bin i. When the method of maximum likelihood is applied to this probability we have

$$\ln\ LF = \sum_i (l(i)\ \ln\ m(i) - m(i)) \tag{4.4}$$

where a constant term, independent of the parameters, has been neglected[38][47]. The function used in the fitting of ^{218}Po, ^{216}Po and ^{214}Po is a Gaussian above the peak and a Lorentzian below the peak. This form showed reasonably good fits to the part of the line far below the peak, with satisfactory χ^2 for peaks containing 10 000 counts. The χ^2 for the fit had low probability if the peak has very good statistics (500, 000 counts). The fit function for the ^{212}Po peak differs because of the tail at high energy from coincident betas from ^{212}Bi. It is represented by a Lorentzian with different widths above and below the peaks[47].

These functions are approximations to the real alpha peak shape, which is given by a convolution of a Gaussian (describing the resolution) and the shape function, a fractional polynomial. This convolution has no analytic expression. The approximation is made as the derivative of the fit function is needed in the fitting procedure[41].

Once all three passes have been made, the energy efficiency in each energy window is determined, as is the overlap of ^{214}Po with ^{216}Po. The fitted spectrum is displayed on the screen where the user can change the range of axes, the bounds of the energy windows and/or refit the spectrum. The default settings from the ^{222}Rn spike run can also be used by READESC to fit the spectrum. Once the energy windows are set, READESC processes all the spectra for the ESC run up to the spectrum used for the fit.

Corrections for dead-time or power failures are also done by READESC. If a power failure occurs, the real time, dead time and counts in the spectrum are reset to zero when power is restored. The acquisition resumes automatically at this point. In processing all the spectrum files, READESC will prompt to correct for the power failure and perform the fit twice to give a fit to the total spectrum. A shift is also applied to the size interval of a spectrum if the dead time exceeds 0.5%. All the information set by READESC is written to a file to be used by FITESC to determine the activities of ^{224}Ra and ^{226}Ra and the equivalent concentrations of ^{232}Th and ^{238}U.

FITESC is built in five main sections and its behaviour is slightly different depending on whether it is a blank or sample run being analyzed.

In the first section the parameters altering the analysis are initialized. The detection efficiency, water flow history (as supplied by the user) and run type are read from the file. The coefficients for the bateman equations from each decay chain are calculated (this is where the overlaps and efficiencies are implemented). The data is then read from the READESC file.

Next, the likelihood function LF is built based equations 4.2 to 4.4. Here $m(i)$ is linearly related to the variables

$$m(i) = \sum_{n} \text{est(n)} \cdot \text{coeff(n,i)} \tag{4.5}$$

where the coefficients are the known functions that only depend on the counting times and fixed parameters, such as half-lives and counting efficiency. The estimators are the activities for ^{224}Ra, ^{228}Th, ^{226}Ra and ^{222}Rn. For a constant background rate

$$\begin{aligned} \text{coeff(n,i)} &= \text{stop(i) - start(i)} \\ &= \tau(i) \end{aligned} \tag{4.6}$$

and for a rate that declines exponentially

$$\begin{aligned}\text{coeff(i)} &= \frac{(e^{-\lambda(n)\cdot \text{start(i)}} - e^{-\lambda(n)\cdot \text{stop(i)}})}{\lambda(n)} \\ &= \delta(n,i)/\lambda(n)\ . \end{aligned} \tag{4.7}$$

For a rate that grows exponentially

$$\text{coeff(n,i)} = \tau(i) - \delta(n,i)/\lambda(n)\ . \tag{4.8}$$

The fit function for each isotope consists of the sum of two (or more) time varying terms. The ^{214}Po spectrum consists of a decreasing term from residual ^{222}Rn decaying to ^{218}Po and an increasing term from extracted ^{226}Ra decays. The ^{216}Po spectrum consists of a decreasing term from extracted ^{224}Ra plus an increasing term from extracted ^{228}Th decaying to ^{224}Ra. The ^{218}Po spectrum consists of an increasing term from extracted ^{226}Ra decays plus a decreasing term from residual ^{222}Rn decaying to ^{218}Po. Part of this peak is also from ^{212}Bi so it includes an increasing term from extracted ^{228}Th decays and a decreasing term from extracted ^{224}Ra. In addition to these components, a fraction of the tail from the higher energy alpha due to overlaps is included. The overlap for ^{214}Po into ^{216}Po is 1.6% for ESC7, as set by the ^{222}Rn spike. The other overlaps, ^{212}Po on ^{214}Po and ^{216}Po on ^{218}Po, are scaled with respect to this overlap (between 1 - 3% depending on resolution). The overlap of ^{212}Bi on ^{218}Po is based on the 36.2% branching ratio for ^{212}Bi and 63.8% for ^{212}Po. ^{212}Po is not used in the fit[47].

The fit function for ^{214}Po is then (neglecting intermediate decays)

$$\begin{aligned} m &= \varepsilon_{214} \cdot [N_{226} \cdot \lambda_{226} \cdot (\tau - \frac{\delta_{226}}{\lambda_{222}}) \\ &\quad + N_{222} \cdot \lambda_{222} \cdot \frac{\delta_{226}}{\lambda_{222}}] \end{aligned} \tag{4.9}$$

where

ε_{214} = detection efficiency for ^{214}Po

N_{226} = number of ^{226}Ra atoms at the start of counting

N_{222} = number of ^{222}Rn atoms at the start of counting

λ_{226} = decay constant for ^{226}Ra

λ_{222} = decay constant for ^{222}Rn

τ = stop - start

$\delta_{226} = e^{-\lambda_{226}\cdot \mathrm{start}} - e^{-\lambda_{226}\cdot \mathrm{stop}}.$

The fit functions for ^{216}Po and ^{218}Po have similar forms based on their respective parent isotope contributions and overlaps. The three functions are combined to give a single LF which is maximized.

The fit function for a blank run differs from that of a sample because the beads were prepared long before counting started so it is assumed that all the observed ^{224}Ra comes from ^{228}Th in equilibrium and is decaying at a constant rate. The activities of ^{228}Th and ^{224}Ra are assumed to be equal and there is no excess ^{224}Ra at the start of counting. Therefore, in the fitting function of a blank run, the amplitudes from ^{228}Th and ^{224}Ra are kept equal[47].

In the third section of FITESC, maximization of the likelihood function is performed by searching for the parameters that yield a minimum of the negative of the logarithm of the likelihood function. If the minimum occurs at a boundary or during an error search it may be desired to fix one or more parameters to a set value.

The fourth section of FITESC calculates the confidence ranges. This is done by setting up the fit vectors of the number of counts in each counting interval and calculating the χ^2 for the fit. The number of counts in the measured fit are checked to be the same as in the spectra. The confidence regions are determined by finding the values of an estimator that reduces the LF from its value at the maximum by the same amount as for a Gaussian function. This is the procedure used to set confidence ranges in the MINOS subroutine of the CERN program MINUIT[47].

Finally, the concentration for the top-most isotope in the uranium or thorium chain, in units of g/cm^3, is calculated by

$$C_{water} = \frac{m_M \cdot e^{-\lambda_{Ra}(t^{Eoe}-t_S^{Soc})}\left[a_{spl}(t_S^{Soc}) - e^{-\lambda_{supp}(t_S^{Soc}-t_B^{Soc})} \cdot a_{blk}(t_B^{Soc})\right]}{\varepsilon_{extr} \cdot \lambda_{top} \cdot N_A \cdot f_i \cdot 1000.0 \cdot \sum_{i=1}^{N_{extr}} \left[\frac{\phi_i}{\lambda_{Ra}} \cdot (1 - e^{-\lambda_{Ra}(t_i^{stop}-t_i^{start})}) \cdot e^{-\lambda_{Ra}(t^{Eoc}-t_i^{stop})}\right]} \tag{4.10}$$

where

λ_{Ra} = decay constant of radium isotope of interest

λ_{supp} = decay constant of isotope supporting blank activity(^{228}Th or ^{226}Ra)

λ_{top} = decay constant of top-most isotope

t^{Eoe} = time when extraction ended

t_B^{Soc}, t_S^{Soc} = time of start of counting the blank/sample

m_M = molar mass of top-most isotope in the chain (g/mol)

ε_{extr} = extraction efficiency

N_A = Avogadro's number

f_i = isotopic fraction of top-most isotope

N_{extr} = number of uninterrupted extraction periods

ϕ_i = average flow during extraction period i

$t_i^{stop/start}$ = stop/start times of extraction period i

1000.0 = converts liters to cm^3

and $a_{spl}(t_S^{Soc})$ and $a_{spl}(t_B^{Soc})$ are the activities obtained from the maximum liklihood fit to the combined time spectra from ^{218}Po, ^{214}Po and ^{216}Po.

Plots of each energy window are generated. These plots show the number of counting intervals (corrected for dead-time and power failures) and the number of counts in each interval. In addition, the χ^2 value is given over the number of degrees of freedom (DoF) as well as the probability of the goodness of the fit (GOF). The resulting activity levels for the supported and unsupported isotopes, from both the ^{232}Th and ^{238}U chains are given in decays per day (dpd), with the statistical uncertainties given at a 68% (1σ) confidence level.

Figures 4.6 to 4.8 show the fits of ^{218}Po, ^{214}Po and ^{216}Po for the blank and sample runs of the 99/09/16 assay of the LTF background. Figures 4.9 to 4.11 show the fits for the first experimental assay, 99/11/16.

4.4 The LTF Radium Background

The first two radium assays to determine the LTF background were done with no radon background assays as the equipment for the radon assays was not available. The third assay of the LTF background was intended to be done in conjunction with a repeated radon assay of the same UPW sample in the chamber, however, the radon assay was deemed unnecessary as the results from the original assay were acceptable, in that a procedural change did not show appreciable effects on the radon assay results. The final LTF background radium assay was done in conjunction with a radon assay, as was intended from a procedural standpoint. Performing the assays together allowed for an immediate refill of the system to begin a new exposure time.

4.4.1 Results

The results of the four LTF background runs are listed in Table 4.2. The top portion of the table shows the calculated equivalent concentrations of ^{232}Th and ^{238}U with their respective GOF values. The lower portion of the table shows the fit activity of

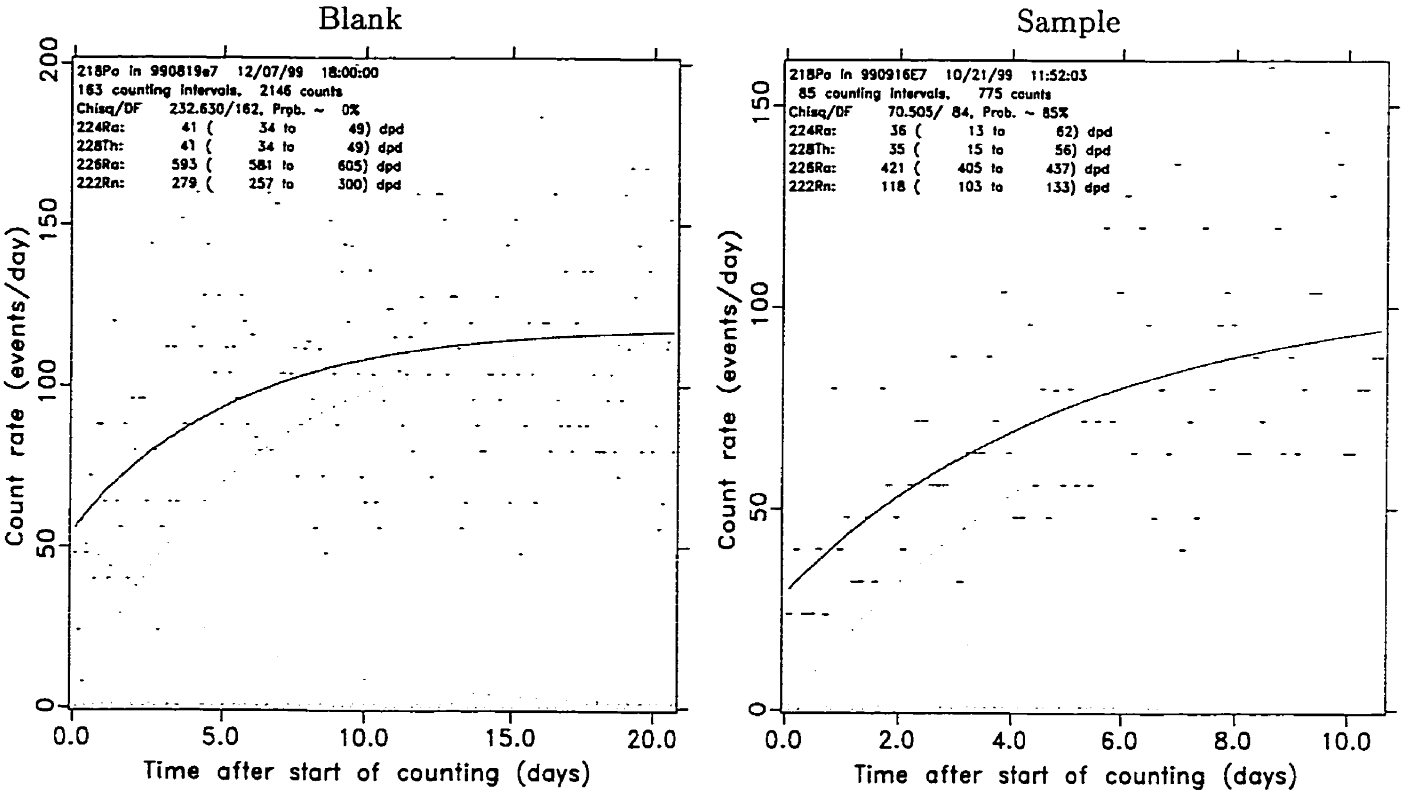

Figure 4.6: Fitted ^{218}Po activity curves for the blank and sample from LTF background assay 99/09/16. The horizontal tabs indicate the counts in a three hour interval, the fit is given by the solid line with the dashed lines at 1σ. The contributions from the supported and unsupported isotopes are given as dotted lines.

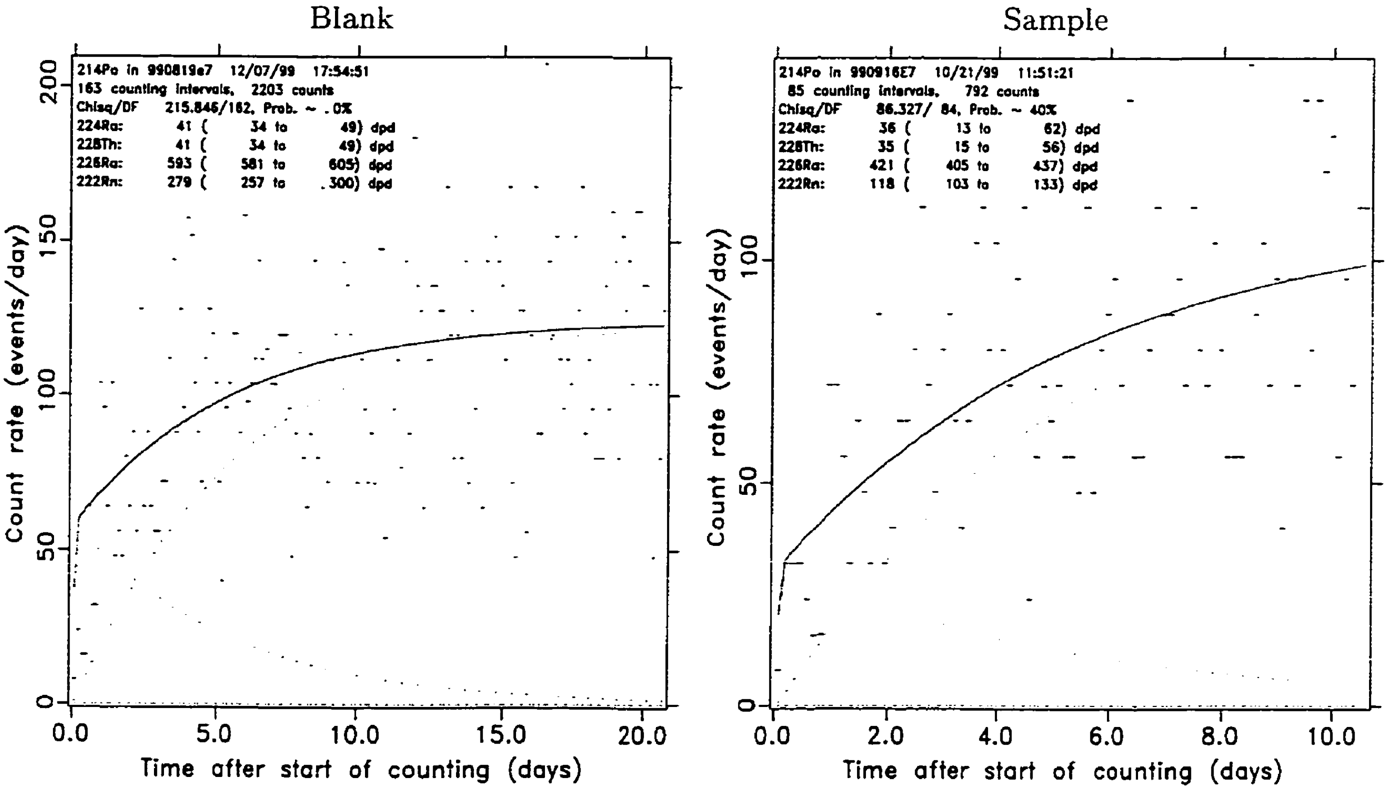

Figure 4.7: Fitted ^{214}Po activity curves for the blank and sample from LTF background assay 99/09/16.

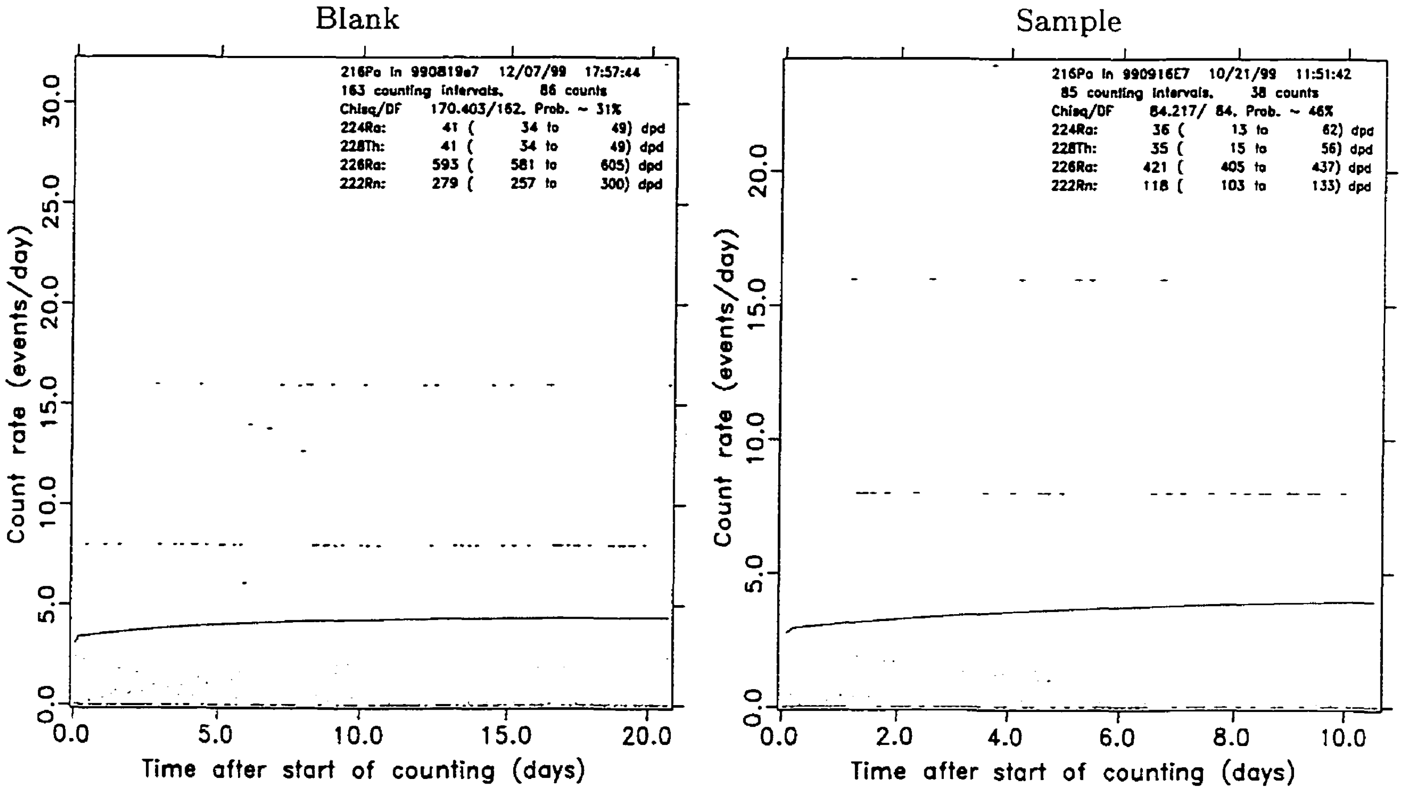

Figure 4.8: Fitted activity curves for the blank and sample from LTF background assay 99/09/16.

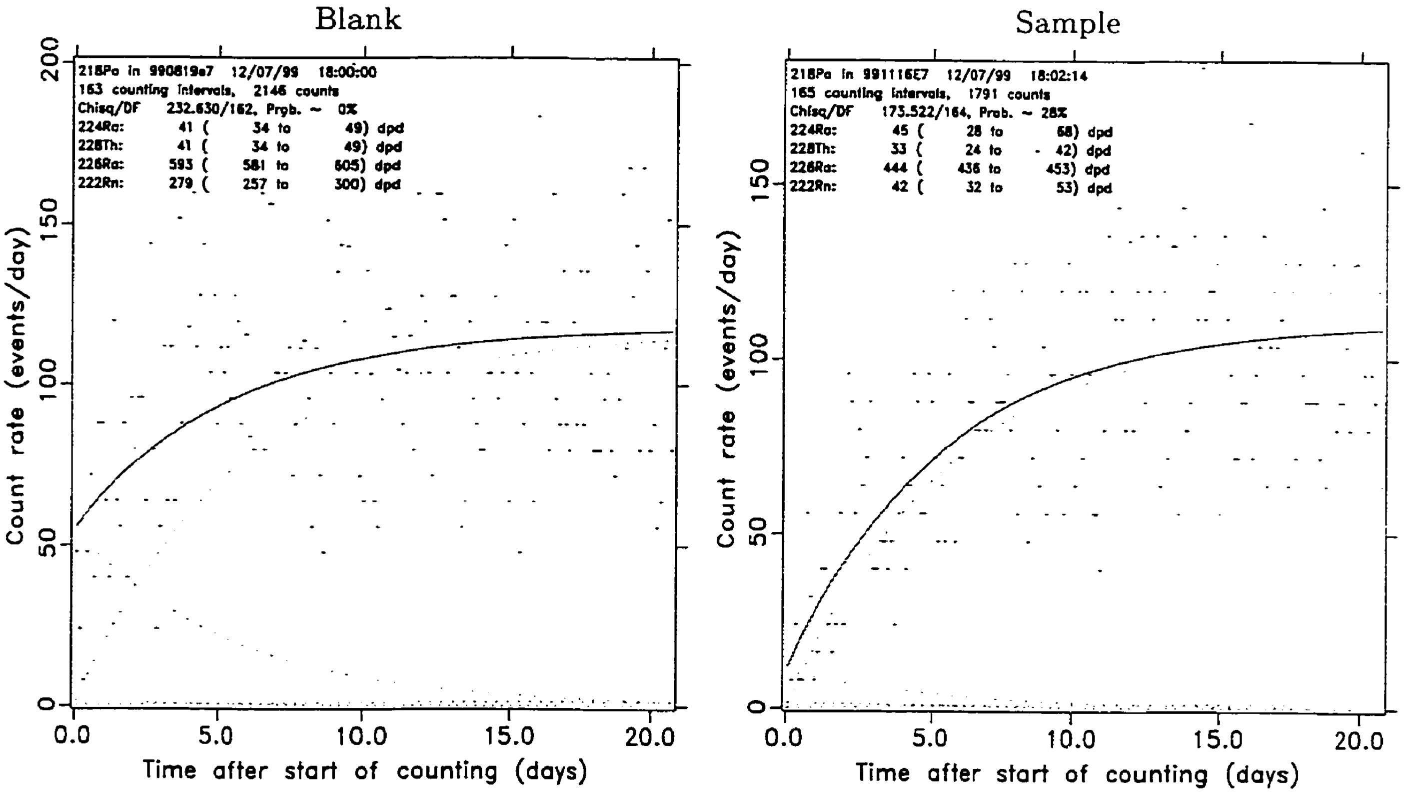
Blank

Sample

Figure 4.9: Fitted ^{218}Po activity curves for the blank and sample from LTF experimental assay 99/11/16.

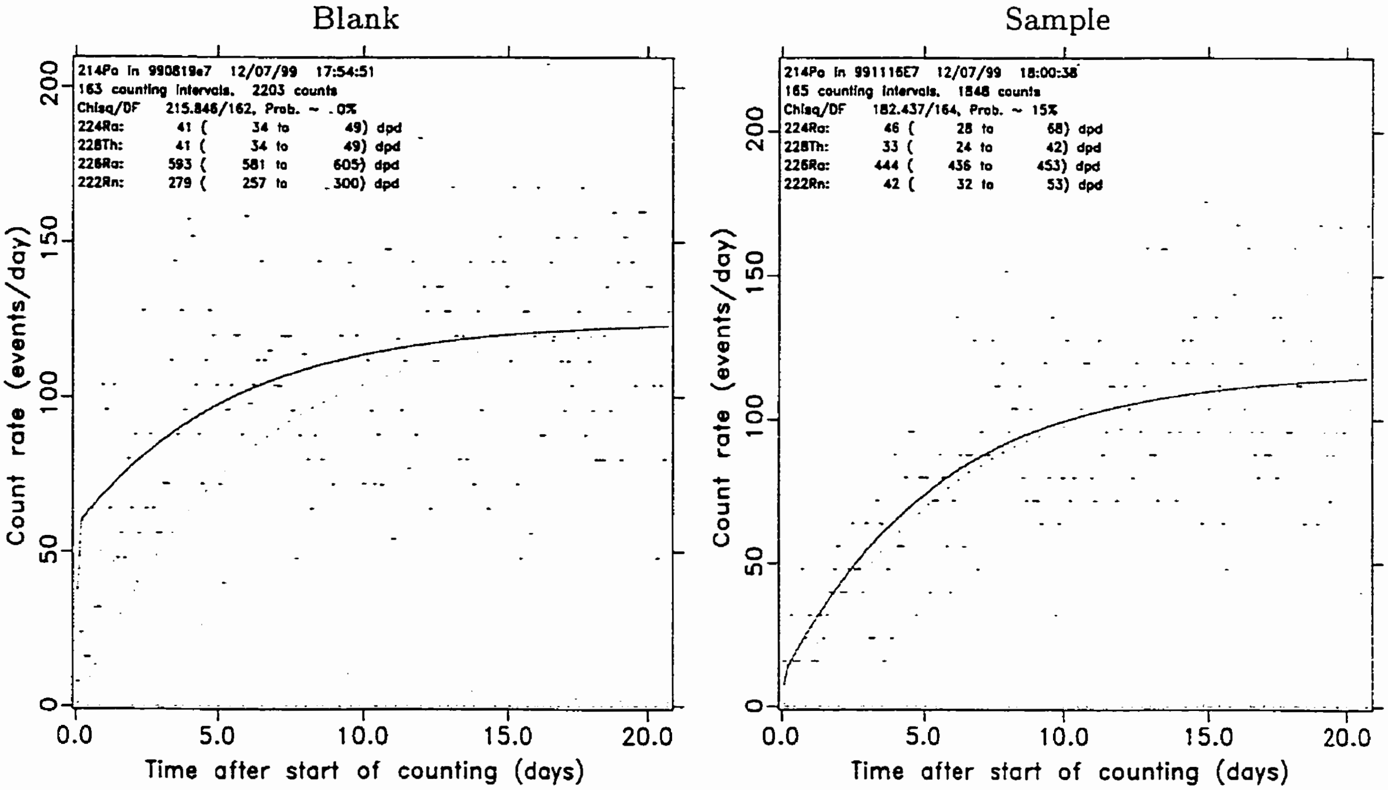

Figure 4.10: Fitted ^{214}Po activity curves for the blank and sample from LTF experimental assay 99/11/16.

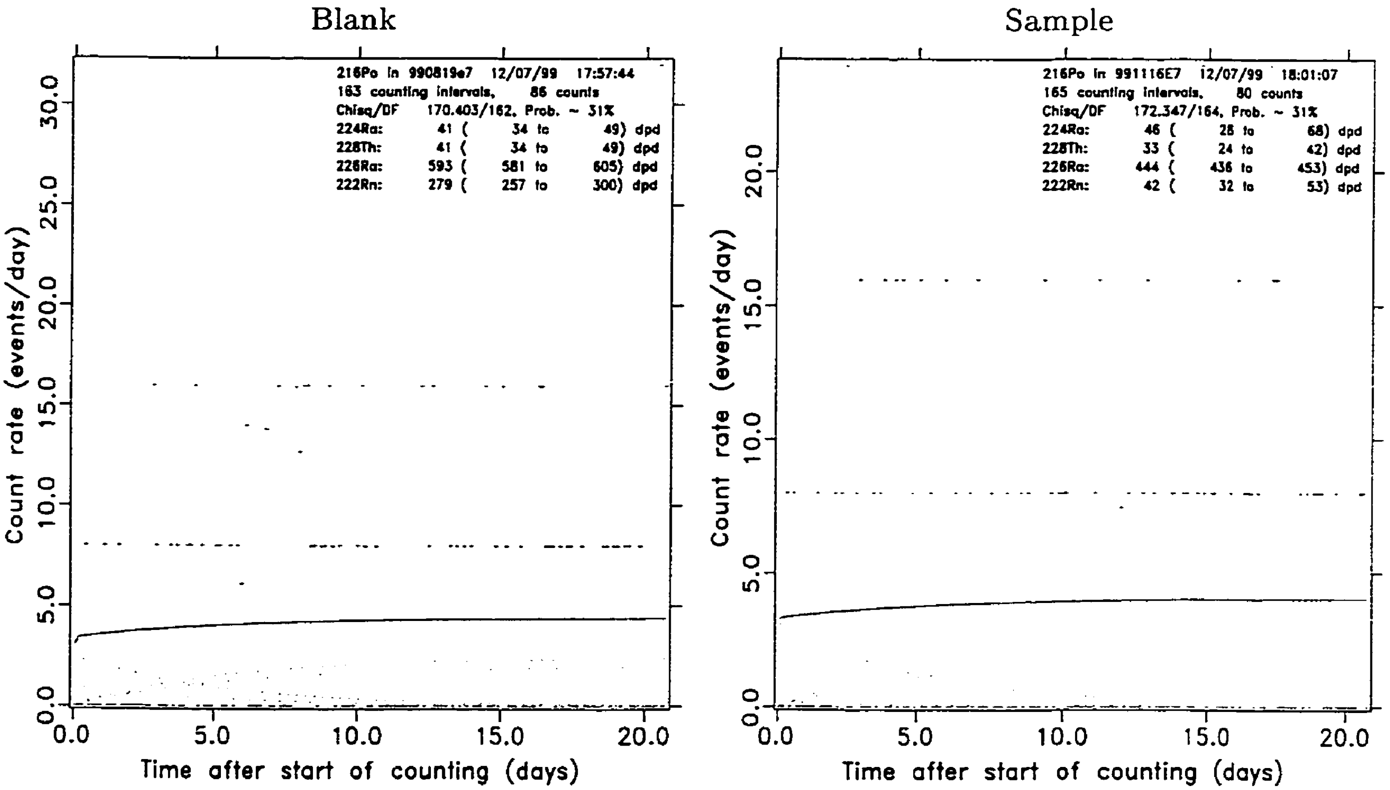

Figure 4.11: Fitted activity curves for the blank and sample from LTF experimental assay 99/11/16.

^{224}Ra and ^{226}Ra from which the above concentrations were calculated.

In all the background assays of the LTF, both ^{224}Ra and ^{226}Ra show results for the sample activity that are either lower than the blank run or within statistical uncertainty of it. However, runs 99/05/28 and 99/10/08 showed activity levels for ^{224}Ra slightly higher than those measured for the blank. These results are used to give the upper limit activity levels for ^{224}Ra at the end of the extraction in Table 4.3. The upper limit activity for ^{226}Ra cannot be determined as all the runs gave results where the activity of the sample was lower than that of the blank (SLB).

The average upper level background activity for ^{224}Ra is calculated to be 45 dpd. The resulting concentrations of ^{232}Th and ^{238}U in UPW have upper limit average values of 9.8 $\times 10^{-12}$ g/g and 3.6 $\times 10^{-12}$ g/g respectively, using the 68% statistical certainty level from the fits. These levels are well above the total concentrations of ^{232}Th and ^{238}U in 1000 tonnes of D_2O of 3.7 $\times 10^{-15}$ g/g and 4.5 $\times 10^{-14}$ g/g respectively. However, given the small volume of the LTF chamber it was suspected that the sensitivity levels for the prototype system would not reach that required to assay small components at the SNO D_2O concentration levels.

The first three background assays were conducted using ESC7 with the same column (11) for each of the extractions. The last assay was conducted using a different column (13) on ESC5 to see if there was a significant difference in results from one ESC to another. Since the SNO radium assays are done using any of the ESC with any of the columns all of the ESCs are characterized fully and the columns used are seen to be clean. As expected, there was no significant difference in using a different ESC and column.

It was suspected that the reason for a sample signal below that of the blank was that MnO_x fines had been lost from the column and/or that a small volume of water was used in the assay. As stated before, the columns had not been pre-rinsed to remove >0.1 μm fines, as is now standard procedure for SNO Ra assays.

Extraction Date	Type	Water Volume (l)	Flow Rate *lpm*	ESC	g Th/cm^3 H$_2$O	g U/cm^3 H$_2$O	Goodness of Fit Prob. (%)
99/05/28	First Ra BGND	7.2 ± 0.1	0.70 ± 0.01	7	$1.0\times10^{-11}(1^{+1.40}_{-1.00})$	$0.0\ (0.0\text{-}3.0\times10^{-12})$	23.
99/07/22	Second Ra BGND	7.9 ± 0.1	1.70 ± 0.02	7	$0.0\ (0.0\text{-}1.3\times10^{-11})$	$0.0\ (0.0\text{-}6.0\times10^{-12})$	43.
99/09/16	Third Ra BGND	7.5 ± 0.1	3.41 ± 0.09	7	$0.0\ (0.0\text{-}1.2\times10^{-11})$	$0.0\ (0.0\text{-}2.8\times10^{-12})$	66.
99/10/08	Fourth Ra BGND	7.9 ± 0.1	0.47 ± 0.01	6	$3.9\times10^{-12}(1^{+3.12}_{-1.00})$	$0.0\ (0.0\text{-}2.7\times10^{-12})$	1.

Extraction Date	ESC	Type	Counting Time (d)	Overlap (%)	Decays ^{224}Ra/day	Decays ^{228}Th/day	Decays ^{226}Ra/day	Decays ^{222}Rn/day	Fit Prob. (%)
99/05/28	7	Blank	18.91	1.6	62(54-71)	62(54-71)	438(427-449)	150(133-167)	3.
	7	Sample	9.66	1.6	83(57-112)	58(35-83)	382(365-399)	105(90-120)	23.
99/07/22	7	Blank	5.51	1.6	59(44-75)	59(44-75)	652(610-695)	70(52-90)	45.
	7	Sample	22.85	1.6	19(0-43)	51(41-61)	390(382-398)	171(156-186)	43.
99/09/16	7	Blank	20.76	1.6	41(34-49)	41(34-49)	593(582-605)	279(257-300)	0.0
	7	Sample	10.65	1.6	36(13-62)	35(15-56)	421(405-437)	118(103-133)	66.
99/10/08	6	Blank	9.78	2.0	39(30-49)	39(30-49)	285(269-301)	55(42-68)	85.
	6	Sample	12.51	2.0	47(25-74)	31(16-47)	275(262-288)	229(212-247)	1.

Table 4.2: Results of analysis of Ra extraction backgrounds on the LTF.

Extraction Date	Exposure Time (d)	Blank Activity (dpd)	Sample Activity (dpd)	Difference (dpd)	Upper Limit at EOE (dpd)
99/05/28	2.75	62 ± 9	83 ± 28	21 ± 29	50
99/10/08	21.92	39 ± 10	47 ± 25	12 ± 27	39

Table 4.3: LTF background upper limit activity levels at the end of extraction for ^{224}Ra.

The results from the LTF background runs are of interest in examining the effect of small volume flushes on the blank signal of a column. The question is; if a column has its blank measured and is then pre-rinsed, does the intrinsic activity level become effectively lowered? A study was conducted to try to identify the effect of small volume flushes on MnO_x intrinsic activity[48].

An MnO_x column was counted twice for its blank signal in a three month interval, then mounted on the rinsing skid of the salt plant in the surface lab. The lines were flushed for twenty minutes, then 5.6 l of UPW were flushed through the column, it was immediately dried for four hours, then counted on an ESC for one week. After the weeks counting, the column had another 5.1 l flushed through it, was dried and recounted for a week. Finally, a volume 10.2 l was flushed through the column, to give a total volume of 20.9 l. The column was dried and counted again. The uncertainty is large enough that the degree of change in the activity level cannot be discerned. The uncertainty in ^{226}Ra is even larger and no trend is apparent for the uranium data. The results are given in Table 4.4.

No conclusions were drawn from the experiment but suggested improvements to the sensitivity of the experiment were made. The uncertainties in the thorium chain can be substantially reduced by counting the column for a longer period of time (two to three weeks). Leaving the ESC chamber under vacuum two days prior to the experiment will allow for all the ^{212}Pb to decay away, allowing the full ^{212}Po peak to be used. In addition, the flushes would be kept uniform to 5 l per flush. A reduction in the errors in the thorium results may allow for the determination of lowering trends, however, the experiments are extensive and were not part of the scope of this thesis.

As mentioned above, there is a rinsing skid available in the surface laboratory. Although this water would not be representative of that used in the LTF extraction, the rinsing of the column could prevent the reduction of radium lost to fines. If the column used in an LTF experiment is rinsed and then has its intrinsic background levels counted in a blank run, this column could then be used with greater accuracy in an LTF experiment. This is providing that there is no evidence of supported ^{228}Th and ^{226}Ra resulting from the flushes on the rinse skid.

In the expression defining the distribution coefficient, K_d, it is evident that the ratio of the volume of water to the volume of resin in the experiment will affect the K_d value greatly. To determine the coefficient, large volumes of water were flushed through the column (on the order of tonnes). Thus, although the flow rates in LTF experiments have been kept well below the 20 BVM level used in the K_d experiments, the volumes of water used have been quite low and K_d values may be affected.

The SNO radium assay system was optimized using a 1 l column with 50 tonnes of water. The chamber of the LTF only holds 8 l of water, making a 1 l column far too large. However, the column cannot be too small or the extraction efficiency will be compromised. A larger chamber volume for the LTF coupled with a reduced column size would lead to an increase in the sensitivity of the system.

Extraction		Water				Goodness of
Date	Flow path	Volume (l)	ESC	g Th/cm^3 H$_2$O	g U/cm^3 H$_2$O	Fit Prob. (%)
99/10/19	Flush 5.6 L total	5.6	2	0.0 (0.0-1.9 $\times$ 10^{-11})	0.0 (0.0-6.2 $\times$ 10^{-12})	7.
99/10/26	Flush 10.7 L total	5.1	2	$8.5 \times 10^{-12}(1^{+1.55}_{-1.00})$	0.0 (0.0-6.4 $\times$ 10^{-12})	78.
99/11/03	Flush 20.9 L total	10.2	2	0.0 (0.0-1.3 $\times$ 10^{-11})	$2.3 \times 10^{-11}(1^{+1.20}_{-1.00})$	25.

Extraction			Counting	Overlap	Decays	Decays	Decays	Decays	Fit
Date	ESC	Type	Time (d)	(%)	^{224}Ra/day	^{228}Th/day	^{226}Ra/day	^{222}Rn/day	Prob. (%)
99/10/12	2	Blank 2	6.91	1.1	42(32-53)	42(32-53)	195(171-219)	162(144-181)	60.
99/10/19	2	Sample 5.6 L	6.64	1.1	30(6-60)	62(27-99)	181(160-203)	117(102-132)	7.
99/10/26	2	Sample 10.7 L	5.86	1.1	54(37-71)	0(0-23)	154(134-174)	60(49-72)	78.
99/11/03	2	Sample 20.9 L	1.38	1.1	0(0-16)	450(268-684)	309(174-443)	28(13-46)	25.

Table 4.4: Results of analysis of small volume flush tests (surface, UPW H$_2$O)

4.5 Radium Leached from Viton

The same samples of viton that were used in the radon assays, were also used to assay radium in the LTF. The radium assay followed immediately after the radon assay, as in the final radium background run of the LTF. The leach rate of ^{226}Ra or ^{224}Ra from viton was not known prior to these experiments. The 20.04 and 20.78 day exposure times allowed for ^{224}Ra (3.64 day half-life) to reach equilibrium with the chamber water. It was hoped that the increased radon signal for viton, shown in previous experiments, would correlate with a larger level of Ra^{++} going into solution in the LTF chamber. Table 4.5 shows the results of assaying the same sample of viton twice.

Although the radon assay showed very strong signals for the sample of viton, the radium assays still gave SLB results for ^{226}Ra and ^{224}Ra. Although the statistics are poor, the upper limit value for the ^{224}Ra activity from the second viton assay is given in Table 4.6.

After removing the ^{224}Ra background activity of 45 dpd for the LTF, the upper limit activity for ^{224}Ra leached from viton is 7 dpd. The area of the viton sample measured was 0.437 ± 0.051 m^2, giving an upper limit ^{224}Ra leach rate for viton of 16 ^{224}Ra/day·m^2.

After measures are taken to improve the sensitivity of the radium assay system of the LTF, it would be desirable to perform a Ra assay using a Ra spiked sample of water. This would give invaluable information on the systematics of the LTF radium assay system as well as adding to the investigations into the effects of small volume flushes on MnO_x intrinsic activity. Again, this is difficult due to the LTF being in the SNO laboratory but after careful characterization of the LTF background the use of a very low level spike may be possible. Finally, an experiment with a spike with two columns in series would give an adequate measurement of the extraction efficiency for the system.

Extraction Date	Type	Water Volume (*l*)	Flow Rate (*lpm*)	ESC	g Th/cm^3 H_2O	g U/cm^3 H_2O	Goodness of Fit Prob. (%)
99/11/16	LTF Oxford Viton I	4.3 ± 0.1	0.36 ± 0.01	7	0.0 (0.0-9.4 $\times 10^{-12}$)	0.0 (0.0-2.2 $\times 10^{-12}$)	12.
99/12/07	LTF Oxford Viton II	4.2 ± 0.1	0.75 ± 0.02	5	$4.7 \times 10^{-10}(1^{+1.49}_{-1.00})$	0.0 (0.0-4.6 $\times 10^{-12}$)	71.

Extraction Date	ESC	Type	Counting Time (d)	Overlap (%)	Decays ^{224}Ra/day	Decays ^{228}Th/day	Decays ^{226}Ra/day	Decays ^{222}Rn/day	Fit Prob. (%)
99/11/16	7	Blank	20.76	1.6	56(46-66)	56(46-66)	515(499-531)	191(173-210)	22
	7	Sample	20.82	1.6	46(28-68)	33(24-42)	445(436-453)	42(32-53)	12.
99/12/07	5	Blank	6.88	1.5	53(41-66)	53(41-66)	393(360-426)	230(207-254)	54.
	5	Sample	7.77	1.5	72(44-103)	49(20-81)	265(247-283)	69(56-82)	71.

Table 4.5: Results of analysis of two consecutive Ra extractions from a sample of viton in the LTF.

Extraction Date	Exposure Time (d)	Blank Activity (dpd)	Sample Activity (dpd)	Difference (dpd)	Upper Limit at EOE (dpd)
99/12/07	20.78	53 ± 13	72 ± 30	19 ± 33	52

Table 4.6: Second viton assay upper limit activity levels at the end of extraction for ^{224}Ra.

Chapter 5

Conclusions

The results presented in this thesis have shown the LTF to be an adequate system for assaying radon. The background activity level for ^{222}Rn in the facility was found to be 61.63 $\pm$ 3.67 dpd. This value is quite similar to the 55.3 dpd that was estimated for the system. A sample of viton gave a radon emanation rate of 1409 $\pm$ 105 Rn/hr $\cdot$ m^2, which was consistent with the levels for other similar materials measured using a different method. The sensitivity of the system for radium detection was not sufficient to allow for measurements down to the level of the UPW in the SNO cavity, however, an understanding of the sensitivity of a prototype system of this size allows for better design of a larger volume system. The upper limits of the background concentrations of ^{232}Th and ^{238}U in the UPW of the system were measured to be 9.8×10^{-12} g ^{232}Th/g UPW and 3.6×10^{-12} g ^{238}U/g UPW, while the lower limit concentrations were both 0.0. The average upper limit of the background activity of ^{224}Ra in the LTF is 45 dpd. The sample signal lower than blank signal (SLB) results for ^{226}Ra assays of the LTF background did not allow for a calculation to be made. The upper limit ^{224}Ra leach rate for viton was measured to be 16 ^{224}Ra/m$^2\cdot$day. Again SLB results prevented any calculations to be made using ^{226}Ra data.

It is apparent that further characterization of the LTF's radon and radium systems are needed in order for it to function as a measurement facility for the low level materials used in SNO. Much of this work involves further understanding the SNO assay systems, since the LTF systems were modelled after the larger SNO systems that existed and had been previously characterized. The following sections suggest methods of optimizing the systems of the LTF in order to have it available for study programs in SNO. Once these activities have taken place, a full scale LTF would be very useful for monitoring radon emanation rates from materials intended for use in the SNO water volume. The system would also be capable of measuring very high leach rates. If a material shows a very strong radon emanation rate, it could be monitored to see if its radium leach rate is correspondingly high.

5.1 Optimizing the LTF Radon Assay System

The radon gas board, Lucas cell, DAQ and DAN systems used for the LTF radon assay system have been extensively studied and characterized. The system parameter that requires further study is the extraction efficiency. The factors affecting the extraction of the radon gas from the LTF chamber are the uniformity of the nitrogen bubbles (size and flow), the amount of gas used in the assay and perhaps the type of gas used.

Initially, the intrinsic background of the empty LTF chamber may be further quantified by repeated measurements, providing the necessary data for defining statistical and systematic uncertainties. After this work has been completed, a ^{222}Rn spike needs to be introduced into a sample of water to be assayed in the LTF. This may require relocation of the system due to the restrictions of the SNO laboratory for sources but a better understanding of the empty chamber background level will allow for determining the strength of the spike. An injection technique, used in the SNO collaboration for ^{222}Rn spikes, may be utilized. This involves exposing water to lab air with a known intrinsic level of ^{222}Rn until equilibrium is reached. The water can then be injected into the system and the spike level is controlled by the amount of spiked water added to UPW. The intrinsic background level for the LTF has been measured at 61.63 ± 3.67 dpd, which is equivalent to 7.2×10^{-4} Bq. The surface lab air radon content of 0.33 pCi/l is equivalent to 1.2×10^{-2} Bq for 1 l of air used. This would be an excellent spike level as it should give us a strong signal but not be too high for the SNO laboratory. A spiked sample experiment may need to be repeated in order to make necessary changes to the parameters affecting the extraction efficiency.

5.2 Optimizing the LTF Radium Assay System

Two main factors have been identified as contributing to the uncertainties of the LTF radium assay system. First, the effect of fines from the MnO_x must first be addressed in order to further characterize the LTF itself. Pre-rinsing of the column used in an LTF assay would allow comparisons to be made to large volume assays as the preparations would be the same. The column could be pre-rinsed on surface using the salt plant skid or underground on the larger SNO water system rinse skid. This may be addressed in the further studies of the effects of small volume flushs on the intrinsic activity of MnO_x column blanks. It may be seen that it is necessary to count a column blank, pre-rinse the column then recount the blank for any assay done in the future, until sufficient data on the effect of rinsing the column is acquired.

Considering the large volume of UPW used to define the distribution coefficient, K_d, for MnO_x assays in SNO and the SLB results obtained in the LTF assays, it is apparent that the chamber volume must be increased. Constructing a 1 kl chamber would allow for assays to be performed with 6 times the sensitivity of the existing facility and would house materials with much larger surface areas. It may also be possible to design a smaller volume column dedicated to relatively small volume assays, however, the extraction efficiency should not be compromised by a change in the column size. Recent results for the extraction efficiency of radium from UPW using standard MnO_x show a 93.5 ± 22.4% efficiency for ^{226}Ra and 97.4 ± 2.1% for ^{224}Ra[29].

Once the systematics of the LTF are understood, the intrinsic background of the LTF can be determined with statistical and systematic uncertainties by reliably measuring the background many times. Once the background levels are known, a radium spike or a barium tracer may be used in a sample of water to quantify the extraction efficiency of the LTF radium assay system.

REFERENCES

[1] John N. Bahcall, Sarbani Basu and M. H. Pinsonneault *Phys. Lett.* **B433**, 1-8 (1998).

[2] John N. Bahcall, *Neutrino Astrophysics*, Cambridge University Press. Cambridge, 1989.

[3] J. N. Bahcall, *Astrophysical Journal*, **467**, 475 (1996).

[4] G. T. Ewan *et al.*, *Sudbury Neutrino Proposal*, SNO-STR-87-12 (1987).

[5] R. Davis Jr. *et al.*, *Phys. Rev. Lett.*, **20**, 1205 (1968).

[6] J. N. Bahcall, *Phys. Rev. Lett.*, **23**, 251 (1969).

[7] A. Breaux *et al.*, *National Technical Information Service* U.S. Department of Commerce, 1998.

[8] B. Pontecorvo, *Zh. Eksp. Teor. Fiz.*, **53**, 1717 (1967) [*Sov. Phys.* JETP **26**, 984 (1968)].

[9] S. P. Mikheyev and A. Yu. Smirnov, *Nuovo Cimento*, **C9**, 17 (1986); *Yad. Fiz.* **42**, 1441 (1985) [*Sov. J. Nucl. Phys.* **42**, 913 (1985)].

[10] L. Wolfenstein, *Phys. Rev.* **D17**, 2369 (1978) and *Phys. Rev.* **D20**, 2634 (1979).

[11] John N. Bahcall and Plamen I. Krastev, *Phys. Lett.* **B436/3-4**, 243 (1998).

[12] Y. Suzuki, Solar Neutrino Results from Super-Kamiokande, in *Proceedings, XVIII International Conference on Neutrino Physics and Astrophysics, Neutrino '98*, *Nucl. Phys.* **B77**, 35-42 (1999).

[13] Y. Fukuda *et al. Phys. Rev. Lett.*, **81**, 1562-1567 (1998).

[14] E. D. Hallman and A. B. McDonald, *Physics in Canada*, **55**, 101 (1999).

[15] H. H. Chen, *Phys. Rev. Lett.*, **55**, 1534 (1985).

[16] John N. Bahcall, *Phys. Rev.* **D44**, 1644 (1991).

[17] John Bahcall *et al.*, *Phys. Rev.* **C54**, 411 (1996).

[18] J. Bogu *et al. Nucl. Instr. and Meth.* **A449**, 172 (2000).

[19] Darren R. Grant, *Process and Monitor Degasser Systems for the SNO Heavy Water Systems*, M.Sc. Thesis, Carleton University, Ottawa, Ontario, Canada (1998).

[20] J. Wilhelmy, G. Miller, LANL, Private communication.

[21] E.D. Earle, SNO, Private communication.

[22] K. McFarlane, SNO, Private communication.

[23] M. Liu, H. W. Lee, A. B. McDonald, *Nucl. Instr. and Meth.* **A329**, 291 (1993).

[24] A. Noble, M. Shatkay, J. -X. Wang in the *SNO Water Review*. 1996.

[25] H. Lee, Queen's University, Private communication.

[26] H. Lee, *Re-estimate of Emanated Radon Load in the H_2O*, SNO-STR-98-013 (1998).

[27] H. Lee, *D_2O Radon Load*, SNO-STR-99-DRAFT (1999).

[28] Shawn Fostner, Henry Lee, Ilan Levine, *Measurements of Radon in the SNO Detector*, SNO-STR-00-DRAFT (2000).

[29] J. Farine, *Trends in MnO_x Radium Assays Rev. 1*, SNO-STR-00-DRAFT (2000).

[30] William W. Nazaroff, Anthony V. Nero, Jr., *Radon and its Decay Products in Indoor Air*, John Wiley & Sons, 1988.

[31] W. Jost, *Diffusion in Solids, Liquids, Gases*, Academic Press, 1960.

[32] Manqing Liu, *^{222}Rn Emanation Into Vacuum*, M.Sc. Thesis, Queen's University, Kingston, Ontario, Canada (1991).

[33] Xiang Zhu, *Study of Vacuum Degassing for SNO Water System*, M.Sc. Thesis, Queen's University, Kingston, Ontario, Canada (1992).

[34] M. Balata *et al.*, *Nucl. Instr. and Meth.*, **A370**, 605 (1996).

[35] David R. Lide, *Handbook of Chemistry and Physics*, CRC Press, 73^{rd} Edition, 1992-93.

[36] Glenn F. Knoll. *Radiation Detection and Measurement*, John Wiley & Sons, 2^{nd} Editon, 1989.

[37] Jian-Xiong Wang *et al.*, *Nucl. Instr. and Meth.*, **A421**, 601 (1999).

[38] Philip R. Bevington, D. Keith Robinson, *Data Reduction and Error Analysis for the Physical Sciences*, McGraw Hill, 2^{nd} Edition, 1992.

[39] V. S. Uras *et al.*, *Summary of Radon Emanation Results*, SNO-STR-93-045 (1993).

[40] Jay Welbourne, *Analysis of Outgassing ESC Data*, SNO-STR-99-DRAFT (1999).

[41] J. Farine *et al.*, *MnO_x Radium Assay Technique Systematic Error Study*, SNO-STR-00-DRAFT (2000).

[42] Cathy Shewchuk, Michal Shatkay, David Sinclair, *Radium Removal/Monitoring in the SNO Experiment Using MnO, XAD-7 Resin*, SNO-STR-94-001 (1994).

[43] T. Andersen *et al.*, *Recent Results on Extraction Efficiencies, Systematics and Fines with MnO_2 Coated Beads*, SNO-STR-95-022 (1995).

[44] M. Shatkay, C. Hargrove, F. Dalnoki-Veress, *Pre-rinsing of MnO_x column for use in SNO*, SNO-STR-97-040 (1997).

[45] Tom Andersen, *Development of Systems for the Sudbury Neutrino Observatory.* Ph. D Thesis, University of Guelph, Guelph, Ontario, Canada (1997).

[46] J. Farine, CRPP, Private communication.

[47] J. Farine, B. Cleveland, *READESC and FITESC Data Analysis Suite for MnO_x Assays*, SNO-STR-00-DRAFT (2000).

[48] J. Farine, *Effect of small volume flushs on MnO_x intrinsic activity*, SNO-STR-00-DRAFT (2000).